Dissecting novel regulatory mechanisms of S100A1 on cardiac function

Inauguraldissertation

zur

Erlangen der Würde eines Doktors der Philosophie

vorgelegt der

Philosophisch-Naturwissenschaftlichen Faklutät

der Universität Basel

von

Melanie Börries

aus Oldenburg in Oldenburg, Deutschland

Freiburg, 2007

Genehmigt von der Philosophisch-Naturwissenschaftlichen Fakultät

auf Antrag von

Herrn Prof. Ueli Aebi, Herrn PD Harald Herrmann und

Frau PD Dr. Cora-Ann Schoenenberger

Basel, den 6. Juli 2005

Prof. Dr. Hans-Jakob Wirz

Dekan der Philosophisch Naturwissen-

schaftlichen Fakultät

To my husband,
Oliver Maier-Börries

Table of Contents

Chapter 1

Introduction

1.1 Calcium: a universal, intracellular second messenger

Calcium (Ca^{2+}) is a highly versatile intracellular signal that can regulate many different cellular functions like cell growth and differentiation, gene expression, apoptosis and necrosis, cell motility and muscle contraction (Berridge, 1993; Berridge et al., 2000; Carafoli et al., 2001). To achieve this versatility, the Ca^{2+}-signalling system operates in many different ways to regulate cellular processes (Fig. 1.1, (Berridge et al., 2003)). Changes in Ca^{2+} levels can occur in microseconds or hours such as in gene transcription or cell proliferation. The level of intracellular Ca^{2+} is determined by a balance between the *on* reactions that introduce Ca^{2+} into the cytoplasm and the *off* reactions through which the Ca^{2+}-signal is removed by the combined action of buffers, pumps and exchangers (Fig. 1.1).

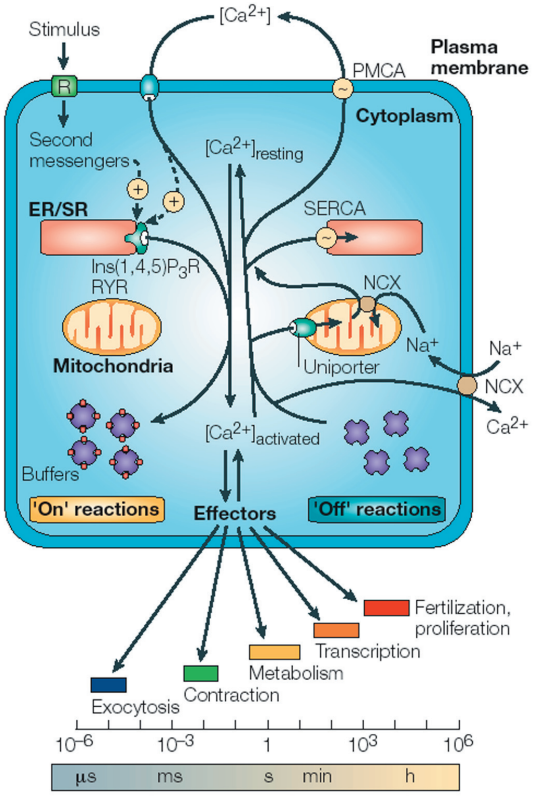

Figure 1.1: Ca^{2+}-signalling dynamics and homeostasis. During the *on* reactions, stimuli induce both the entry of external Ca^{2+} and the formation of second messengers that release internal Ca^{2+} that is stored within the endoplasmic reticulum (ER/SR). Most of this Ca^{2+} (shown as red circles) is bound to buffer, whereas a small proportion binds to the effectors that activate various cellular processes that operate over a wide temporal spectrum. During the *off* reactions, Ca^{2+} leaves the effectors and buffers and is removed from the cell by various exchangers and pumps. The Na^+/Ca^{2+} exchanger (NCX) and the plasma-membrane Ca^{2+}-ATPase (PMCA) extrude Ca^{2+} to the outside, whereas the sarco(endo)plasmic reticulum Ca^{2+}-ATPase (SERCA) pumps back into the ER. Mitochondria also have an active function during the recovery process in that they sequester Ca^{2+}rapidly through a uniporter, and this then released more slowly back into the cytosol to be dealt with by the SERCA and the PMCA. *Ins(1,4,5)P3R, inositol-1,4,5-triphosphate receptor; RYR, ryanodine receptor.* From Berridge et al., 2003.

During the *on* reaction, a small proportion of the Ca^{2+} binds to different effectors that are responsible for stimulating numerous Ca^{2+}-dependent processes (Fig. 1.1).

The Ca^{2+}-binding sites of the majority of proteins involved in transducing Ca^{2+}-signals have a structural motif in common, a lelix-loop-helix, termed the EF-hand. The term EF-hand motif was introduced by Kretzinger and is based on the first three-dimensional structure of parvalbumin, the founding member of this family (Kretsinger and Nockolds, 1973). EF-hand proteins exhibit both high selectivity for Ca^{2+} and the ability to respond rapidly and efficiently to modest (hundred-fold) changes in Ca^{2+} concentration. Part of the EF-hand protein members, for example parvalbumin, act intracellulary as so called Ca^{2+}-buffer proteins whereas other family members act as so called Ca^{2+}-sensor proteins. Prominent examples for the latter are the S100 proteins (Donato, 1999; Nelson and Chazin, 1998). This diversity in function for a single family of proteins is intriguing and has prompted to further studies.

1.2 Cardiac excitation-contraction coupling

Cardiac excitation-contraction coupling represents the process from electrical excitation of the myocyte to contraction of the heart. The ubiquitous second messenger Ca^{2+} plays essential role in cardiac electrical activity and is a direct activator of the myofilaments which cause contraction. During the cardiac action potential, Ca^{2+} enters the cell through depolarization-activated Ca^{2+}-channels (L-Type voltage-operated channels). This inward Ca^{2+} current (ICa), contributes to the action potential plateau (Fig 1.2 (Bers, 2002)). Ca^{2+} entry in term, triggers Ca^{2+}-release from the sarcoplasmic reticulum (SR). This process is commonly known as Ca^{2+}-induced Ca^{2+}-release process, CICR (Roderick et al., 2003).

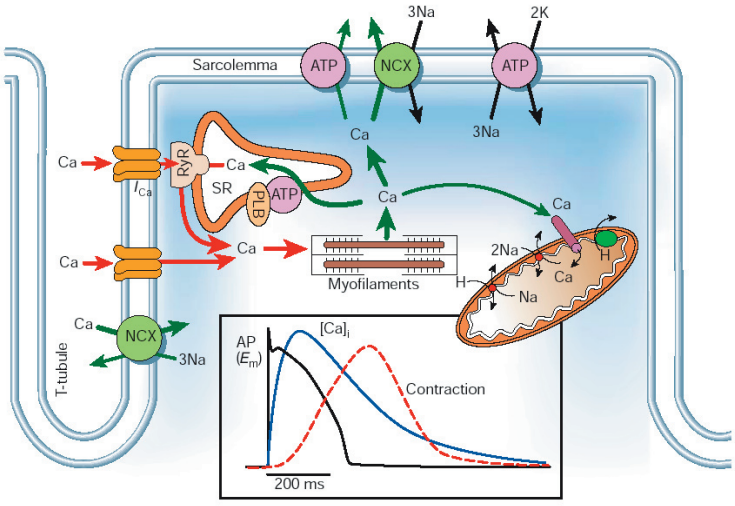

Figure 1.2: Ca^{2+}**transport in ventricular myocytes.** Inset shows the time course of an action potential (AP, black), Ca^{2+}-transient (blue) and contraction (red) measured in rabbit ventricular myocyte at 37°C. *NCX, Na^+/Ca^{2+}-exchanger; ATP, ATPase; PLB, phospholamban; SR, sarcoplasmic reticulum.* From Bers, 2002.

The combination of Ca^{2+} influx and release from the SR raises the free intracellular Ca^{2+} concentration ($[Ca^{2+}]_i$), allowing Ca^{2+} to bind to the myofilament protein troponin C, which then switches on the contractile machinery. For relaxation to occur $[Ca^{2+}]_i$ must decline, allowing Ca^{2+} to dissociate from troponin. The four pathways resonsible for Ca^{2+} transport out involve the SR Ca^{2+}-ATPase (SERCA), sarcolemmal Na^+/Ca^{2+}-exchange (NCX), sarcolemmal Ca^{2+}-ATPase or mitochondria Ca^{2+} uniport (Figure 1.2).

1.3 S100 proteins

S100 is a multigenic family of low molecular weight (Mr beween 9 and 13 kDa) Ca^{2+}-binding proteins of the EF-hand type. The EF-hand was devised by Kretsinger and Nockolds over 30 years ago as a graphical description of the Ca^{2+}-binding motiv observed in parvalbumin ((Fig. 1.3 (Kretsinger and Nockolds, 1973)).

Figure 1.3: A symbolic representation of the EF-hand motif. Helix E winds down the index fingers, whereas helix F winds up the thumb of a right hand. When Ca^{2+}-ion binds, helix F moves from the closed (apoprotein, light grey) to the open (holoprotein, dark grey) conformation. From Lewit-Bentley and Rety, 2000.

The first member of the S100 family was discovered in 1965 as an unfractioned bovine brain mixture of S100B and S100A1, called 'S100' because of its solubility in a 100% satured ammonium sulfate solution (Moore, 1965). Several years later bovine brain S100 protein was shown to consist of two distinct, but strictly related proteins, S100A1 and S100B which termed out not to be brain-specific (Isobe and Okuyama, 1978; Isobe and Okuyama, 1981). The nomenclature of S100 proteins is given by the gene location within the cluster on chromosome 1q21 and is designed by consecutive Arabic numbers placed behind the stem symbol S100A, for example S100A1. In contrast, S100 genes from other chromosomal regions should carry the stem symbol S100 followed by a single letter, like S100B that is localized on chromosome 21q22.

An S100 protein is characterized by the presence of two Ca^{2+}-binding motifs of the EF-hand type interconnected by an intermediate region often referred to as the hinge region (Fig. 1.4).

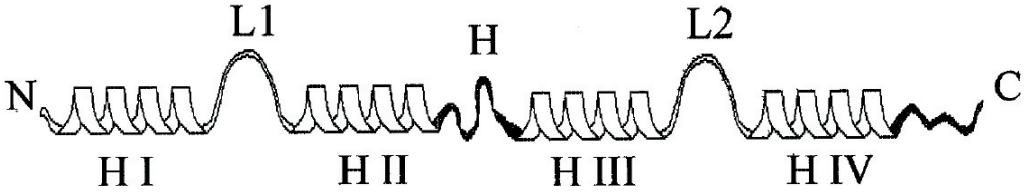

Figure 1.4: Schematic representation of the secondary structure of an S100 protein. Each Ca^{2+}-binding loop (L1 and L2, in the N- and C-terminal half, respectively) is flanked by α-helices (helices I and II, and helices III and IV for L1 and L2, respectively). A linker region (hinge region, H) connects helix II-III. Helix IV is followed by a C-terminal extension. From Donato et al., 2001.

In each Ca^{2+}-binding motif of the EF-hand type, a Ca^{2+}-binding loop is flanked by α-helices, resulting in the characteristic helix-loop-helix arrangement. The C-terminal EF-hand contains the classical Ca^{2+}-binding motif with a canonical Ca^{2+}-binding loop, common to all EF-hand proteins. This Ca^{2+}-binding motif has a typical sequence signature of 12 amino acids (Fig 1.5) and is flanked by helices III and IV. The N-terminal EF-hand is different from the classical EF-hand motif, the Ca^{2+}-binding loop is unconventional, longer and rearranged, and is characteristic for S100 proteins. Therefore, this EF-hand with a 14-amino-acid consensus sequence motif, which is flanked by helices I and II, is called the 'S100-specific' or 'pseudo-EF-hand' (Fig 1.5 (Heizmann and Cox, 1998; Marenholz et al., 2004)).

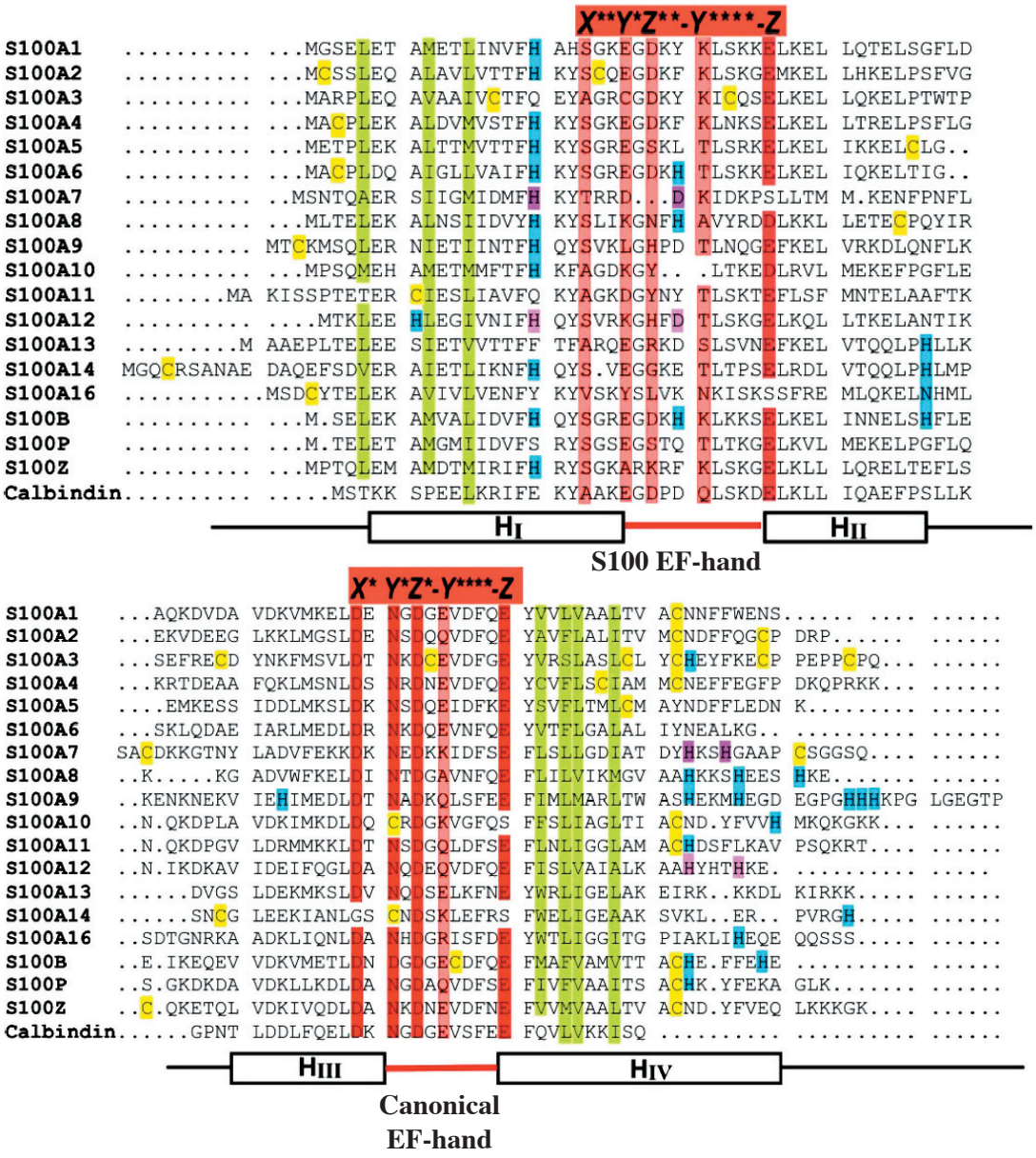

Figure 1.5: Schematic representation of the secondary structure of an S100 protein. Each Ca^{2+}-binding loop (L1 and L2, in the N- and C-terminal half, respectively) is flanked by α-helices (helices I and II, and helices III and IV for L1 and L2, respectively). A linker region (hinge region, H) connects helix II-III. Helix IV is followed by a C-terminal extension. From Marenholz et al., 2004.

Hence, the two Ca^{2+}-binding sites in an S100 protein bind Ca^{2+} with different affinities, a higher affinity in the case of the C-terminal site and a much lower affinity in the case of the N-terminal site (Donato, 1986). The highest sequence identity among S100 members is found in the Ca^{2+}-binding sites. The hinge region and the C-terminal extension display the least extent of sequence identity, suggesting the possibility that these two regions might play a role in the specification of biological activity of individual S100 proteins (Heizmann and Cox, 1998). In some cases, such as S100A1 and S100B, some conserved residues are found

at the same positions in the hinge region and the C-terminal extension, which explains in part the large overlap of the regulatory roles attributed to these two S100 members (Donato, 1999).

Within cells, most of S100 proteins exist as homodimers in which the two monomers are related by a two-fold axis of rotation and are held together by non-covalent bonds (Fig. 1.6A (Donato, 2001)). This has been demonstrated for S100A1, S100A1, S100A6, S100A7, S100A8, S100A10, S100A11, S100A12 and S100B, by nuclear magnetic resonance (NMR) spectroscopy, X-ray crystallography, or multiple anomalous wavelength dispersion (Drohat et al., 1996; Drohat et al., 1998; Kilby et al., 1996; Moore, 1965; Moroz et al., 2000; Potts et al., 1995; Rety et al., 2000; Rety et al., 1999; Rustandi et al., 2002; Sastry et al., 1998). Only a single member of the S100 family, calbindin 3, occurs as a monomer.

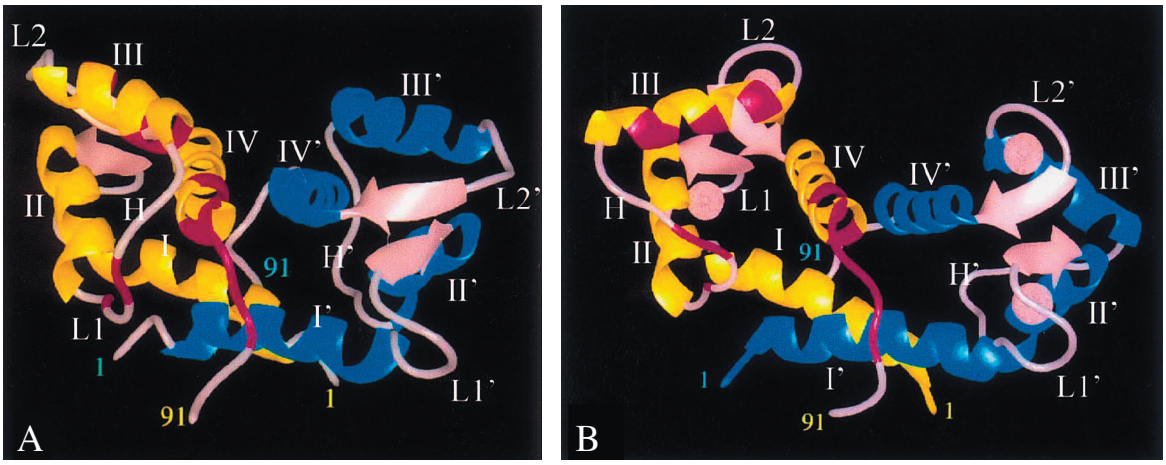

Figure 1.6: Structure of Ca^{2+}-free (A) and Ca^{2+}-loaded (B) $S100B_2$ dimer (taken as an example of S100 dimer). One S100B monomer is in yellow and the other is in blue. Helices are indicated by Roman numerals (I-IV in one monomer, and I'-IV' in the other monomer. Binding of Ca^{2+} to each S100B monomer cause a reorientation of helix III relative to all other helices with consequent reorientation of the hinge region and the (H) (compare A with B). These changes result in the exposure to the solvent of a surface defined by residues (in magenta) in helices III and IV, the hinge region and the C-terminal extension. Ca^{2+} ions are represented by light-pink dots within Ca^{2+}-binding loops (L1, L2 in one monomer, and L1', L2' in the other monomer). Note that the Ca^{2+}-loaded $S100B_2$ dimer is more extended than the Ca^{2+}-free dimer (B). From Donato, 2001.

Dimerization of S100 proteins seems important for their biological activites. Structural information (Fig. 1.6) suggests that upon Ca^{2+}-binding, helix III becomes perpendicular to helix IV as a consequence of a remarkable change of the interhelical angle between these two helices (Drohat et al., 1998; Smith and Shaw, 1998). Due to this change, the hinge region swings out. As a result of these structural changes, a cleft forms in each monomer, which is defined by residues in the hinge region, helices III and IV and the C-terminal extension,

and is buried in monomeric apo S100. Residues defining this cleft are believed to be important for the Ca^{2+}-dependent recognition of S100 target proteins. However, one member, S100A10, does not undergo Ca^{2+}-dependent conformational changes as it is in a permanent 'Ca^{2+}-on' state (Gerke and Weber, 1985; Rety et al., 1999).

It is generally accepted that within cells, S100 proteins regulate the activity of effector proteins (target proteins). Because this regulation is modulated by Ca^{2+}, S100 proteins are also considered Ca^{2+}-sensor proteins. One exception to this paradigm is the monomeric calbindin D9k for which no target protein has identified. Instead, calbindin D9K buffers cytosolic Ca^{2+} and is thus is a Ca^{2+} modulator protein.

S100 proteins exhibit cell- and tissue-specific expression and have been linked to Ca^{2+}-dependent regulation of a variety of S100 isoform-specific intracellular activities such as protein phosphorylation, enzyme activity, cell proliferation and differentiation, dynamics of cytoskeletal constituents, structural organization of membranes, intracellular Ca^{2+}-homeostasis and inflammation (Donato, 2003; Heizmann and Cox, 1998; Zimmer et al., 1995). In addition growing evidence indicates that members of the S100 protein family also exert extracellular effects on their target cells (Donato, 2003; Most et al., 2003a). Although S100 proteins apparently lack the classic signaling sequences required for secretion, some S100 proteins seem to reach the extracellular space through secretory pathways that neither involve the common endoplasmic reticulum/Golgi nor the alternative interleukin-1 route (Rammes et al., 1997). The number of downstream functions affected by extracellular S100 proteins is increasing. For instance, S100B, S100A4 and S100A12 have been shown to promote differentiation of embryonic neurons (Mikkelsen et al., 2001; Novitskaya et al., 2000; Selinfreund et al., 1991). Some extracellular activities of S100 proteins such as S100A12 and S100B are apparently mediated through interaction with the multiligand receptor for advanced glycation end products (RAGE)(Hofmann et al., 1999; Huttunen et al., 2000). In addition S100 proteins play an important role in the pathology of diseases, like in neoplasias, neurodegenerative disorders, inflammatory diseases and cardiomyopathies (Ehlermann et al., 2000; Most et al., 2003a; Most et al., 2004; Sheng et al., 1994; Wicki et al., 1997).

1.4 S100 A1

S100A1 is the most abundant S100 protein isoform in striated muscle (Donato, 2003; Kato and Kimura, 1985). Based on the observation that cardiac-restricted S100A1 overexpression enhances Ca^{2+}-cycling and cardiac contractility performance *in vitro* and *in vivo* (Most et al., 2001; Most et al., 2003b;Most et al, 2004; Remppis et al., 2002; Remppis et al., 2004), S100A1 has been earmarked as a novel positive inotropic intracellular regulator of heart function. These effects are primarily attributed to improved cardiac sarcoplasmic reticulum (SR) Ca^{2+}-handling. A recent study also provided evidence that S100A1 improves SR Ca^{2+}-fluxes and contractile force in skeletal muscle (Most et al., 2003c). In contrast to conventional positive inotropic agents, S100A1-mediated chronic cardiac inotropic actions in normal myocardium are independent of β-adrenergic signaling, with no alteration of heart rate or signs of myocardial hypertrophy or fibrosis (Most et al., 2003b). In addition, S100A1-deficient mice showed an impaired cardiac-contractility response to hemodynamic stress (Du et al., 2002). Consistently, S100A1 has been found to be downregulated in human and animal models of heart failure (Remppis et al., 1996; Tsoporis et al., 2003).

Furthermore, S100A1 stimulates the sarcomeric, myosin-associated giant kinase twitchin in a Ca^{2+}-dependent manner in vitro (Heierhorst et al., 1996). Twitchin is a member of a family of giant protein kinases involved in regulation of muscle contraction and the mechanoelastic properties of the sarcomere in invertebrates. Titin, the corresponding protein in vertebrates, was recently shown to interact with S100A1 (Yamasaki et al., 2001). S100A1 was proposed to provide a mechanism to free the thin filaments from titin and reduce titin-based tension before active contraction (Yamasaki et al., 2001).

Similar to other S100 protein members, S100A1 also exhibits extracellular functions (Donato, 2003; Most et al, 2003a). Although no evidence for its secretion has been offered so far, S100A1 induces neurite extension activity and also exhibits a pro-survival effect on neurons (Donato, 2003; Huttunen et al., 2000). Moreover, it has been shown that S100A1 is released into the extracellular space in considerable amounts during ischemic myocardial injury via an unknown mechanism (Kiewitz et al., 2000).

In the current thesis, the molecular mechanisms of S100A1 on cardiac function have been examined. Analysis of the internalization of S100A1 revealed a novel pro-survival pathway of extracellulary added S100A1 (Chapter 2). Furthermore, restoring S100A1 protein expression by adenoviral gene transfer can rescue defective contractile performance of failing myocardium *in vitro* and *in vivo* (Chapter 3). In addition, we were able to gain insight into the mechanism through which S100A1 differentially modulates sarcolemmal and sarcoplasmic Ca^{2+}-handling in ventricular cardiomyocytes depending on the subcellular location of this protein (Chapter 4). Last but not least, we identified new target proteins of S100A1, all of which are involved in energy metabolism. S100A1 directly interacts with the F_1-ATPase in a Ca^{2+}-dependent manner and is able to increase the ATP content of neonatal rat cardiomyocytes (Chapter 5). Overall, this work presents new knowledge on the cardiac regulator protein S100A1 and provides insight into the molecular mechanisms of this protein.

1.6 References

Berridge, M.J. 1993. Cell signalling. A tale of two messengers. Nature. 365:388-9.

Berridge, M.J., M.D. Bootman, and H.L. Roderick. 2003. Calcium signalling: dynamics, homeostasis and remodelling. Nat Rev Mol Cell Biol. 4:517-29.

Berridge, M.J., P. Lipp, and M.D. Bootman. 2000. The versatility and universality of calcium signalling. Nat Rev Mol Cell Biol. 1:11-21.

Bers, D.M. 2002. Cardiac excitation-contraction coupling. Nature. 415:198-205.

Carafoli, E., L. Santella, D. Branca, and M. Brini. 2001. Generation, control, and processing of cellular calcium signals. Crit Rev Biochem Mol Biol. 36:107-260.

Donato, R. 1986. S-100 proteins. Cell Calcium. 7:123-45.

Donato, R. 1999. Functional roles of S100 proteins, calcium-binding proteins of the EF-hand type. Biochim Biophys Acta. 1450:191-231.

Donato, R. 2001. S100: a multigenic family of calcium-modulated proteins of the EF-hand type with intracellular and extracellular functional roles. Int J Biochem Cell Biol. 33:637-68.

Donato, R. 2003. Intracellular and extracellular roles of S100 proteins. Microsc Res Tech. 60:540-51.

Drohat, A.C., J.C. Amburgey, F. Abildgaard, M.R. Starich, D. Baldisseri, and D.J. Weber. 1996. Solution structure of rat apo-S100B(beta beta) as determined by NMR spectroscopy. Biochemistry. 35:11577-88.

Drohat, A.C., D.M. Baldisseri, R.R. Rustandi, and D.J. Weber. 1998. Solution structure of calcium-bound rat S100B(betabeta) as determined by nuclear magnetic resonance spectroscopy. Biochemistry. 37:2729-40.

Du, X.J., T.J. Cole, N. Tenis, X.M. Gao, F. Kontgen, B.E. Kemp, and J. Heierhorst. 2002. Impaired cardiac contractility response to hemodynamic stress in S100A1-deficient mice. Mol Cell Biol. 22:2821-9.

Ehlermann, P., A. Remppis, O. Guddat, J. Weimann, P.A. Schnabel, J. Motsch, C.W. Heizmann, and H.A. Katus. 2000. Right ventricular upregulation of the Ca^{2+} binding protein S100A1 in chronic pulmonary hypertension. Biochim Biophys

Acta. 1500:249-55.

Gerke, V., and K. Weber. 1985. The regulatory chain in the p36-kd substrate complex of viral tyrosine-specific protein kinases is related in sequence to the S-100 protein of glial cells. Embo J. 4:2917-20.

Heierhorst, J., B. Kobe, S.C. Feil, M.W. Parker, G.M. Benian, K.R. Weiss, and B.E. Kemp. 1996. Ca^{2+}/S100 regulation of giant protein kinases. Nature. 380:636-9.

Heizmann, C.W., and J.A. Cox. 1998. New perspectives on S100 proteins: a multi-functional Ca^{2+}-, Zn^{2+}- and Cu^{2+}-binding protein family. Biometals. 11:383-97

Hofmann, M.A., S. Drury, C. Fu, W. Qu, A. Taguchi, Y. Lu, C. Avila, N. Kambham, A. Bierhaus, P. Nawroth, M.F. Neurath, T. Slattery, D. Beach, J. McClary, M. Nagashima, J. Morser, D. Stern, and A.M. Schmidt. 1999. RAGE mediates a novel proinflammatory axis: a central cell surface receptor for S100/calgranulin polypeptides. Cell. 97:889-901.

Huttunen, H.J., J. Kuja-Panula, G. Sorci, A.L. Agneletti, R. Donato, and H. Rauvala. 2000. Coregulation of neurite outgrowth and cell survival by amphoterin and S100 proteins through receptor for advanced glycation end products (RAGE) activation. J Biol Chem. 275:40096-105.

Isobe, T., and T. Okuyama. 1978. The amino-acid sequence of S-100 protein (PAP I-b protein) and its relation to the calcium-binding proteins. Eur J Biochem. 89:379-88.

Isobe, T., and T. Okuyama. 1981. The amino-acid sequence of the alpha subunit in bovine brain S-100a protein. Eur J Biochem. 116:79-86.

Kato, K., and S. Kimura. 1985. S100ao (alpha alpha) protein is mainly located in the heart and striated muscles. Biochim Biophys Acta. 842:146-50.

Kiewitz, R., C. Acklin, E. Minder, P.R. Huber, B.W. Schafer, and C.W. Heizmann. 2000. S100A1, a new marker for acute myocardial ischemia. Biochem Biophys Res Com mun. 274:865-71.

Kilby, P.M., L.J. Van Eldik, and G.C. Roberts. 1996. The solution structure of the bovine S100B protein dimer in the calcium-free state. Structure. 4:1041-52.

Kretsinger, R.H., and C.E. Nockolds. 1973. Carp muscle calcium-binding protein. II.

Structure determination and general description. J Biol Chem. 248:3313-26.

Lewit-Bentley, A., and S. Rety. 2000. EF-hand calcium-binding proteins. Curr Opin Struct Biol. 10:637-43.

Marenholz, I., C.W. Heizmann, and G. Fritz. 2004. S100 proteins in mouse and man: from evolution to function and pathology (including an update of the nomenclature). Biochem Biophys Res Commun. 322:1111-22.

Mikkelsen, S.E., V. Novitskaya, M. Kriajevska, V. Berezin, E. Bock, B. Norrild, and E. Lukanidin. 2001. S100A12 protein is a strong inducer of neurite outgrowth from primary hippocampal neurons. J Neurochem. 79:767-76.

Moore, B.W. 1965. A soluble protein characteristic of the nervous system. Biochem Biophys Res Commun. 19:739-44.

Moroz, O.V., A.A. Antson, G.G. Dodson, K.S. Wilson, I. Skibshoj, E.M. Lukanidin, and I.B. Bronstein. 2000. Crystallization and preliminary X-ray diffraction analysis of human calcium-binding protein S100A12. Acta Crystallogr D Biol Crystallogr. 56 (Pt 2):189-91.

Most, P., J. Bernotat, P. Ehlermann, S.T. Pleger, M. Reppel, M. Borries, F. Niroomand, B. Pieske, P.M. Janssen, T. Eschenhagen, P. Karczewski, G.L. Smith, W.J. Koch, H.A. Katus, and A. Remppis. 2001. S100A1: a regulator of myocardial contractility. Proc Natl Acad Sci U S A. 98:13889-94.

Most, P., M. Boerries, C. Eicher, C. Schweda, P. Ehlermann, S.T. Pleger, E. Loeffler, W.J. Koch, H.A. Katus, C.A. Schoenenberger, and A. Remppis. 2003a. Extracellular S100A1 protein inhibits apoptosis in ventricular cardiomyocytes via activation of the extracellular signal-regulated protein kinase 1/2 (ERK1/2). J Biol Chem. 278:48404-12.

Most, P., S.T. Pleger, M. Volkers, B. Heidt, M. Boerries, D. Weichenhan, E. Loffler, P.M. Janssen, A.D. Eckhart, J. Martini, M.L. Williams, H.A. Katus, A. Remppis, and W.J. Koch. 2004. Cardiac adenoviral S100A1 gene delivery rescues failing myocardium. J Clin Invest. 114:1550-63.

Most, P., A. Remppis, S.T. Pleger, E. Loffler, P. Ehlermann, J. Bernotat, C. Kleuss, J.

Heierhorst, P. Ruiz, H. Witt, P. Karczewski, L. Mao, H.A. Rockman, S.J. Duncan, H.A. Katus, and W.J. Koch. 2003b. Transgenic overexpression of the Ca^{2+}-binding protein S100A1 in the heart leads to increased in vivo myocardial contractile performance. J Biol Chem. 278:33809-17.

Most, P., A. Remppis, C. Weber, J. Bernotat, P. Ehlermann, S.T. Pleger, W. Kirsch, M. Weber, D. Uttenweiler, G.L. Smith, H.A. Katus, and R.H. Fink. 2003c. The C terminus (amino acids 75-94) and the linker region (amino acids 42-54) of the Ca^{2+}-binding protein S100A1 differentially enhance sarcoplasmic Ca^{2+} release in murine skinned skeletal muscle fibers. J Biol Chem. 278:26356-64.

Nelson, M.R., and W.J. Chazin. 1998. Structures of EF-hand Ca^{2+}-binding proteins: diversity in the organization, packing and response to Ca^{2+}-binding. Biometals. 11:297-318.

Novitskaya, V., M. Grigorian, M. Kriajevska, S. Tarabykina, I. Bronstein, V. Berezin, E. Bock, and E. Lukanidin. 2000. Oligomeric forms of the metastasis-related Mts1 (S100A4) protein stimulate neuronal differentiation in cultures of rat hippocampal neurons. J Biol Chem. 275:41278-86.

Potts, B.C., J. Smith, M. Akke, T.J. Macke, K. Okazaki, H. Hidaka, D.A. Case, and W.J. Chazin. 1995. The structure of calcyclin reveals a novel homodimeric fold for S100 Ca^{2+}-binding proteins. Nat Struct Biol. 2:790-6.

Rammes, A., J. Roth, M. Goebeler, M. Klempt, M. Hartmann, and C. Sorg. 1997. Myeloid-related protein (MRP) 8 and MRP14, calcium-binding proteins of the S100 family, are secreted by activated monocytes via a novel, tubulin-dependent pathway. J Biol Chem. 272:9496-502.

Remppis, A., T. Greten, B.W. Schafer, P. Hunziker, P. Erne, H.A. Katus, and C.W. Heizmann. 1996. Altered expression of the Ca^{2+}-binding protein S100A1 in human cardiomyopathy. Biochim Biophys Acta. 1313:253-7.

Remppis, A., P. Most, E. Loffler, P. Ehlermann, J. Bernotat, S. Pleger, M. Borries, M. Reppel, J. Fischer, W.J. Koch, G. Smith, and H.A. Katus. 2002. The small EF-hand Ca^{2+}-binding protein S100A1 increases contractility and Ca^{2+} cycling in rat cardiac

myocytes. Basic Res Cardiol. 97 Suppl 1:I56-62.

Remppis, A., S.T. Pleger, P. Most, J. Lindenkamp, P. Ehlermann, C. Schweda, E. Loffler, D. Weichenhan, W. Zimmermann, T. Eschenhagen, W.J. Koch, and H.A. Katus. 2004. S100A1 gene transfer: a strategy to strengthen engineered cardiac grafts. J Gene Med. 6:387-94.

Rety, S., D. Osterloh, J.P. Arie, S. Tabaries, J. Seeman, F. Russo-Marie, V. Gerke, and A. Lewit-Bentley. 2000. Structural basis of the Ca^{2+}-dependent association between S100C (S100A11) and its target, the N-terminal part of annexin I. Structure Fold Des. 8:175-84.

Rety, S., J. Sopkova, M. Renouard, D. Osterloh, V. Gerke, S. Tabaries, F. Russo-Marie, and A. Lewit-Bentley. 1999. The crystal structure of a complex of p11 with the annexin II N-terminal peptide. Nat Struct Biol. 6:89-95.

Roderick, H.L., M.J. Berridge, and M.D. Bootman. 2003. Calcium-induced calcium release. Curr Biol. 13:R425.

Rustandi, R.R., D.M. Baldisseri, K.G. Inman, P. Nizner, S.M. Hamilton, A. Landar, D.B. Zimmer, and D.J. Weber. 2002. Three-dimensional solution structure of the calcium-signaling protein apo-S100A1 as determined by NMR. Biochemistry. 41:788-96.

Sastry, M., R.R. Ketchem, O. Crescenzi, C. Weber, M.J. Lubienski, H. Hidaka, and W.J. Chazin. 1998. The three-dimensional structure of Ca^{2+}-bound calcyclin: implications for Ca^{2+}-signal transduction by S100 proteins. Structure. 6:223-31.

Selinfreund, R.H., S.W. Barger, W.J. Pledger, and L.J. Van Eldik. 1991. Neurotrophic protein S100 beta stimulates glial cell proliferation. Proc Natl Acad Sci U S A. 88:3554-8.

Sheng, J.G., R.E. Mrak, and W.S. Griffin. 1994. S100 beta protein expression in Alzheimer disease: potential role in the pathogenesis of neuritic plaques. J Neurosci Res. 39:398-404.

Smith, S.P., and G.S. Shaw. 1998. A novel calcium-sensitive switch revealed by the structure of human S100B in the calcium-bound form. Structure. 6:211-22.

Tsoporis, J.N., A. Marks, D.B. Zimmer, C. McMahon, and T.G. Parker. 2003. The myocardial protein S100A1 plays a role in the maintenance of normal gene expressi on in the adult heart. Mol Cell Biochem. 242:27-33.

Wicki, R., C. Franz, F.A. Scholl, C.W. Heizmann, and B.W. Schafer. 1997. Repression of the candidate tumor suppressor gene S100A2 in breast cancer is mediated by site-specific hypermethylation. Cell Calcium. 22:243-54.

Yamasaki, R., M. Berri, Y. Wu, K. Trombitas, M. McNabb, M.S. Kellermayer, C. Witt, D. Labeit, S. Labeit, M. Greaser, and H. Granzier. 2001. Titin-actin interaction in mouse myocardium: passive tension modulation and its regulation by calcium/ S100A1. Biophys J. 81:2297-313.

Zimmer, D.B., E.H. Cornwall, A. Landar, and W. Song. 1995. The S100 protein family: history, function, and expression. Brain Res Bull. 37:417-29.

Chapter 2

Extracellular S100A1 protein inhibits apoptosis in ventricular cardiomyocytes via activation of the extracellular signal-regulated protein kinase 1/2 (ERK1/2)

Patrick Most*, Melanie Boerries*, Carmen Eicher, Christopher Schweda, Philipp Ehlermann, Sven T. Pleger, Eva Loeffler, Walter J. Koch, Hugo A. Katus, Cora-Ann Schoenenberger‡ and Andrew Remppis‡

*Both authors contributed equally to this study

‡ Both authors contributed and supported this study equally

2.1 Abstract

S100A1 is a Ca^{2+}-binding protein of the EF-hand type, which belongs to the S100 protein family. It is specifically expressed in myocardium at high levels and is considered to be an important regulator of cardiac contractility. Since S100A1 protein is released into the extracellular space during ischemic myocardial injury, we examined the cardioprotective potential of extracellular S100A1 protein on ventricular cardiomyocytes in vitro. In this report we show that extracellularly added S100A1 protein is endocytosed into the endosomal compartment of neonatal ventricular cardiomyocytes via a Ca^{2+}-dependent clathrin-mediated process. S100A1-uptake protects neonatal ventricular cardiomyocytes from 2-deoxyglucose and oxidative-stress induced apoptosis *in vitro*. S100A1-mediated anti-apoptotic effects involve specific activation of the extracellular signal-regulated kinase 1/2 pro-survival pathway, including activation of phospholipase C, protein kinase C, mitogen-activated protein kinase kinase 1 (MEK1) and ERK 1/2. In contrast, neither transsarcolemmal Ca^{2+}-influx via the L-type channel, nor protein kinase A activity seem to take part in the S100A1-mediated signaling pathway. In conclusion, this study provides evidence for S100A1 protein serving as a novel cardioprotective factor in vitro. These findings warrant speculation that injury-dependent release of S100A1 protein from cardiomyocytes may serve as an intrinsic mechanism to promote survival of myocardium *in vivo*.

2.2 Introduction

S100A1, a low-molecular weight (Mr 10.000) Ca^{2+}-binding protein belongs to a multigenic family (21 members) of non-ubiquitous Ca^{2+}-modulated proteins to form an important sub-class of EF-hand proteins. Importantly, S100 proteins exhibit cell- and tissue-specific expression and have been linked to Ca^{2+}-dependent regulation of a variety of S100 isoform-specific intracellular activities such as protein phosphorylation, enzyme activity, cell proliferation and differentiation, dynamics of cytoskeletal constituents, structural organization of membranes, intracellular Ca^{2+}-homeostasis and inflammation (for reviews see (1-3)). S100A1 is the most abundant S100 protein isoform in striated muscle and has been identified as a novel positive inotropic intracellular regulator of cardiac as well as skeletal muscle Ca^{2+}-homeostasis and contractility (4-8).

However, growing evidence indicates that members of the S100 protein family also exert extracellular effects on their target cells (3). Although S100 proteins apparently lack signaling sequences required for secretion, some S100 isoforms seem to follow secretory pathways that involve neither the classical endoplasmic reticulum/Golgi nor the alternative interleukin-1-like route (9). For instance, S100A8 and S100A9, expressed at high concentrations by myelomonocytic cells, are secreted by a novel tubulin-dependent pathway and then exert important roles in the regulation of inflammatory processes (9). Similarly, extracellular functions for S100B, which is is secreted by astrocytes, have been extensively described (10). After secretion, S100B appears to exert both trophic and pro-survival effects on neurons via activation of the Ras/mitogen-activated protein (MAP) kinase pathway (11,12). Neurotrophic effects have also been reported for extracellular S100A4 and S100A12 protein based on the activation of the extracellular signal-regulated protein kinase (ERK1/2) signaling pathway (13,14).

It has been shown that S100A1 protein is released into the extracellular space in considerable amounts during ischemic myocardial injury via an unknown mechanism (15). Based on these observations, we raised the hypothesis that extracellular S100A1 protein may exert protective effects on myocardial cells. To address this question, the current study focuses on the characterization of extracellular effects of S100A1 protein on cardiac myocytes and

related molecular mechanisms in vitro. Indeed, our study identifies S100A1 protein as a novel cardioprotective factor since we could demonstrate for the first time that extracellular S100A1 protein can protect cardiomyocytes from apoptosis based on Ca^{2+}-dependent clathrin-mediated endocytotic uptake resulting in a specific activation of the pro-survival ERK1/2 signaling pathway.

2.3 Experimental Procedures

Reagents

Monodansylcadaverine (M-4008), chlorpromazine (C-8138) and verapamil (V-4629) were purchased from Sigma while myr-PKI (476485), calphostin-c (208725), U-73122 (662035), and PD98095 (513000) were obtained from Calbiochem. Myr-FRCRCF was custom-made by Eurogentec (Belgium) as prviously described (16,17). Anti-RAGE Ab was obtained from Chemicon (MAB5328).

Expression and purification of human recombinant S100A1 protein

Expression and purification of human recombinant S100A1 protein in E.coli was performed as previously described (6). After dialysis against PBS (pH 7.4), aliquots of purified S100A1 were stored at -80°C. Coupling of S100A1 with tetramethyl-rhodamine (Rh-S100A1) was carried out by Eurogentec.

Cell culture

Isolation of neonatal ventricular cardiomyocytes (NVCM) was performed as previously described (18). NVCM were cultured for 3 days either on plastic culture dishes, glass coverslips or cell-locates‘ (Eppendorf) in DME media (Biochrom) supplemented with penicillin/streptomycin (100U/ml), L-glutamine (2 mM) and 0.5% FCS Gold (PAA Laboratories Gmbh) (standard medium) at 37°C in a 95% air-5% CO2 humidified atmosphere. To induce apoptosis, 2-day old cultures were either incubated in glucose-free standard medium or DME media containing 2-deoxyglucose (3mM) or H2O2 (100 μM), respectively, for an additional 18 h. NVCM were treated with 1 μM human recombinant S100A1 where indicated.

Indirect Immunofluorescence and Phase contrast images

3-day old NVCM grown on glass coverslips were incubated with Rh-S100A1 (1 μM) as indicated, washed three times with PBS (pH 7.4), fixed in 4% paraformaldehyde and permeabilized with 0.2% Triton X-100 in PBS. Following three PBS washes, coverslips were incubated in 0.1% bovine serum albumine for 30 min to block nonspecific sites. Subsequently, cells were labeled with either anti-α-actinin (Sigma, 1/3000), anti-transferrin (Sigma, 1/500) or anti-caveolin-3 (Santa Cruz, 1/500) antibodies. Following incubation of the primary antibody for 1 h in the dark, coverslips were washed four times with PBS and then the corresponding ALEXA Fluor 488-conjugated secondary antibody (Molecular Probes, 1/800) was added for 1 h. After several washes with PBS, coverslips were mounted in Mowiol. Confocal images (CLSM) were obtained using a 100x oil objective on a Leica TCS SP laser scanning confocal microscope. Digitized confocal images were processed by Leica software and Adobe Photoshop. For phase contrast images, an inverse microscope (Olympus IX 70) equipped with a SensiCam CCD camera of PCO, was used. Images were subsequently processed with TILLvisION4.01 software (Tillphotonics).

Trypan Blue Exclusion, Cytochrome c Release, Caspase-3 Activity and MTT assay

The fraction of dead cells was determined by counting trypan blue stained cells on cell-locate slides. Viable NVCM were tested for electrical excitability by field stimulation. On each cell-locate slide, a total number of at least 150 cells were inspected. Cytochrome c release and caspase-3 activity were assessed by Quantikine“ M Mouse Cytochrome c Immunoassay (R&D Systems, Cat.Nr. MCTC0) and Caspase-3 Colorimetric Assay (R&D Systems, Cat. Nr. BF3100), respectively, as outlined by the manufactures protocol. MTT assay based on reduction of tetrazolium salt 3,[4,5-dimethylthiazol-2-yl]-2,5-diphenyltetrazolium bromide (MTT) was purchased from Trevigen (4890-25-K) and carried out according to the manufactures protocol.

Western Blot and MAPK Activity

Western blots using specific antibodies were performed to assess protein levels of

phosphorylated/non-phosphorylated MAP kinases p44/42 (ERK1/2; Cell Signaling # 9101/9102), p38 (Cell Signaling # 9211/9212), p54/46 (SAPK/JNK; Cell Signaling # 9251/9252), cardiac actin (Biogene Ac1-20.4.2) and S100A1 protein (SA 5632, Eurogentec). Cell cultures were rinsed in PBS and scraped off the dish in lysis buffer (PBS pH 7.4, SDS 2%, 2 mM EGTA/EDTA) containing a mixture of 1% v/v phosphatase inhibitors (Sigma; Phosphatase inhibitor cocktail I/II) and protease inhibitor (1 tablet/5ml) (Roche; Mini complete EDTA free protease inhibitor). To determine Rh-S100A1-uptake, NVCM were first washed extensively with EGTA/EDTA buffer (PBS, pH 7.4, 2 mM EGTA/EDTA) and then lysed. Blots were developed with the Avidix chemiluminescence detection system (Tropix, Applied Biosystems, Foster City, CA) and quantified by densitometry.

Statistical analyses

Data are presented as mean ± SEM. Unpaired student´s t-test and a two way repeated ANOVA analysis were performed to test for differences between groups. A value of $P < 0.05$ was accepted as statistically significant.

2.4 Results

Ca^{2+}-dependent clathrin-mediated endocytosis of extracellular S100A1 protein in NVCM

Before studying the effect of extracellularly added S100A1 protein on NVCM, the purity of human recombinant S100A1 protein was analyzed by SDS-PAGE and the specificity of S100A1 was confirmed by western blots probed with an custom-made antibody that specifically recognizes human S100A1 (SA5632) (data not shown) as recently described (6).
Incubation of NVCM with 1 μM rhodamine-conjugated recombinant S100A1 protein (Rh-S100A1) for 5, 30 and 120 min in the presence of 2 mM extracellular Ca^{2+} ($[Ca^{2+}]_e$) resulted in a vesicular accumulation of the protein in the cytosol as shown by CLSM (Fig. 2.1). Consistent with a cytosolic distribution of internalized S100A1 protein, images taken at the level of the nucleus revealed nuclear exclusion of Rh-S100A1. Simultaneous indirect immunofluorescence labeling of Rh-S100A1 treated NVCM with an anti-α-actinin antibody

revealed regular striated Z-line pattern typical of cardiomyocytes. Despite a reported interaction of S100A1 protein with the Z-line component capZ (19), internalized Rh-S100A1 protein seemed not localize to the Z-lines.

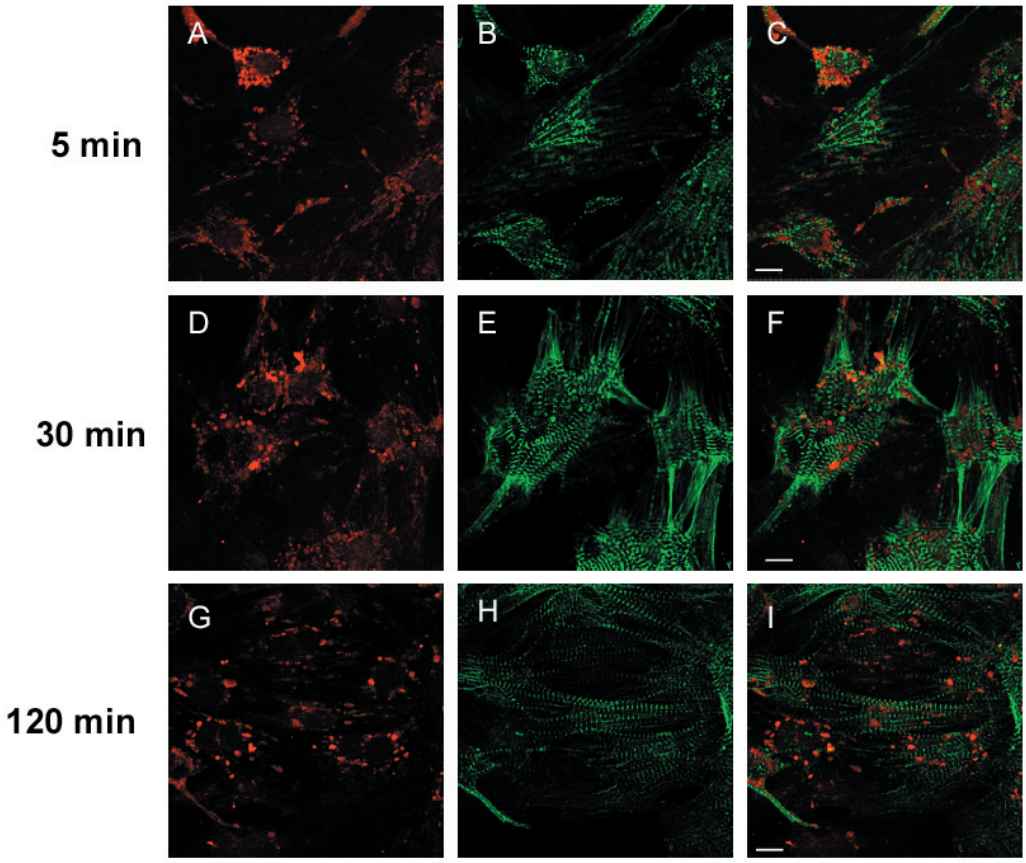

Figure 2.1: Localization of internalized Rh-S100A1 protein in NVCM. (A,D,G) In 3–day old cardiomyocyte cultures, rhodamine-coupled S100A1 (Rh-S100A1, red) is detected intracellularly five minutes after its addition to the culture medium. The overall intracellular distribution of Rh-S100A1 is similar 30 and 120 min after addition to the culture medium. (B,E,H) To identify cardiomyocytes, the same cultures were immunostained with an anti-α-actinin/Alexa Fluor 488-anti-mouse antibody (green), which reveals a distinct striated pattern. (C,F,I) Merged images confirming the uptake of Rh-S100A1 by NVCM. Bar, 10 μm.

This suggests that internalized and endogenous S100A1 protein are present in distinct cellular compartments probably serving dual functions in the cardiomyocyte. To further examine the specificity of S100A1-uptake, parallel NVCM cultures were incubated with corresponding concentrations of rhodamine alone. However, in these Rh-treated cells, we did not detect any dye uptake (data not shown). In contrast to NVCM cultured in Ca^{2+}-containing standard medium, a vesicular accumulation of Rh-S100A1 protein was not observed in cells that were kept in Ca^{2+}-free medium containing 2 mM EGTA (Fig. 2.2, B-G). This absence indicates that the uptake of exogenous S100A1 is dependent on Ca^{2+}. Analysis of homogenates from control NVCM and cells treated with S100A1 in the presence and absence of

Ca^{2+} by anti-S100A1 western blotting further confirmed the Ca^{2+}-dependence of S100A1 internalization (Fig 2.2A). Moreover, if NVCM cultures were incubated for 20 min with anti-S100A1 antibody (SA 5632) prior to the addition of recombinant S100A1, uptake of S100A1 protein was also be inhibited (Fig. 2.2H). As expected for a specific inhibition, the antibody-mediated 'clearing' was dose-dependent and thus, an unspecific cellular uptake of the protein driven by the rhodamine tag could be excluded. In contrast, despite previous reports that have identified RAGE as a potential S100 protein receptor, intracellular uptake of S100A1 could not be prevented by a 30 min preincubation with an anti-RAGE antibody (10μg/ml) that recognizes the ligand-binding domain of the receptor (MAB5328; data not shown) (11,20).

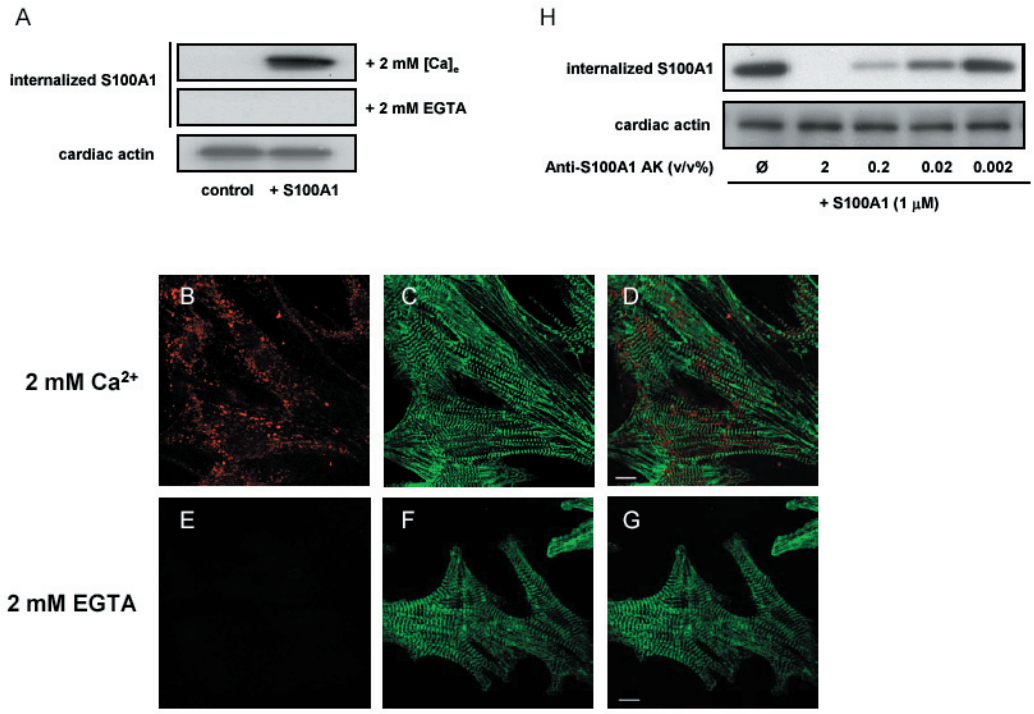

Figure 2.2: Ca^{2+}-dependence of S100A1 internalization. (A) Western blot of homogenates of untreated (control) and S100A1-treated NVCM in the presence of 2 mM Ca^{2+} (upper panel) or 2 mM EGTA (middle panel) probed with an antibody that is specific for human S100A1. Addition of 2 mM EGTA to the medium prevents cellular uptake of Rh-S100A1. Probing with an antibody that recognizes cardiac actin (bottom panel) demonstrates that protein loading in individual lanes was comparable. (B) Fluorescence image showing the cellular uptake of exogenously added Rh-S100A1 (red) in the presence of 2 mM $[Ca^{2+}]_e$ after 30 min. Immunostaining with an anti-α-actinin antibody (C) reveals the striated pattern typical for cardiomyocytes. (D) Merged image of Rh-S100A1 and Alexa Fluor 488-anti-actinin in the presence of 2 mM $[Ca^{2+}]_e$. Bar, 10 μm. (E) Internalization of Rh-S100A1 does not occur in the presence of 2 mM EGTA. (F) Immunostaining of Rh-S100A1-treated NVCM in the presence of 2 mM EGTA with an anti-α-actinin/Alexa Fluor 488-anti-mouse antibody. (G) Merged image of (E) and (F) reveals only the striated pattern typical for cardiomyocytes, but without Rh-S100A1-uptake. Bar, 10 μm. (H) Western blot of homogenates prepared from S100A1-treated (1μM) NVCM cultures that were incubated with different amounts of anti-S100A1 antibody (SA 5632, v/v %). Uptake of extracellularly added S100A1 is inhibited by SA 5632 in a dose-dependent manner. The band representing human S100A1 is no longer detected if SA 5632 is present in the culture medium at 2% (v/v).

To gain insight into the pathway of S100A1 internalization, Rh-S100A1 treated NVCM were labeled with an anti-caveolin-3/Alexa Fluor 488-anti-mouse antibody (Fig. 2.3), which is a marker for the caveolin-mediated uptake (21). Merging corresponding rhodamine and Alexa Fluor 488 confocal images clearly showed that the caveolin-3 staining pattern is distinct from that of Rh-S100A1 vesicles (Fig. 2.3C). In contrast, immunolabeling of Rh-S100A1 treated NVCM with an anti-transferrin antibody, which is a marker for the endosomal compartment revealed that Rh-S100A1 vesicles colocalize with transferrin and are therefore part of the endosomal compartment (Fig. 2.3, D-F) (22,23).

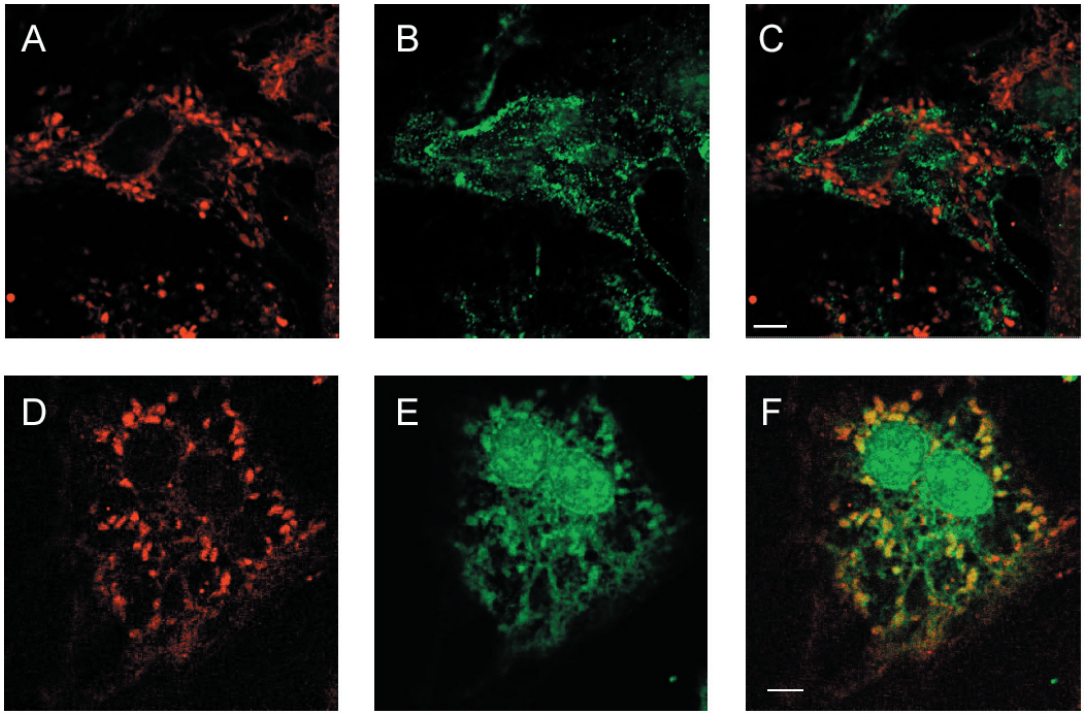

Figure 2.3: Colocalization of internalized Rh-S100A1 with the endosomal compartment. (A) Vesicular accumulation of Rh-S100A1 in the cytoplasm. (B) Immunostaining of Rh-S100A1-treated NVCM with an anti-caveolin-3/Alexa Fluor 488-anti-mouse antibody, which outlines the caveolin-mediated pathway. (C) Overlay of (A) and (B) shows no colocalization. (D) Vesicular accumulation of Rh-S100A1 in the cytoplasm. (E) Labeling of the endosomal compartment in Rh-S100A1-treated NVCM with an anti-transferrin/Alexa Fluor 488-anti-mouse antibody. (F) Overlay of (A) and (B) reveals colocalization of Rh-S100A1 and transferrin. Bar, 5 μm.

To substantiate that a clathrin-mediated uptake rather than a caveolin-dependent process is involved in S100A1 internalization, we examined the effects of two inhibitors of clathrin-mediated endocytosis, monodansylcadaverine (MDC) and chlorpromazine (CPZ) (24,25), on the uptake of S100A1. As illustrated by western blots of homogenates of cells incubated with S100A1 in the presence of inhibitors, that were probed with an anti-human S100A1

antibody (Fig. 2.4A), MDC and CPZ resulted in a dose-dependent inhibition of S100A1 internalization. Consistently, CLSM images of NVCM incubated with S100A1 in the presence of MDC revealed an absence of Rh-S100A1-uptake (Fig. 2.4B).

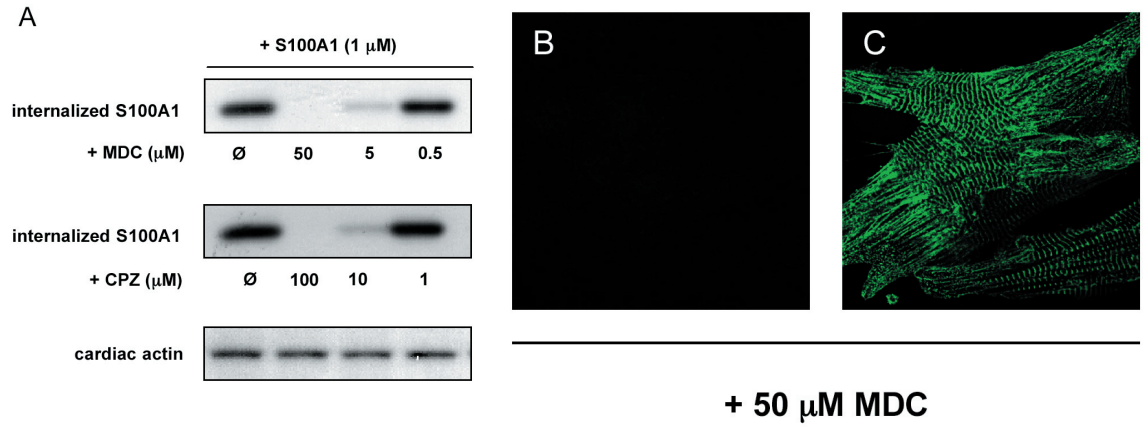

Figure 2.4: Clathrin-mediated endocytosis of S100A1 in NVCM. (A) Western blots of homogenates of S100A1-treated NVCM incubated in the presence of monodansylcadaverine (MDC; upper panel) and chlorpromazine (CPZ; lower panel), respectively. Internalized S100A1 is detected with an anti-human S100A1 specific antibody (SA 5632) whereas an anti-cardiac actin antibody was used to normalize amounts of protein loaded in individual lanes (bottom panel). Inhibition of S100A1-uptake via the clathrin-mediated pathway by MDC and CPZ is dose-dependent. (B) Fluorescence image of Rh-S100A1-treated (1 μM) NVCM incubated with standard medium containing 50 μM MDC. Vesicular accumulation of Rh-S100A1 in the cytoplasm is not detected if clathrin-mediated endocytosis is blocked by MDC. (C) Immunolabeling of the same coverslip with an anti-a-actinin/Alexa Fluor 488-anti-mouse antibody confirms the presence of cardiomyocytes. Bar, 10 μm.

In conclusion, our data strongly suggest that extracellular S100A1 protein is internalized and routed for the endosomal compartment of NVCM via a Ca^{2+}-dependent, clathrin-mediated endocytotic pathway. Because RAGE apparently does not mediate internalization of extracellular S100A1 protein in NVCM in our experimental setting, S100A1 protein may be endocytosed by another, yet to be identified receptor.

Activation of the ERK1/2 signaling pathway by endocytosed S100A1

Since signaling proteins of the mitogen-activated protein kinase (MAPK) pathways in particular have been linked to the endosomal compartment (for review see (25)), we next investigated whether endocytotic uptake of S100A1 protein might affect MAPK activity in NVCM. For this purpose, western blots of homogenates were probed with antibodies that specifically recognize either the unposphorylated or the phosphorylated form of the respective protein. Figure 2.5A shows that addition of 1 μM S100A1 to NVCM in the presence of

2 mM $[Ca^{2+}]_e$ resulted in a specific increase of p44/42 (ERK1/2) phosphorylation (3.8-fold, upper panel) compared to control cells.

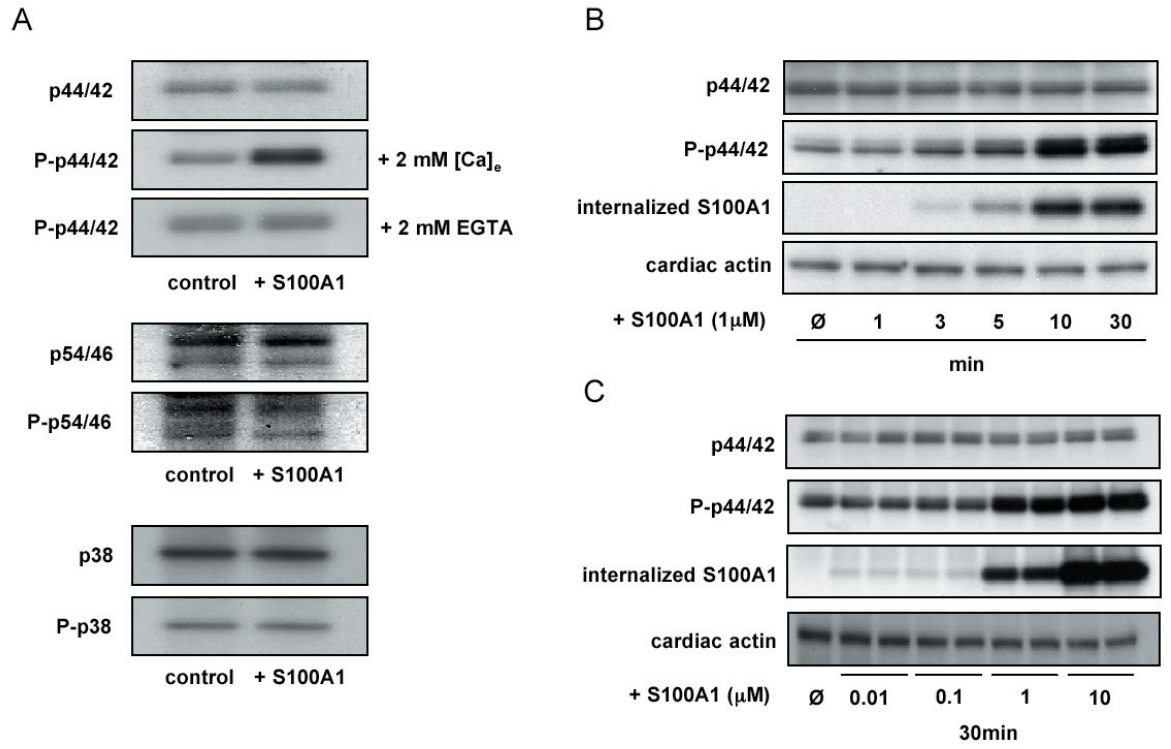

Figure 2.5: Extracellular S100A1 addition specifically increases levels of phosphorylated ERK1/2 (P-p44/42). (A) The effects of extracellularly added S100A1 (1 μM) on the levels of unphosphorylated and phosphorylated p44/42 (ERK1/2; top), p55/46 (SAPK/JNK; middle) and p38 (bottom) are shown by Western blots of cell extracts from untreated (control) and S100A1-treated cardiomyocytes (+S100A1; 1μM) probed with specific antibodies. Top, Ca^{2+}-mediated uptake of S100A1 leads to a 3.8±0.3-fold increase in p44/42 phosphorylation (P-p44/42; middle panel) compared to control ($P<0.01$, n=3), whereas the levels of unphosphorylated p44/42 (upper panel) remain constant. Inhibition of S100A1-uptake by 2 mM extracellular EGTA (lower panel) prevents ERK1/2 activation. Middle and bottom, p54/46 and p38 phosphorylation state are not affected by endocytosed S100A1. (B) Time-dependence of S100A1-induced activation of p44/42 phosphorylation (P-p44/42). The increase in p44/42 phosphorylation coincides with an increased level of internalized S100A1 over time. Maximal S100A1-uptake and P-p44/42 levels are reached after 10 min. (C) Dose-dependent activation of ERK1/2 phosphorylation. NVCM were incubated with increasing amounts of S100A1 (0.01-10 μM) for 30 min. A significant ($P<0.01$) increase of P-p44/42 is detected at 1 μM and 10 μM S100A1 stimulation.

Consistently, if S100A1-uptake is prevented by the presence of 2 mM EGTA (see Fig. 2.2 A), S100A1-mediated activation of ERK1/2 was absent. In contrast, the extent of phosphorylation of SAPK/JNK (p54/46, middle panel) and p38 (lower panel) following Ca^{2+}-dependent S100A1-uptake was comparable to that of control cells (Fig. 2.5A). Incubation of NVCM with S100A1 protein (1 μM) in the range of 1 to 30 min showed a time-dependence of ERK1/2 activation (Fig. 2.5B), while a 30 min application of increasing concentrations of extracellular S100A1 protein (0.01-10 μM; Fig. 2.5C) resulted in a dose-dependent en-

hancement of ERK1/2 phosphorylation. Concomitantly, the concentration of endocytosed S100A1 protein increased (Fig. 2.5, B and C). Inhibition of S100A1 endocytosis by 50 μM monodansylcadaverine effectively abrogated the S100A1-mediated increase in ERK1/2 phosphorylation (Fig. 2.6 A). Furthermore, S100A1-mediated activation of ERK 1/2 could be prevented by preincubation with PD98095 (2-10 μM) (Fig. 2.6B), a specific inhibitor of MEK1 (26,27).

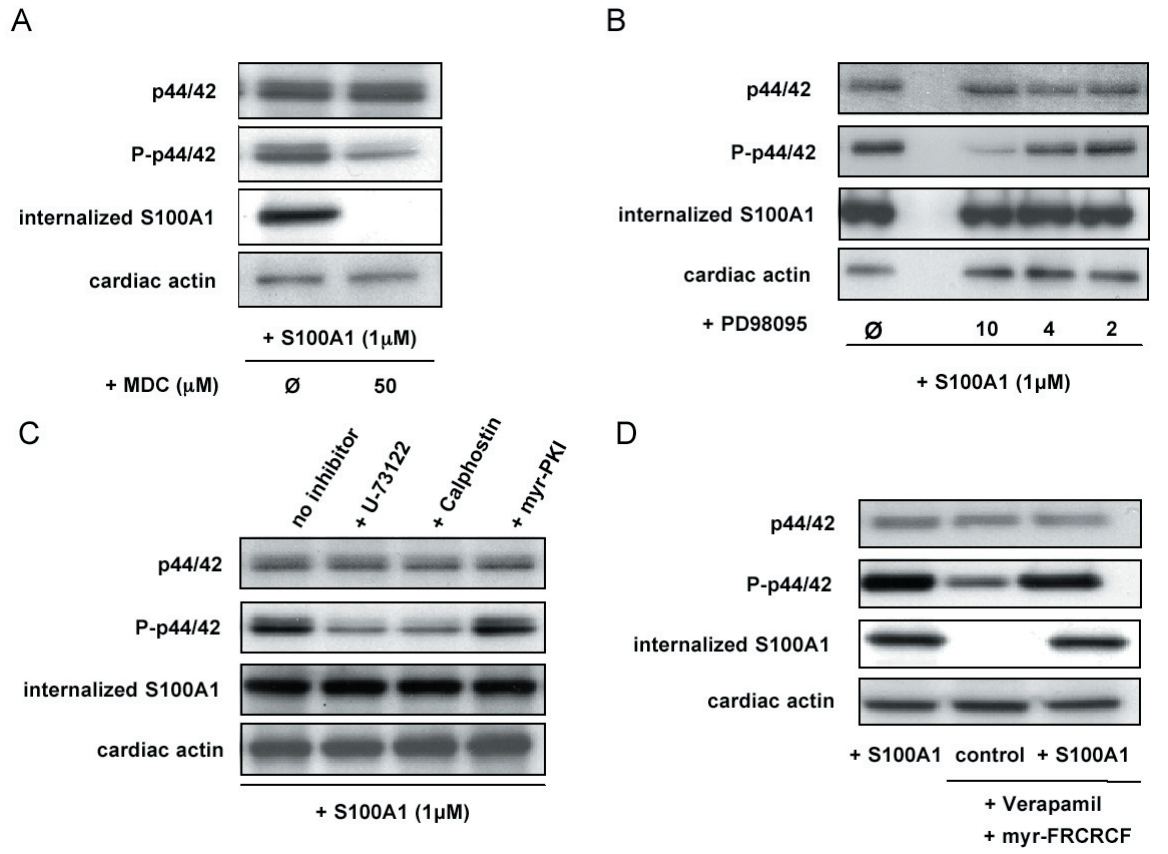

Figure 2.6: Effects of S100A1 on the signaling pathway upstream of ERK1/2. (A) Western blot of extracts from cells treated with S100A1 in the presence of 50 μM MDC, probed with specific antibodies, S100A1-uptake as well as S100A1-mediated increase of ERK1/2 phosphorylation is inhibited. (B) Addition of increasing amounts of MEK1 inhibitor PD98095 (2, 4, 10 μM) to S100A1-stimulated NVCM. Western blots of homogenates show that S100A1-uptake is not affected by PD98095, whereas the levels of phosphorylated ERK1/2 are reduced in a dose-dependent manner. (C) Effects of PLC, PKC and PKA inhibition on S100A1-mediated activation of ERK1/2 phosphorylation. In the presence of PLC inhibitor U-73122 levels of P-p44/42 are significantly reduced. A similar effect is observed by inhibition of PKC with calphostin-c. In contrast, inhibition of PKA by myr-PKI has no effect on the levels of P-p44/42. Probing the Western blot with an anti-S100A1 antibody shows that S100A1 endocytosis (internalized S100A1) is not influenced by the inhibitors of PLC, PKC and PKA. (D) Effects of transsarcolemmal Ca^{2+}-influx on ERK1/2 phosphorylation. Simultaneous inhibition of L-type Ca^{2+}-channel (5 μM verapamil) and NXC (10 μM myr-FRCRCF) leads to a reduction of P-p44/42 levels in untreated (control) cells and S100A1-treated cells by approximately 40%. Both S100A1-uptake (internalized S100A1) and S100A1-mediated activation of ERK1/2 are not significantly perturbed. Equal protein loading in individual lanes was confirmed by comparable levels of cardiac actin.

Since extracellular neurotrophic effects of S100A4 protein on rat hippocampal neurons depends on phospholipase C (PLC), which has also been linked to the endosomal compartment, we investigated the influence of PLC inhibition by U-73122 (5 μM) on S100A1-mediated ERK1/2 activation (13,25). As illustrated in Figure 2.6 C, it appears that inhibition of PLC completely prevented the S100A1-induced enhancement of ERK1/2 phosphorylation. Because receptor-mediated activation of PLC is known to subsequently enhance protein kinase C (PKC) activity, we next tested whether S100A1-mediated enhancement of ERK1/2 activity requires activation of PKC. Interestingly, in the presence of calphostin-c (0.5 μM), a potent inhibitor of PKC (13), S100A1-induced enhancement of ERK1/2 phosphorylation was abrogated (Fig. 2.6C). Since activation of cAMP-dependent protein kinase (PKA) has also been linked to ERK1/2 signaling, we likewise explored the effect of PKA inhibition on S100A1-dependent ERK1/2 activation by a cell permeable specific PKA inhibitor (28). However, preincubation of NVCM with myristolated PKA inhibitor 14-22 amide (myr-PKI, 5 μM) for 30 min, did not affect S100A1-mediated enhancement of ERK1/2 activity (Fig. 2.6C). This finding suggests that the modulation of the ERK1/2 signaling pathway by S100A1 does not involve PKA.

Transsarcolemmal Ca^{2+}-influx has been shown to be another modulator of ERK1/2 signaling (28). Because exogenous addition of S100A1 protein to immature cardiomyocytes has been shown to increase L-type Ca^{2+}-channel (dihydropyridine receptor, DHPR) activity and thus Ca^{2+}-influx (29), we explored the effect of extracellularly added S100A1 protein on ERK1/2 signaling in response to inhibition of transsarcolemmal Ca^{2+}-influx. For this purpose, DHPR was blocked with verapamil (5 μM) and the sodium-calcium exchanger (NCX) with a cell-permeable specific NCX inhibitor, myr-FRCRCF (10 μM), In both cases, the inhibitors slightly reduced the extent of ERK1/2 phosphorylation in control cells as well as in S100A1-treated cardiomyoctyes, but did not perturb the S100A1-uptake and S100A1-mediated activation of ERK1/2 phosphorylation (S100A1 vs. control +3.2±0.4-fold, n=3, $P<0.01$; S100A1 vs. control (verapamil/myrFRCRCF) +2.8±0.2-fold, n=3, $P<0.01$) (Fig. 2.6D).

Taken together, our results strongly support the notion that endocytosed S100A1 protein specifically increases ERK1/2 activity via the PLC-PKC-MEK1 pathway. In contrast, PKA

and transsarcolemmal Ca^{2+}-influx did not appear to be involved in S100A1-mediated activation of ERK1/2.

S100A1 inhibits NVCM apoptosis via ERK1/2 signaling

Previous studies which have demonstrated that ERK1/2 activation is associated with protection from apoptosis in cardiomyocytes (26,30-33), prompted us to examine whether S100A1-induced ERK1/2 signaling may exert cardioprotective effects on cardiomyocytes. To assess if S100A1 addition provides protection from apoptotic stimuli, NVCM were incubated in 2-deoxyglucose- containing (2-DOG) glucose-free medium for 18h as described previously (26) and in 2-DOG containing the MEK1 inhibitor PD98095. Figure 2.7 shows corresponding phase contrast images of NVCM cultured in standard medium in comparison to cells cultured in 2-DOG. Addition of S100A1 to NVCM cultured in standard medium did not significantly alter cell morphology (Fig. 2.7, A and B). Apoptosis is induced when NVCM were cultured in 2-DOG rather than standard medium (Fig. 2.7C) and cells display a rounded morphology. In the presence of S100A1 (Fig. 2.7D), the rounding up of 2-DOG was prevented and cell morphology is similar to that of untreated cells cultured in standard medium (Fig. 2.7A). The S100A1-induced protection from apoptosis abolished in the presence of the MEK1 inhibitor PD98095 (Fig. 2.7F).

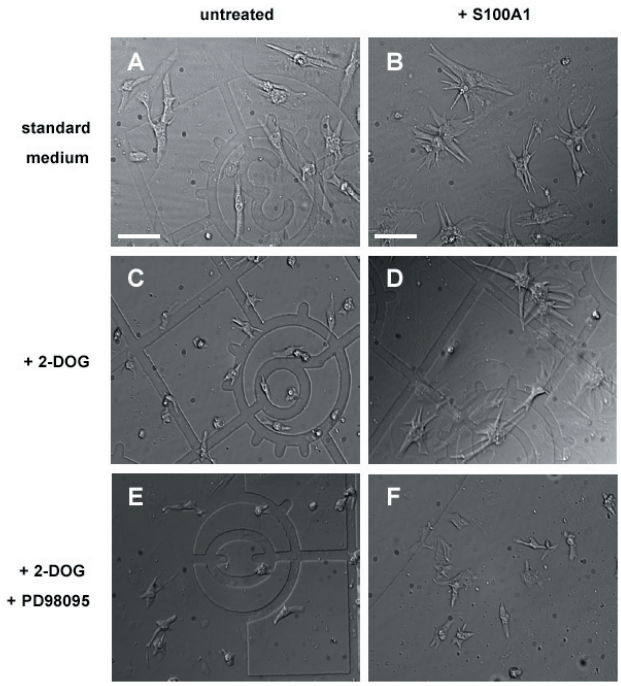

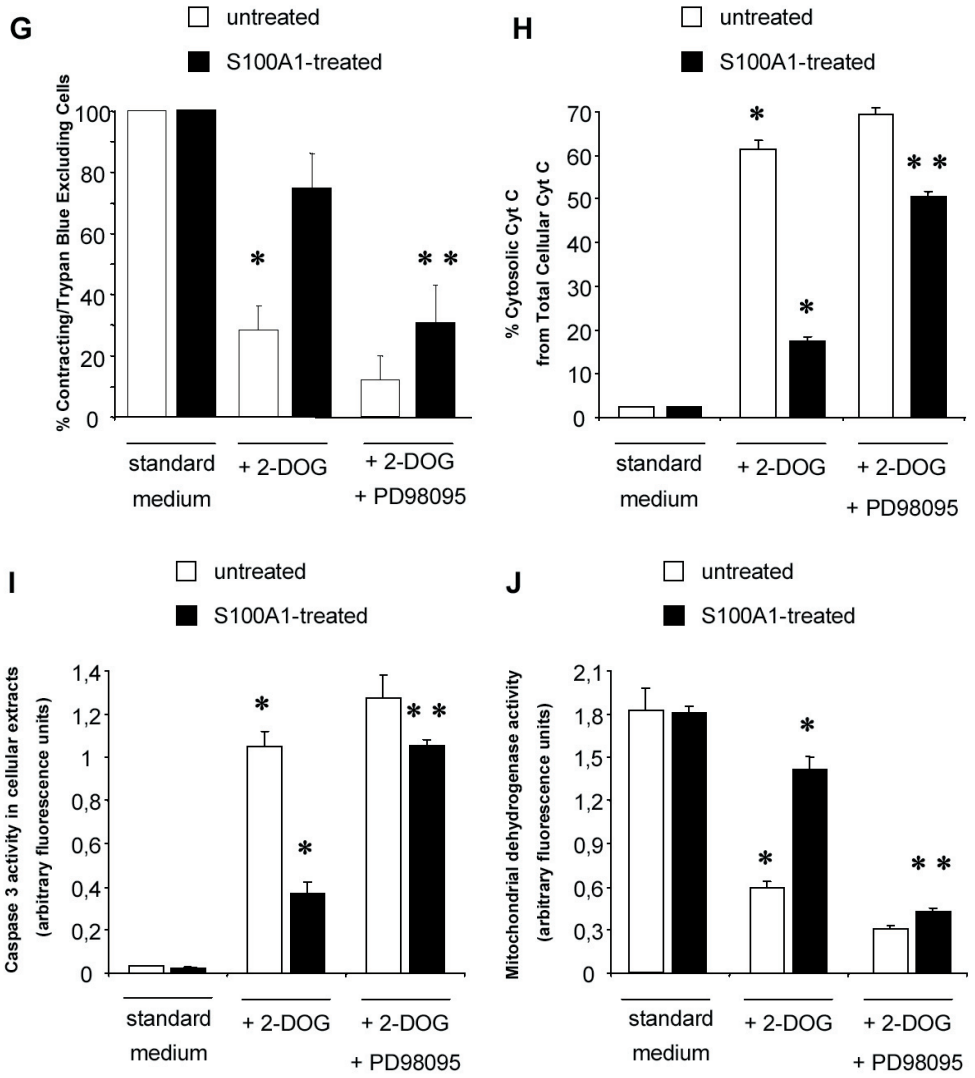

Figure 2.7: Antiapoptotic effect of S100A1 protein on NVCM. (A-F) Phase contrast images of NVCM under different culture conditions. (A) Untreated cells in standard culture medium (containing glucose) (control). (B) Addition of S100A1 (1 μM) to NVCM in standard medium does not significantly alter their morphology. (C) NVCM cultured for 18 h in medium containing the apoptosis inducing 2-deoxyglucose (2-DOG; 3 mM) without S100A1 display a rounded morphology. (D) If S100A1 is added to the cells, cells cultured in 2-DOG extend cellular processes and assume a morphology similar to that of control cells (A). (E) Untreated cells cultured as in (C) but in the presence of the MEK1 inhibitor PD98095 do not spread. (F) In the presence of PD98095, 2-DOG induced apoptosis is not overcome by S100A1 addition. Bar, 50 μm. (G) Anti-apoptotic effect of S100A1 involves the ERK1/2 pathway. Compared to control NVCM (standard medium, no S100A1; 100%), only 28 ± 3.6% of cells (n = 5) cultured in 2-DOG were viable and able to contract. When cells were treated with S100A1 (1 μM) the survival rate of 2-DOG-induced apoptotic cells is ~2-fold higher (79 ± 5.6%, * P<0.01) compared to control cells. Addition of 10 μM PD98095 abolishes the S100A1-induced rescue (30 ± 5.8% survival, n=5, ** P<0.01). (H) S100A1 treatment reduces apoptosis-related mitochondrial cytochrome c release by ~2.5-fold (S100A1 17±1.1% vs. untreated 61±2.3%, n=5, * P<0.01, data are expressed as % cytosolic cytochrome c from total cytochrome c (tcytc), tcytc was estimated at approximately 230 ng per 106 cells). This reduction is blocked by 10 μM PD98095 (S100A1-treated 17±1.1% vs. S100A1-treated/PD98095 50.4±2.1%, n=5, ** P<0.01). (I) Apoptosis-related caspase-3 activity is reduced ~1.8-fold by S100A1 treatment (S100A1-treated 0.37±0.08 vs. untreated 1.05±0.1, n=5, * P<0.01). The antiapoptotic effect of S100A1 treatment is effectively inhibited by 10 μM PD98095 (S100A1-treated 0.37±0.08 vs. S100A1-treated/PD98095 1.05±0.046, n=5, ** P<0.01). (J) In comparison to untreated NCVM, S100A1 treatment prevents the 2-DOG-mediated decrease in mitochondrial dehydrogenase activity (S100A1-treated 1.4±0.2 vs. untreated 0.6±0.1, n=5, * P<0.01). This anti-apoptotic effect is inhibited by 10 μM PD98095 (S100A1-treated 1.4±0.2 vs. S100A1-treated/PD98095 0.4±0.1, n=5, ** P<0.01).

Viability of NVCM was assessed by trypan-blue exclusion and electrical field stimulation (Fig. 2.7G). Addition of 1 μM S100A1 protein did not affect viability of cells under standard culture conditions (S100A1-treated 117±8, vs. untreated 119±8, each n=5 cell locates, P=n. s.). However, compared to untreated NVCM (100%), only ~30% of cells cultured in 2-DOG were viable and able to contract. When cells were treated with S100A1 (1 μM) the survival rate of 2-DOG-induced apoptotic cells was ~2-fold higher. Consistent with the morphological data, S100A1-mediated rescue from apoptosis was effectively abolished by the presence of the MEK1 inhibitor PD98095 (10 μM).

As additional indicators of apoptosis, mitochondrial cytochrome c release, caspase-3 and mitochondrial dehydrogenase activity were quantified under different culture conditions (Fig. 2.7, H-J). If S100A1 was added to cells cultured in 2-DOG medium, the cytochrome c release and caspase-3 activity was reduced by ~2.5-fold and ~1.8-fold, respectively (Fig. 2.7 H and I). Again, the S100A1-mediated protection from apoptosis was effectively prevented by addition of 10 μM PD98095. The presence of the inhibitor also blocked a nearly ~1.3-fold higher preservation of mitochondrial dehydrogenase activity in S100A1-treated cells compared to untreated NVCM (Fig. 2.7J). In line with these results the pretreatment of cultured cardiomyocytes with S100A1 similarly inhibited oxidative-stress-induced apoptosis by H_2O_2 (100μM) in our experimental setting (data not shown).

In summary, these results demonstrate that addition of S100A1 protein to cultured neonatal ventricular cardiomyocytes protects them via activation of ERK1/2 signaling from apoptotic stimuli.

2.5 Discussion

To date, the multigene family of Ca^{2+}-binding proteins of the EF-hand type known as S100 proteins has grown to 21 members that are differentially expressed in a large number of cell types. Individual S100 proteins are viewed as cell-specific proteins, which are implicated in the Ca^{2+}-dependent regulation of a variety of activities in the cell (3). Recent evidence indicates that S100 proteins, once secreted or released into the extracellular space, may also exert specific effects on their target cells. For instance, extracellular S100A8 and S100A9 secreted by a novel tubulin-dependent pathway have been ascribed important functions in the regulation of inflammatory processes (9). In addition, secreted S100B, S100A4 and S100A12 have been shown to exert a neurotrophic effect on neurons (11,13,14). In the case of S100B, the trophic effects on neurite outgrowth were accompanied by an increased expression of the anti-apoptotic protein Bcl-2 (11). Since S100A1 is also released into the extracellular space following ischemic myocardial injury (15), we undertook this study addressing the question whether extracellular S100A1 may exert protective effects on cardiac cells.

Our data for the first time provide evidence that extracellular addition of S100A1 protein can protect neonatal ventricular cardiomyocytes from apoptosis in vitro via specific activation of the ERK1/2 signaling pathway. By coupling human recombinant S100A1 protein with rhodamine we were able to trace the uptake of S100A1 into the cytosolic compartment of cultured NVCM. Indirect immunofluorescence staining and uptake experiments under different culture conditions revealed that S100A1 protein is internalized via a Ca^{2+}-dependent clathrin-mediated endocytotic pathway. Interestingly, our results suggest that the cell surface receptor for advanced glycosylated end products (RAGE), which has been reported to interact with S100B (11,20), does not seem to be involved in the endocytosis of S100A1 in NVCM. Therefore, another cell surface receptor is likely to be responsible for S100A1 uptake in NVCM. Recently, internalization of S100A1 protein into embryonic murine cardiomyocytes has been shown to be associated with a decrease in membrane capacitance (29). With regard to the current study, this decrease in membrane capacitance is likely to reflect endocytotic vesicles forming at the plasma membrane, which then pinch off as clathrin-coated vesicles and eventually fuse with the endosomal compartment.

A growing body of evidence indicates that several signaling proteins involved in receptor tyrosine kinase (RTK) and G-protein coupled receptor (GPCR) signal transduction, e.g., PLC, Ras, Raf, MEK1 and ERK1/2, are located in endosomes from where they transduce signals to the cytosol and nucleus (25). In hippocampal neurons, it has been shown that the extracellular addition of S100A4 protein activates the ERK1/2 signaling pathway (13). Correspondingly, our data obtained from western blots probed with antibodies that specifically recognize unphosphorylated or phosphorylated forms of ERK1/2, together with the western blot data obtained when known upstream constituents of the MAPK signaling pathway were inhibited (Fig. 2.8), demonstrate that internalized S100A1 protein specifically activates ERK1/2 in cardiomyocytes both in a time- and dose-dependent manner. Hereby, internalization of S100A1 protein represents an important prerequisite for the activation of ERK1/2 since prevention of S100A1 endocytosis, both in Ca^{2+}-free medium and in the presence of inhibitors of clathrin-mediated endocytosis, resulted in a lack of enhanced ERK1/2 phosphorylation. In contrast, kinases involved in other signaling pathways, such as p38 and SAPK/JNK (p54/46), are not affected.

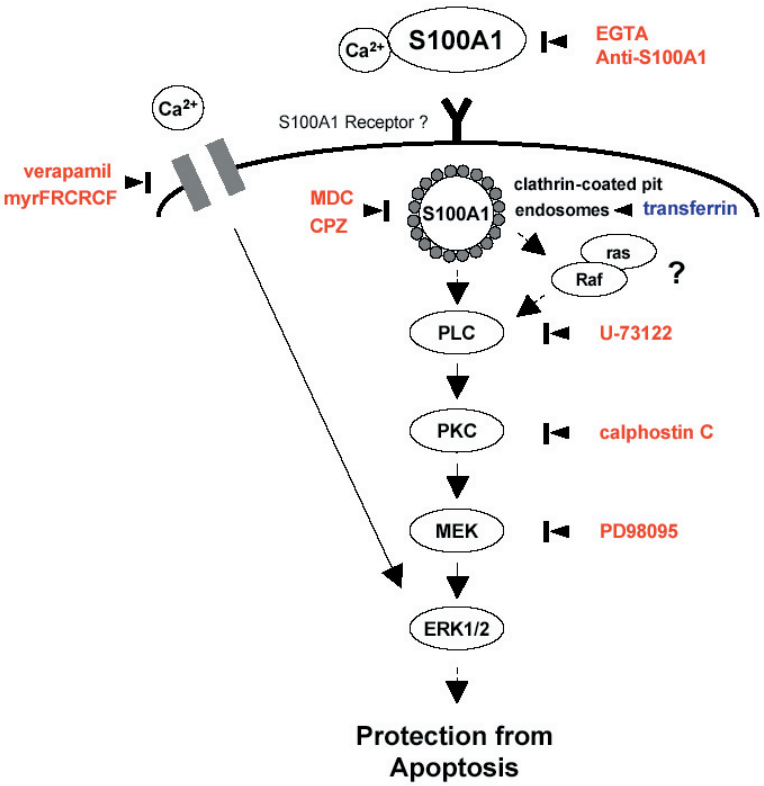

Figure 2.8: Model of S100A1 involvement in ERK1/2 signaling. The model suggests endocytosis of extracellular S100A1 by NVCM via an unknown receptor. Inhibitors of the S100A1-mediated pathway are shown in red while markers are given in blue. *PLC, phospholipase C; PKC, phosphokinase C; MEK1, MAPkinase kinase1; ERK1/2, extracellular signal-regulated kinase 1/2; MDC, monodansylcadaverine; CPZ, chlorpromazine.*

By using several specific inhibitors of intracellular signal transduction constituents (see Fig. 2.8), we could identify that S100A1-mediated activation of ERK1/2 signaling involves activation of PLC and PKC, which have been closely linked to the endosomal compartment (25). A stimulation of ERK1/2 activation by PKC has been previously reported (34). Based on our collective findings, we have developed a model of how S100A1 participates in the ERK1/2 signaling cascade (Figure 2.8). As depicted by the model, our data further provide evidence that sarcolemmal Ca^{2+}-influx mediated by the L-type channel does not participate in the S100A1-mediated enhancement of ERK1/2 phosphorylation. These findings are in contrast to work by Gomez and coworkers, which shows that glucagon-like peptide 1 (GPL-1)-mediated activation of ERK1/2 requires Ca^{2+}-influx through L-type channel in a mouse pancreatic β-cell line (28). Moreover, in their experimental system, inhibiting PKA activity diminished GPL-1-mediated ERK1/2 activation, whereas inhibition of PKA showed no significant effect on the S100A1-mediated ERK1/2 activation in NVCM. In addition, an unchanged phosphorylation state at serine16 in phospholamban in NVCM after addition of S100A1 revealed no evidence for enhanced PKA activity in our experimental setting (data not shown). From these differences we conclude that S100A1-mediated ERK1/2 activation follows a different signaling pathway than GPL-1. Taken together our results strongly support the notion that internalized S100A1 protein is routed to the endosomal compartment where it specifically activates the ERK1/2 signaling pathway.

Since an activation of the ERK1/2 signaling pathway by different means has been reported to protect cardiomyocytes from apoptosis (26,30,32,33,35), we evidently examined whether S100A1 treatment had a similar effect on the viability of neonatal cardiomyocytes in response to the apoptosis inducing agent 2-deoxyglucose. Indeed, our data show that S100A1 protein dramatically enhances the survival of cardiomyocytes in response to 2-DOG. S100A1-treated cells at the same time display a reduced release of mitochondrial cytochrome c, a diminished caspase-3 activity and maintain their mitochondrial dehydrogenase activity. In accordance, the pretreatment of cultured cardiomyocytes with S100A1 similarly inhibited oxidative-stress-induced apoptosis by H_2O_2 (100μM) in our experimental setting (data not shown) further corroborating the cytoprotective effect of S100A1 protein.

Consistent with the S100A1 signaling pathway outlined in Figure 2.8, these pro-survival parameters are effectively blocked if MEK1 is inhibited by PD98095. Taken together, the data of our study provide convincing evidence that the antiapoptotic effect of S100A1-uptake in vitro is brought about by enhanced ERK1/2 signaling. The results of the present study provide the basis for the working model shown in Figure 2.8, which illustrates the downstream signaling pathways involved in the antiapoptotic actions of extracellular S100A1 on cardiomyocytes. In conclusion, our study identifies extracellular S100A1 protein as a novel antiapoptotic factor that enhances survival of neonatal cardiomyocytes *in vitro* via activation of the PLC-PKC-MAP kinase kinase1-ERK1/2 pathway.

The mechanism by which a considerable amount of S100A1 is released into the extracellular space during ischemic myocardial injury is yet unknown. Since other S100 proteins are secreted either by a Ca^{2+}- or tubulin-dependent pathway, one might consider a similar mechanism for myocardial S100A1 release. Based on these considerations, we hypothesize that in vivo, S100A1 extrusion from myocardial cells under pathological conditions might promote the survival of the surrounding myocardium. Because S100A1 protein levels are reduced in heart failure (36) and S100A1 gene-deletion resulted in progressive deterioration of cardiac function *in vivo* (8), S100A1 protein deficiency may not only result in impaired contractility of the failing heart, but may also contribute to an enhanced susceptibility of injured or failing cardiomyocytes to apoptosis. Undoubtedly, elucidating the detailed molecular mechanism of myocardial S100A1 release is now imminent, as are studies that provide insight into the pathophysiological relevance of the cardioprotective effect of S100A1 protein on cardiac cells *in vivo*.

2.6 Acknowledgments

This work was supported in part by grants from the Forschungsförderungsprogramm Medizinische Fakultät der Universität Heidelberg 93/2002 and 61/2003 (to Patrick Most), Deutsche Forschungsgemeinschaft (1083/1-1 to Andrew Remppis), the M.E. Müller Foundation and the Kanton of Basel Stadt (to M. Boerries and C-A. Schoenenberger). Sven T. Pleger was supported by the Boehringer Ingelheim Stiftung.

2.7 Abbreviations

CPZ, chlorpromazine; CLSM, confocal images; 2-DOG, 2-deoxyglucose; DME, Dulbecco‘s modified Eagle‘s medium; EGTA, ethyleneglycol-bis (beta-aminoethylether)- N,N‘-tetraacetic acid; ERK1/2, extracellular signal-regulated kinase 1/2; FCS, fetal calf serum; GLP-1, glucagon-like peptide 1; kD, kilodalton(s); μm, micrometer(s); M, molar; MAPK, mitogen-activated protein kinase; MDC, monodansylcadaverin; min, minute; NVCM, neonatal ventricular cardiomyocytes; n, number in a study or group; PAGE, polyacrylamide gel electrophoresis; PBS, phosphate-buffered saline; PKA, protein kinase a; PKC, protein kinase C; PLC, phospholipase; RAGE, receptor for advanced glycosylated end products; SEM, standard error of the mean; t test, Student‘s t test.

2.8 References

1. Zimmer, D. B., Cornwall, E. H., Landar, A., and Song, W. (1995) Brain Res Bull 37, 417-429
2. Heizmann, C. W., and Cox, J. A. (1998) Biometals 11, 383-397.
3. Donato, R. (2003) Microsc Res Tech 60, 540-551.
4. Most, P., Bernotat, J., Ehlermann, P., Pleger, S. T., Reppel, M., Borries, M., Niroomand, F., Pieske, B., Janssen, P. M., Eschenhagen, T., Karczewski, P., Smith, G. L., Koch, W. J., Katus, H. A., and Remppis, A. (2001) Proc Natl Acad Sci U S A 98, 13889-13894.
5. Most, P., Remppis, A., Pleger, S. T., Löffler, E., Ehlermann, P., Bernotat, J., Kleuss, C., Heierhorst, J., Ruiz, P., Witt, H., Karczewski, P., Mao, L., Rockman, H. A., Duncan, S. J., Katus, H. A., and Koch, W. J. (2003) J Biol Chem. 278, 33809-33817
6. Most, P., Remppis, A., Weber, C., Bernotat, J., Ehlermann, P., Pleger, S. T., Kirsch, W., Weber, M., Uttenweiler, D., Smith, G. L., Katus, H. A., and Fink, R. H. (2003) J Biol Chem 278, 26356-26364
7. Remppis, A., Most, P., Löffler, E., Ehlermann, P., Bernotat, J., Pleger, S. T., Börries, M., Repper, M., Fischer, J., Koch, W. J., Smith, G. L., and Katus, H. A. (2002) Basic Res Cardiol 97, I/56-I/62

8. Du, X. J., Cole, T. J., Tenis, N., Gao, X. M., Kontgen, F., Kemp, B. E., and Heierhorst, J. (2002) Mol Cell Biol 22, 2821-2829.

9. Rammes, A., Roth, J., Goebeler, M., Klempt, M., Hartmann, M., and Sorg, C. (1997) J Biol Chem 272, 9496-9502

10. Davey, G. E., Murmann, P., and Heizmann, C. W. (2001) J Biol Chem 276, 30819-30826

11. Huttunen, H. J., Kuja-Panula, J., Sorci, G., Agneletti, A. L., Donato, R., and Rauvala, H. (2000) J Biol Chem 275, 40096-40105.

12. Alexanian, A. R., and Bamburg, J. R. (1999) Faseb J 13, 1611-1620.

13. Novitskaya, V., Grigorian, M., Kriajevska, M., Tarabykina, S., Bronstein, I., Berezin, V., Bock, E., and Lukanidin, E. (2000) J Biol Chem 275, 41278-41286.

14. Mikkelsen, S. E., Novitskaya, V., Kriajevska, M., Berezin, V., Bock, E., Norrild, B., and Lukanidin, E. (2001) J Neurochem 79, 767-776.

15. Kiewitz, R., Acklin, C., Minder, E., Huber, P. R., Schafer, B. W., and Heizmann, C. W. (2000) Biochem Biophys Res Commun 274, 865-871.

16. Convery, M. K., Levi, A. J., Khananshvili, D., and Hancox, J. C. (1998) Pflugers Arch 436, 581-590.

17. Hobai, I. A., Khananshvili, D., and Levi, A. J. (1997) Pflugers Arch 433, 455-463.

18. Pinson, A. (1990) In: Piper H.M. (ed.) Cell Culture Techniques in Heart and Vessel. Research Springer Verlag Berlin Heidelberg New York, 20-35

19. Bianchi, R., Garbuglia, M., Verzini, M., Giambanco, I., Ivanenkov, V. V., Dimlich, R. V., Jamieson, G. A., Jr., and Donato, R. (1996) Biochim Biophys Acta 1313, 258-267.

20. Hofmann, M. A., Drury, S., Fu, C., Qu, W., Taguchi, A., Lu, Y., Avila, C., Kambham, N., Bierhaus, A., Nawroth, P., Neurath, M. F., Slattery, T., Beach, D., McClary, J., Nagashima, M., Morser, J., Stern, D., and Schmidt, A. M. (1999) Cell 97, 889-901.

21. Conner, S. D., and Schmid, S. L. (2003) Nature 422, 37-44.

22. Rizzo, M. A., Shome, K., Watkins, S. C., and Romero, G. (2000) J Biol Chem 275,

23911-23918.

23. Pol, A., Calvo, M., and Enrich, C. (1998) FEBS Lett 441, 34-38.
24. Howe, C. L., Valletta, J. S., Rusnak, A. S., and Mobley, W. C. (2001) Neuron 32, 801-814.
25. Sorkin, A., and Von Zastrow, M. (2002) Nat Rev Mol Cell Biol 3, 600-614.
26. Bueno, O. F., De Windt, L. J., Tymitz, K. M., Witt, S. A., Kimball, T. R., Klevitsky, R., Hewett, T. E., Jones, S. P., Lefer, D. J., Peng, C. F., Kitsis, R. N., and Molkentin, J. D. (2000) Embo J 19, 6341-6350.
27. Davies, S. P., Reddy, H., Caivano, M., and Cohen, P. (2000) Biochem J 351, 95-105.
28. Gomez, E., Pritchard, C., and Herbert, T. P. (2002) J Biol Chem 277, 48146-48151.
29. Reppel, M., Remppis, A., Sasse, P., Roell, W., Most, P., Hescheler, J., Katus, H. A., and Fleischmann, B. K. (2002) European Heart Journal 23 [Supplement], 41, P363
30. Aikawa, R., Komuro, I., Yamazaki, T., Zou, Y., Kudoh, S., Tanaka, M., Shiojima, I., Hiroi, Y., and Yazaki, Y. (1997) J Clin Invest 100, 1813-1821.
31. De Windt, L. J., Lim, H. W., Haq, S., Force, T., and Molkentin, J. D. (2000) J Biol Chem 275, 13571-13579.
32. Mehrhof, F. B., Muller, F. U., Bergmann, M. W., Li, P., Wang, Y., Schmitz, W., Dietz, R., and von Harsdorf, R. (2001) Circulation 104, 2088-2094.
33. Parrizas, M., Saltiel, A. R., and LeRoith, D. (1997) J Biol Chem 272, 154-161.
34. Braz, J. C., Bueno, O. F., De Windt, L. J., and Molkentin, J. D. (2002) J Cell Biol 156, 905-919
35. Sheng, Z., Knowlton, K., Chen, J., Hoshijima, M., Brown, J. H., and Chien, K. R. (1997) J Biol Chem 272, 5783-5791.
36. Remppis, A., Greten, T., Schafer, B. W., Hunziker, P., Erne, P., Katus, H. A., and Heizmann, C. W. (1996) Biochim Biophys Acta 1313, 253-257.

Chapter 3

Cardiac adenoviral S100A1 gene delivery rescues failing myocardium

Patrick Most*, Sven T. Pleger*, Mirko Völkers*, Beatrix Heidt, Melanie Boerries,Dieter Weichenhan, Eva Löffler, Paul M.L. Janssen, Andrea D. Eckhart, Jeffrey Martini, Matthew L. Williams, Roger J. Hajjar Hugo A. Katus, Andrew Remppis, Walter J. Koch

* Authors contributed equally to this study

3.1 Abstract

Cardiac-restricted overexpression of the Ca^{2+}-binding protein S100A1 has been shown to lead to increased myocardial contractile performance *in vitro* and *in vivo*. Since decreased cardiac expression of S100A1 is a characteristic of heart failure, we tested the hypothesis that S100A1 gene transfer could restore contractile function of failing myocardium. Adenoviral S100A1 gene delivery normalized S100A1 protein expression in a post-infarction rat heart failure model and reversed contractile dysfunction of failing myocardium *in vivo* and *in vitro*. S100A1 gene transfer to failing cardiomyocytes restored diminished intracellular Ca^{2+}-transients and sarcoplasmic reticulum (SR) Ca^{2+}-load mechanistically due to increased SR Ca^{2+}-uptake and reduced SR Ca^{2+}-leak. Moreover, S100A1 gene transfer decreased elevated intracellular Na^{+}-concentrations to levels seen in non-failing cardiomyocytes, reversed reactivated fetal gene expression and restored energy supply in failing cardiomyocytes. Intracoronary adenoviral-mediated S100A1 gene delivery *in vivo* to the post-infarcted failing rat heart normalized myocardial contractile function and Ca^{2+}-handling providing physiologic significance to results found in myocytes. Thus, the present study demonstrates that restoration of S100A1 protein levels in failing myocardium by gene transfer may be a novel therapeutic strategy for the treatment of heart failure.

3.2 Introduction

Heart failure (HF) remains a leading cause of mortality in the developed world (1) and this, in part, reflects a lack of therapies targeted to the underlying molecular defects that lead to chronic ventricular dysfunction. Although other systems contribute, there is substantial evidence for abnormal intracellular Ca^{2+}-handling being a key component of the impaired contractile performance of the failing heart (2). This defect has been linked to abnormal levels of Ca^{2+}-sensor and regulatory proteins in failing myocardium (3) and restoring diminished key protein levels may therefore represent a strategy to reverse the defect. In this regard, S100A1, a low-molecular weight (Mr 10,000) Ca^{2+}-binding protein is especially interesting with respect to cardiovascular disease. S100A1, a member of the multigenic S100 family, is the most abundant S100 protein isoform in the heart (4) and has been found to be down-regulated in human and animal models of heart failure (5, 6). Importantly, S100A1 has previously been identified as a novel positive inotropic regulator of heart function based on the observation that cardiac-restricted S100A1 overexpression enhances Ca^{2+}-cycling and cardiac contractile performance *in vitro* and *in vivo* (7-10). These effects were mainly due to improved cardiac sarcoplasmic reticulum (SR) Ca^{2+}-handling and a recent study also provided evidence that S100A1 can improve SR Ca^{2+}-fluxes and contractile force in skeletal muscle (11).

In contrast to conventional positive inotropic agents, S100A1-mediated chronic cardiac inotropic actions in normal myocardium were independent of β-adrenergic signaling with no alteration of heart rate or signs of myocardial hypertrophy or fibrosis (8). In support of these results, S100A1-deficient hearts display severe inotropic and lusitropic defects shown both by impaired contractile reserve and rapid progressive deterioration of contractile function in response to acute and chronic hemodynamic stress, respectively (12). Thus, the loss of S100A1 protein in human heart failure may indeed contribute to the Ca^{2+}-dysregulation and deterioration of contractile strength. Interestingly, S100A1 has most recently been shown to inhibit programmed cell death of ventricular cardiomyocytes (13), a process that can significantly contribute to the development and progression of HF.

Most of the data to date showing positive myocardial functional effects with S100A1

overexpression has either been seen in a transgenic mouse model or adenoviral-mediated gene delivery to cultured ventricular cardiomyocytes or engineered heart tissue from non-failing hearts and not in the context of HF. Therefore, it is not known whether restoration of S100A1 protein expression in the failing heart *in vivo* may improve contractile performance and prove to be therapeutic. In this study, we tested this hypothesis using adenoviral-mediated myocardial S100A1 gene delivery to an experimental rat HF model. Our translational approach demonstrates that S100A1 gene transfer can normalize S100A1 protein levels and restore contractile function of failing myocardium *in vitro* and *in vivo* primarily through a normalization and restoration of myocyte Ca^{2+}-homeostasis.

3.3 Methods

Generation of S100A1 adenovirus

To construct the adenovirus containing both the human S100A1 and GFP cDNA (AdS100A1), we used the method described by He et al. (21). An adenovirus containing GFP only (AdGFP) served as a control. The titers of stocks used for these studies measured by plaque assays were $2x10^{11}$ plaque forming units/ml (pfu/ml) for AdS100A1 and 3¥1011 pfu/ml for AdGFP. Aliquots were stored at –80°C.

Experimental rat HF model

All animal procedures and experiments were peformed in accordance with corresponding institutional guidelines. 10-12 weeks old Sprague-Dawley rats of either sex (n=30) were sedated with pentobarbital (65mg/kg IP), intubated and further anesthetized with isoflurane (2% v/v) during mechanical ventilation. Hearts were exposed by median sternotomy, fixed by an apical suture, and a liquid-nitrogen cooled cryoprobe with a diameter of 7 mm was applied for three freeze-thaw cycles on the free LV anterior wall. The chest was then closed and animals were transferred back to their cages receiving appropiate analgesia. Four animals in the cryoinfarction group died during surgery. Sham-operated control animals (n=9) underwent a similar procedure except application of the cryoprobe. Hearts of six cryoin-

farcted animals were sectioned transaxially and size of the infarcted LV area was estimated to 32±3% by triphenyltetrazolium chloride (TTC) staining (Figure 1A) (22). There were no differences in infarct size between any subsequent groups (data not shown).

Cardiac catheterization and *in vivo* intracoronary myocardial adenovirus delivery

12 weeks after surgery closed-chest cardiac catheterization was performed both in anesthetized (Xylazine 5mg/kg BW, Ketamine 100mg/kg BW) sham-operated and cryoinfarcted animals as described (8). A 2.5 F Millar catheter was inserted into the left main carotid artery and advanced into the LV. *In vivo* basal and isoproterenol-stimulated hemodynamic analysis (Bemon32/Amon32 Version 3.2.) included heart rate (beats/min), maximal (LVdP/dtmax) and minimal (LVdP/dtmin) first derivate of LV pressure, LV end-diastolic pressure (LVEDP) and maximal LV systolic ejection pressure (LVESP). Isoproterenol (6μg/kg/min) was administered via the jugular vein and data were aquired when functional parameters reached a stable plateau. Afterwards, *in vivo* cardiac gene delivery was performed as previously described by the Hajjar group (15, 23). Animals were divided in three groups either receiving 200 μl AdS100A1 ($1x10^{10}$ pfu; n=8) or AdGFP ($1x10^{10}$ pfu; n=8) in solution via a 22-G catheter advanced from the apex of the LV to the aortic root. The third failing group (n=8) received saline injection only. The aorta and the main pulmonary artery were clamped distal to the site of the catheter and the solution injected. The clamp was maintained for 10 sec when the heart pumped against a closed isovolumic system allowing the adenovirus to circulate down the coronary arteries and perfuse the heart. In each group one animal died during this procedure. After removal of air and blood, the chest was closed, and animals were extubated and transferred back to their cages. Seven days after gene transfer, *in vivo* cardiac function was reevaluated as described above via the right main carotid artery. After cardiac catheterization, same animals were used for isolation of ventricular cardiomyocytes. Transfection efficieny was monitored by GFP fluorescence (510 nm) in cryosectioned hearts (20 μm sections, 40-fold magnification). To confirm specificity of the GFP emission both the same offset for suppressed background of non-transfected hearts excited at 488 nm was applied to adenovirally transfected hearts (Figure 3.5A-F) and additional measurements

were taken below and above the GFP excitation spectrum (data not shown).

Cardiomyocyte isolation and i*n vitro* gene transfer

Adult LV cardiomyocytes were obtained using a collagenase digestion method as described in detail elsewhere (9). Adenoviral transfection (5 pfu/cell) of isolated ventricular cardiomyocytes from saline-treated failing hearts (n=4) was carried out in HEPES-modified medium 199 (M199) and cells were maintained in M199 for 24 hours at 37°C, 95%O2/5%CO2. Cardiomyocytes used for contractility, Ca^{2+} and Na^{+} measurements were plated with a density of 30.000 cells/cm2 on laminin-coated glass dishes. For analysis of mRNA and protein expression and energetic metabolites, cardiomyocytes were plated with a density of 150.000 and 300.000 cells/cm2, respectively.

Indirect Immunofluorescence

Imaging of adenoviral treated ventricular cardiomyocytes was carried out as described previously with minor modifications (13). Briefly, adenoviral transfection (5 pfu/cell) of isolated cells was carried out on coated glass coverslips. After 24 hrs cells were fixed, permeabilized and labeled with anti-S100A1 (SA 5632, Eurogentec; 1/300), anti-SERCA2 (Alexis; 1/500) or anti-RyR2 (Alexis; 1/500) antibodies, followed by the corresponding Cy3-conjugated (Jackson Immuno Research Lab; 1/3000) and Cy5-conjugated (Jackson Immuno Research Lab; 1/400) secondary antibodies. Confocal images were obtained using a 40x objective on a Leica TCS SP laser scanning confocal microscope. Digitized confocal images were processed by Leica software and Adobe Photoshop.

Cardiomyocyte contractility

Contractile properties of isolated ventricular cardiomyocytes were obtained by video-edge-detection as described previously (7). Analysis of *in vivo* and *in vitro* transfected cardiomyocytes was carried out immediately after isolation and 24 hrs following adenoviral gene transfer, respectively. Analysis of steady state twitches at 2 Hz field stimulation, 37°C and 2 mM extracellular Ca^{2+}-concentration ($[Ca^{2+}]_e$) was performed by custom designed software

written in LabView (version 5.0, National Instruments).

Intracellular Ca^{2+}-transients and SR Ca^{2+}-load

Calibration and assessment of intracellular Ca^{2+}-transients and SR Ca^{2+}-load in field-stimulated ventricular cardiomyocytes was performed as described in details elsewhere (8). Assessment of Ca^{2+}-handling properties in isolated, FURA-2AM loaded *in vivo* and *in vitro*-transfected cardiomyocytes was carried out immediately after isolation and 24 hrs following adenoviral gene delivery, respectively. Steady state transients at 2 Hz field stimulation, 37°C and 2 mM $[Ca^{2+}]_e$ were analyzed by T.I.L.L Vision software (version 4.01). To avoid interference with FURA-2 and GFP emission, FURA-2 emision was assessed both in non-transfected and GFP-transfected cells and GFP emission interference (+5%) was subtracted prior to calibration.

COS-1 cell culture and adenoviral transfection

COS-1 cells were maintained in DMEM supplemented with 10% FCS, penicillin/streptomycin (100 units/ml) and glutamine (2 mM) at 37°C in a 95% air/5% CO2 humidified atmosphere and grown to 80% confluency. Infections of cultured cells with recombinant adenovirus were performed with a multiplicity of 100 viral particles per cell in serum free medium for 6 hours. Cells were either co-infected with S100A1 and SERCA2a adenovirus or each virus alone. Cells were further grown in supplemented DMEM for 48 hours and harvested for preparation of microsomal fractions and western blot analysis in ice-cold PBS (pH 7.4) supplemented with protease inhibitors (1tablet/5 ml) (Roche Applied Science; Mini Complete EDTA free protease inhibitors).

Ca^{2+}-ATPase measurements

Cardiac SR vesicles and microsomal fractions from *in vitro* adenoviral treated failing cardiomyocytes and COS cells, respectively, were prepared by density-gradient centrifugation as previously described (n=3 different preparations) (8, 24). COS microsomal fractions were prepared in the presence of $CaCl_2$ (1 mM) to prevent depletion of overexpressed S100A1

protein. SR Ca^{2+}-ATPase activity was assessed by the use of a pyruvate/NADH coupled enzymatic reaction (19).

SR Ca^{2+}-leak assay

Ca^{2+}-leak from SR vesicles derived from *in vivo* adenoviral treated and control hearts (n=3 in each group) was assessed by the use of the Ca^{2+}-indicator Fluo-3 as described previously (25). S100A1 recombinant human protein and S100A1 peptides (N-terminal; N: amino acid 2-16; hinge region; H: amino acid 42-54; C-terminal; C: amino acids 75-94) were obtained as described elsewhere (11).

[^{3}H]-Ryanodine binding

[^{3}H]-Ryanodine binding experiments were performed from terminal SR vesicle preparations prepared from rat left ventricular myocardium as described (8, 26). Briefly, membranes were incubated at 37°C with 6 nM [^{3}H]ryanodine (Perkin Elmer) in 300 μl of 20 mM PIPES, pH 7.1, 150 mM KCl, 0.5 mM $MgCl_2$, 15 mM NaCl, EGTA 3 mM, 10 mM caffeine, 1% phosphatase inhibitors (Sigma; inhibitor mix I/II), protease inhibitors (1tablet/5 ml) (Roche Applied Science; Mini Complete EDTA free protease inhibitors) and the indicated free Ca^{2+}-concentrations either in the presence or absence of 1 μM human recombinant S100A1 protein. Nonspecific binding was determined using 1000-fold excess of unlabeled ryanodine. After 60 min, aliquots of the samples were diluted in 10 volumes of ice-cold water and placed on Whatman GF/B filters preincubated with 2% polyethyleneimine in water. Filters were washed three times with 5 ml of ice-cold 20 mM PIPES, pH 7.1, 150 mM KCl, 15 mM NaCl. Radioactivity remaining on the filters was determined by liquid scintillation counting to obtain bound [^{3}H]ryanodine.

Western Blotting

Western blots to assess protein levels of S100A1 protein (Sigma, S-2407), SERCA2 (Biomol SA209-0100), NCX (ABR MA3-926), CSQ (calbiochem 208915), cardiac actin (Progen Ac1-20.4.2), PLB (upstate 05-205), Ser16-PLB (upstate 07-052) and GFP (clontech, #837

1-1) were done with samples of *in vitro* (n=3) or *in vivo* (n=7) adenovirally treated myocardium as wells as transfected COS cells (n=3) as described elsewhere (8). S100A1 protein (Mr 10000) from cellular extracts was enriched by sequential size exlusion centrifugation columns (Amicon; Microcon YM-50 and -3).

Co-immunoprecipitations

Co-immunoprecipitation for S100A1 with SERCA2 and RyR2 was investigated in crude membrane preparations from *in vitro* adenoviral-treated failing cardiomyocytes as described previously (8, 27). Interaction of S100A1 with SERCA2 was also tested in cell lysates from adenovirally transfected COS cells. To exclude unspecific binding anti-S100A1 (SA 5632) preincubated with the blocking peptide (hinge, S100A1 amino acids 42-54) was used as a control. Samples were processed by western blot as described above with minor modifications. Co-immunprecipitated samples for S100A1-SERCA2 and S100A1-RyR2 were stained with an anti-S100A1 (SA 5632, custom-made by Eurogentec), anti-SERCA2 (Biomol, SA209-0100) and anti-RyR2 (ABR, MA-3-925) antibody, followed by a corresponding pair of Alexa-Fluor 680 (Molular Probes) and IRDye 800CW (Rockland) coupled secondary antibodes, respectively. Proteins were visualized with an LICOR infrared imager (Odyssey) and pictures were processed by Odyssey v1.2 infrared imaging software.

RNA Isolation, Reverse Transcription and Quantitative Real-Time PCR

Total RNA isolation, reverse transcription and real-time RT-PCR was carried out for rat atrial natriuretic factor (ANF; forward primer 5'-CCCGACCCAGCATGG-3', reverse primer 5'-CAACTGCTTTCTGAAAGGGGTG-3'; annealing temperature 60°C), NCX (forward primer 5'-GCTCATATTACTGTAAGAAAGGGGTG-3', reverse primer 5'-GGCGGCGCTTCCCA-CAATGG-3'; annealing temperature 61°C), a-sk-actin (forward primer 5'-CAGCTCTGGCTCCCAGCACC-3', reverse primer 5'-AATGGCTGGCTTTAATGCTTCA-3'; annealing temperature 60°C) from *in vitro* (n=3) and *in vivo* (n=7) adenoviral treated failing cardiomyocytes by the use of an ABI Prism 7000 Sequence Detection System and the Platinum" SYBR" Green qPCR SuperMix-UDG (Invitrogen) as described elsewhere

(10). 18s rRNA signals were used for normalization (forward primer 5'-TCAAGAACG-AAAGTCGGAGG-3', reverse primer 5'-GGACATCTAAGGGCATCAC-3'; annealing temperature 60°C). After amplification, a melting curve acquired by heating the product to 95°C, cooling to and maintaining at 55°C for 20 sec, then slowly (0.5°C/sec) heating to 95°C was used to determine the specificity of PCR products, which were then confirmed by gel electrophoresis.

Measurement of intracellular Na^+-concentrations

Calibration and assessment of intracellular Na^+-concentration ($[Na^+]_i$) of cardiomyocytes (n=3 different preparations) was accomplished 24 hrs following adenoviral delivery by the use of the Na^+-fluorescent dye SBFI-AM as previously described (28). Analysis of $[Na^+]_i$ was performed at rest and 2 Hz at 37°C and 2 mM $[Ca^{2+}]_e$ with T.I.L.L Vision software (version 4.01).

Assessment of high energetic phosphates

Phosphocreatine (PCr) and adenosine triphosphate (ATP) levels were measured in cellular homogenates 24 hrs after adenoviral treatment (n=3 different preparations) as described previously (29).

Statistics

Data are generally expressed as mean±SEM. An unpaired two-tail student's t-test and two-way repeated measures ANOVA were performed for statistical comparisons. For all tests, a P value of <0.05 was considered as significant.

3.4 Results

Characterization of experimental heart failure model

12 weeks after surgery, cryoinfarcted animals (n=24) (Figure 3.1A) developed post-infarction HF shown by marked LV enlargement (Figure 3.1B) and depressed in vivo basal and β-adrenergic stimulated cardiac function compared with sham-operated control animals (sham-OP, n=9) (Table 3.1).

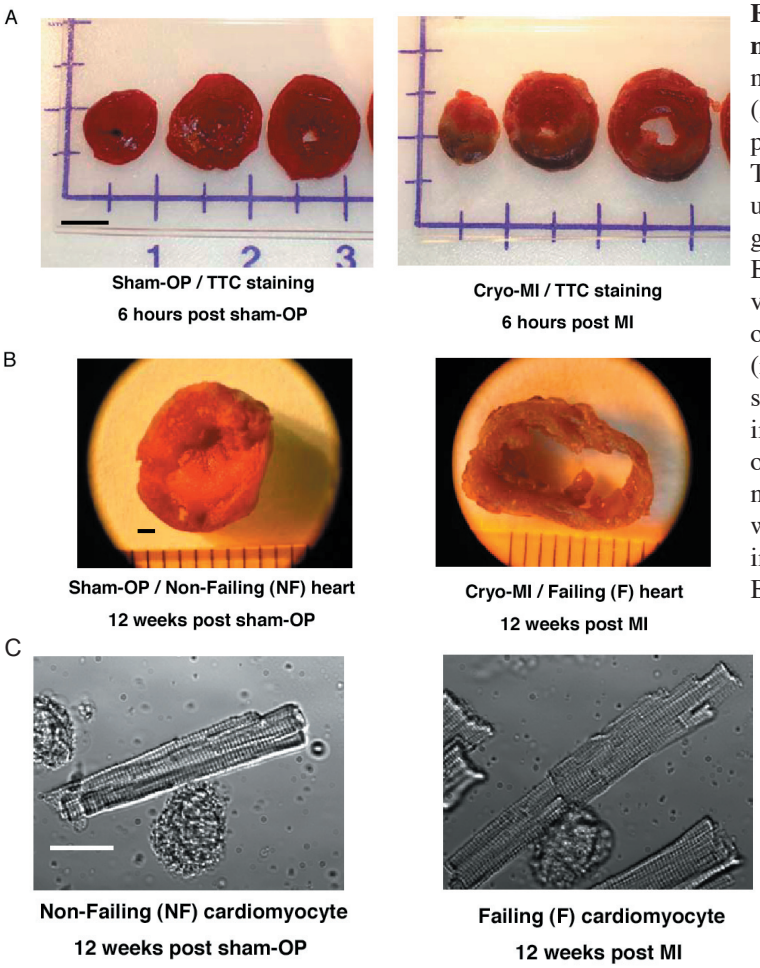

Figure 3.1: Post-infarct heart failure model. (A) Representative TTC-stained cross-sections of a sham-operated (left panel) and a cryoinfarcted (right panel) rat heart 6 hrs after surgery. Transmural cryoinfarcted myocardium emerges as brown tissue with a grey-white border zone (right panel). Bar, 5mm. (B) Representative mid-ventricular cross-sections of a sham-operated (left panel) and cryoinfarcted (right panel) rat heart 12 weeks after surgery. Bar, 1mm. (C) Representative images of a freshly isolated LV cardiomyocyte from a non-failing (left panel) and failing heart (right panel) 12 weeks after surgery. Note the marked increase in end-diastolic length in F. Bar, 25μm.

Similarly, isolated LV cardiomyocytes from cryoinfarcted hearts displayed evidence of HF with significant depression of contractility and Ca^{2+}-cycling (Table 3.2) as well as a marked increase in end-diastolic cell length (EDL) (31%) (Figure 3.1C) compared with non-failing cardiomyocytes obtained from sham-operated rats. Quantitative RT-PCR analysis indicated a significant increase in mRNA levels for ANF (42-fold), NCX (2.7-fold) and α-sk-actin (10-fold) in failing cardiomyocytes (Figure 3.2A).

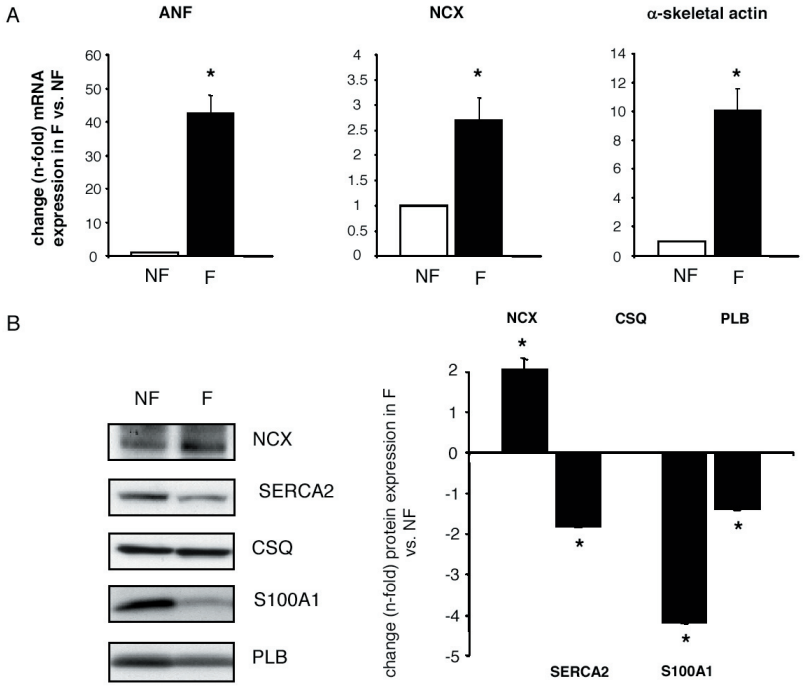

Figure 3.2. Reactivated fetal gene expression and abnormal abundance of Ca^{2+}-regulatory proteins in failing myocardium. (A) Reactivated fetal gene expression (ANF, NCX and α-sk-actin) in failing rat cardiomyocytes (F) versus non-failing sham-operated hearts (NF). (n=6; * P<0.01 F vs. NF). Results were obtained from 5 different hearts in each group 12 weeks after surgery. (B) Abnormal protein expression in failing cryoinfarcted rat hearts. (Left) Representative results of Western blots for NCX, SERCA2, CSQ, S100A1 and PLB from pooled fractions of failing (F) cryoinfarcted rat hearts (F; n=5) and non-failing (NF; n=5) sham-operated control hearts 12 weeks after surgery. (Right) Average change (n-fold) in protein expression in failing (F) cryoinfarcted hearts relative to the sham-operated group (NF). (n=7; * P<0.01 F vs. NF). Data are given as mean±SEM.

Table 3.1 In vivo hemodynamic and biometric parameters of postinfarction rat heart failure model

	Sham-OP / Nonfailing (n = 9)	Failing (n = 24)	% Change vs. sham-OP	P^A
Hemodynamics				
Basal				
HR (min^{-1})	272 ± 09	255 ± 06	–7 %	0.2
LV+dP/dt (mmHg/s)	6777 ± 209	5537 ± 280	–19%	<0.01
LV–dP/dt (mmHg/s)	5887 ± 282	4184 ± 223	–29%	<0.01
LVEDP (mmHg)	8.51 ± 0.53	12.53 ± 0.76	+47%	<0.01
LVESP (mmHg)	100.6 ± 2.2	86.7 ± 2.7	–23%	<0.01
Isoproterenol (6 μg/kg body wt/min)				
HR (min^{-1})	373 ± 14	339 ± 09	–10%	0.5
LV+dP/dt (mmHg/s)	15162 ± 740	9537 ± 639	–38%	<0.01
LV–dP/dt (mmHg/s)	10427 ± 570	5537 ± 280	–47%	<0.01
LVEDP (mmHg)	12.45 ± 1.83	16.81 ± 1.78	+35%	<0.01
LVESP (mmHg)	155.6 ± 5.9	115.6 ± 2.5	–26%	<0.01
Phenotype				
HW (g)	1.03 ± 0.07	1.58 ± 0.7	+53%	<0.01
HW/body wt (mg/g)	3.03 ± 0.16	5.48 ± 0.3	+80%	<0.01

Data were obtained 12 weeks after surgery in anesthetized animals and are presented as mean ± SEM. HR, heart rate; SEP, systolic ejection pressure; HW, heart weight.
[A]Compared by Student's *t* test or ANOVA.

Table 3.2 Contractile and Ca^{2+}-handling properties of NFCs and ventricular FCs

	NFCs	FCs	% Change, FCs vs. NFCs	P^A
Contractile properties	(n = 30)	(n = 33)		
Basal				
Fractional shortening (%)	10.76 ± 0.5	5.80 ± 0.37	−46%	<0.01
−d*l*/d*t* (μm/s)	8.27 ± 0.50	4.09 ± 0.26	−51%	<0.01
+d*l*/d*t* (μm/s)	7.52 ± 0.50	2.91 ± 0.34	−61%	<0.01
EDL (μm)	100.6 ± 2.9	131.0 ± 2.7	+31%	<0.01
Diameter (μm)	24.9 ± 0.74	27.4 ± 0.96	+10%	0.07
Isoproterenol (10^{-6} M)				
Fractional shortening (%)	19.78 ± 1.61	7.67 ± 0.93	−60%	<0.01
−d*l*/d*t* (μm/s)	18.20 ± 1.31	5.52 ± 0.97	−69%	<0.01
+d*l*/d*t* (μm/s)	16.47 ± 1.92	5.05 ± 1.20	−61%	<0.01
% Change in FS% vs. basal	+112%	+32%	−71%	<0.01
Ca^{2+} handling properties	(n = 100)	(n = 94)		
Basal				
Ca^{2+}-transient amplitude (nM)	326 ± 15	231 ± 18	−30%	<0.01
Diastolic Ca^{2+} (nM)	208 ± 10	322 ± 12	+54%	<0.01
Isoproterenol (10^{-6} M)				
Ca^{2+}-transient amplitude (nM)	605 ± 22	346 ± 33	−42%	<0.01
% Change in amplitude vs. basal	+85%	+49%	−42%	<0.01

Data were obtained from freshly isolated cardiomyocytes 12 weeks after surgery and are presented as mean ± SEM. Cells were obtained from 4 different preparation in each group. EDL, end diastolic length; [A]Compared by Student's *t* test or ANOVA.

Moreover, failing cardiomyocytes exhibited a significant decrease in protein levels for S100A1 (4.1-fold), SERCA2 (1.9-fold) and PLB (1.2-fold) compared with non-failing cardiomyocytes (Figure 3.2B). NCX protein in failing cardiomyocytes was up-regulated (2-fold) while CSQ was unchanged compared with non-failing cells (Figure 3.2B). These results show that chronic cryoinfarcted rat hearts have the typical biochemical and functional alterations of failing myocardium.

S100A1 gene transfer restores S100A1 protein levels in failing ventricular cardiomyocytes *in vitro*

To assess the impact of cardiac S100A1 gene transfer on failing ventricular cardiomyocytes in vitro, we treated adult cardiomyocytes isolated from post-infarcted failing rat hearts with a S100A1 adenovirus (AdS100A1). Incubation of failing cardiomyocytes either with AdS100A1 (MOI 5 pfu/cell) or AdGFP (MOI 5 pfu/cell) resulted in a nearly 100% infection rate in both groups as indicated by the expression of the GFP reporter (Figure 3.3A). Analysis of S100A1 protein expression 24 hrs following gene transfer revealed restoration of S100A1 protein in failing cardiomyocytes (F) to levels observed in non-failing cardiomyocytes (NF) (F; 0.9±0.3, NF; 4.2±0.4, F-AdS100A1; 3.9±0.5, P=n.s. NF vs. F-AdS100A1, P<0.05 F-

AdS100A1 vs. F, n=4) (Figure 3.3B). Data are given as relative arbitrary units normalized to CSQ that did not change among the different groups nor did α-cardiac actin. In contrast, AdGFP-treated failing myocytes continued to have diminished expression of S100A1 (F-AdGFP; 0.8±0.3, Figure 3.3B). The increased S100A1 protein seen 24 hrs after AdS100A1 treatment did not change aberrant protein expression of SERCA2 (NF; 4.2±0.4, F; 2.1±0.3, F-AdGFP; 2.2±0.4, F-AdS100A1; 2.4±0.2, n=4), NCX (NF; 0.7±0.1, F; 1.4±0.2, F-AdGFP; 1.6±0.3, F-AdS100A1; 1.5±0.3, n=4) or PLB (NF; 1.1±0.1, F; 0.7±0.2, F-AdGFP; 0.6±0.1, F-AdS100A1; 0.6±0.2, n=4) compared with either AdGFP-treated or untreated failing cardiomyocytes (Figure 3.3B).

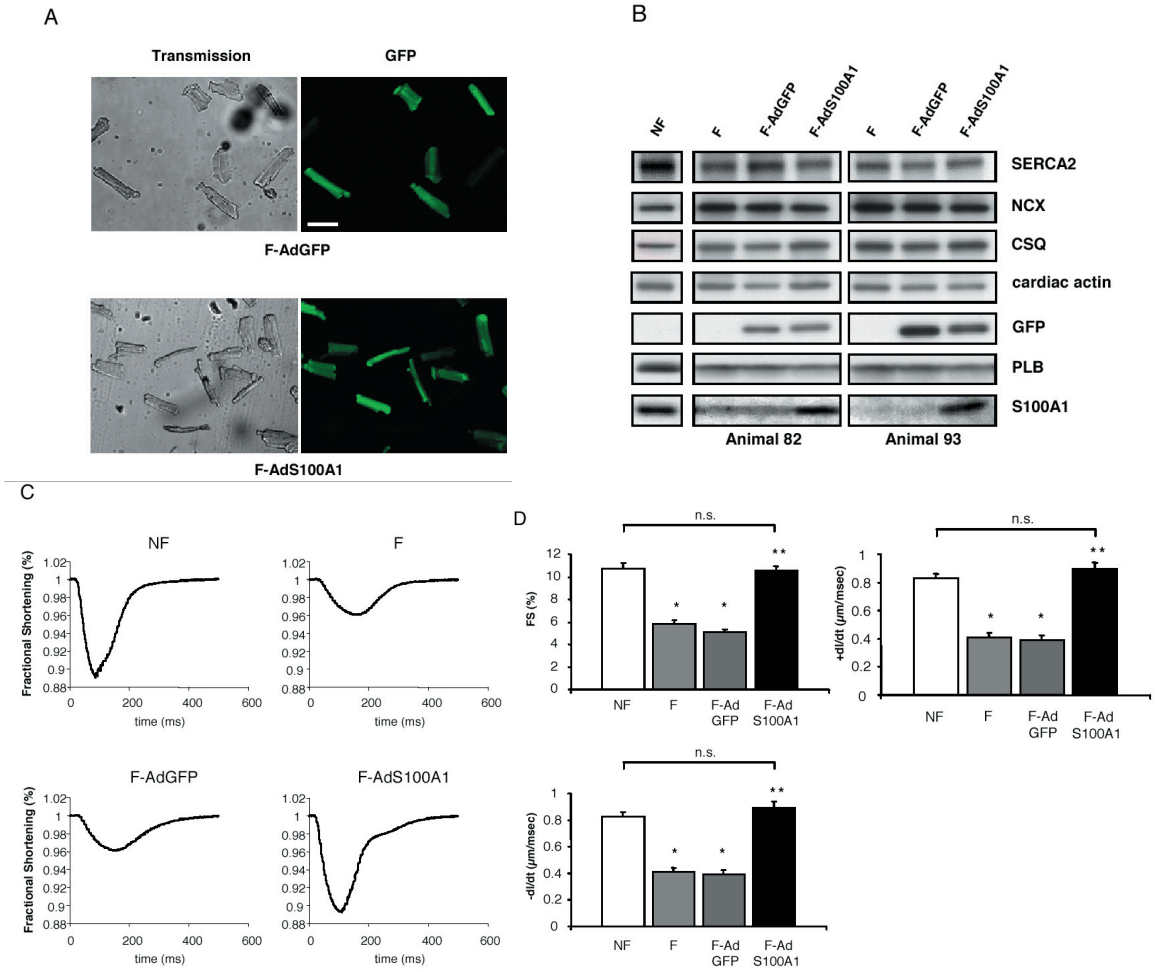

Figure 3.3: S100A1-mediated rescue of contractile dysfunction *in vitro*. (A) Efficiency of adenoviral-mediated gene transfer in failing cardiomyocytes. Representative transmission (left) and GFP emission images (right) from failing cells 24 hrs after adenoviral infection. (upper panel, left) F-AdGFP transmission, (upper panel, right) F-AdGFP 510-nm emission, (lower panel, left) F-AdS100A1 transmission, (lower panel, right) F-AdS100A1 510-nm emission. Bar, 100 μm. (B) Restoration of S100A1 protein levels in failing cardiomyocytes 24 hrs after S100A1 gene transfer. Representative results of Western blots for SERCA2, NCX, CSQ, cardiac actin, GFP, PLB and S100A1 from homogenates both of untreated non-failing (NF) and failing (F) cells and Ad-GFP and Ad-S100A1 transfected failing cardiomyocytes. Note that GFP is only expressed in adenoviral treated failing cells. Data are shown from two different representative preparations (animal 82 and 93). (C) Rescue of contractile function in failing cardiomyocytes (F) after adenoviral S100A1 gene transfer.

Original tracings of fractional shortening (FS%, shown as downward deflection) from a representative non-failing (NF, upper panel, left), failing (F, upper panel, right) and AdGFP-infected (F-AdGFP, lower panel, left) and AdS100A1-infected (F-AdS100A1, lower panel, right) failing cardiomyocyte. (D) Normalization of fractional shortening (FS%; upper panel), rate of cellular shortening (-dl/dt; μm/msec; middle panel) and rate of cellular relengthening (+dl/dt; μm/msec; lower panel) in failing cells after S100A1 gene addition. (n=40 cells from four different preparations in each group; * P<0.01 NF vs. F and F-AdGFP, ** P<0.01 F-AdS100A1 vs. F and F-AdGFP, P=n.s. NF vs. F-AdS100A1). Data are presented as mean±SEM.

Adenoviral S100A1 gene delivery rescues contractile function of failing ventricular cardiomyocytes *in vitro*

Figure 3.3C shows representative steady-state twitches from untreated non-failing (NF) and failing cardiomyocytes (F) (upper panel) and AdGFP- and AdS100A1-treated failing cells (lower panel). Recordings were obtained at 2Hz, 37°C and 2 mM $[Ca^{2+}]_e$ 24 hrs after gene transfer. S100A1 gene delivery significantly increased fractional shortening (FS%) (%: NF; 10.8±0.49, F; 5.8±0.37, F-AdGFP; 5.1±0.27, F-AdS100A1; 10.5±0.39), the rate of cell shortening (-dL/dt) (-μm/msec: NF; 0.82±0.05, F; 0.41±0.03, F-AdGFP; 0.39±0.03, F-AdS100A1; 0.89±0.05) and relenghtening (+dL/dt) (+μm/msec: NF; 0.75±0.05, F; 0.29±0.03, F-AdGFP; 0.27±0.02, F-AdS100A1; 0.67±0.04) in failing cardiomyocytes to levels observed in non-failing cells (Figure 3.3D). AdGFP treatment did not improve contractility of failing cells (Figure 3.3D).

S100A1 gene delivery normalizes Ca^{2+}-handling in failing ventricular cardiomyocytes *in vitro*

Figure 3.4A displays representative steady-state Ca^{2+}-transients obtained under basal conditions from non-failing (NF) and failing cardiomyocytes (F) 24 hrs after AdGFP or AdS100A1 treatment. S100A1 gene transfer significantly increased the Ca^{2+}-transient amplitude (nM) in failing cardiomyocytes to a degree observed in non-failing control cells (nM: NF; 326±23, F; 231±14, F-AdGFP; 225±33, F-AdS100A1; 300±25), whereas, infection with AdGFP did not improve decreased Ca^{2+}-transient amplitudes (Figure 3.4B). In addition, AdS100A1-treated cells showed a significant accelerated decay of Ca^{2+}-transient as assessed by the decay-constant t (data not shown). Moreover, S100A1 gene transfer also significantly reduced the elevated diastolic Ca^{2+}-overload ($[Ca^{2+}]_i$) observed in AdGFP-treated and untreated failing cells (nM: NF; 208±13, F; 322±25, F-AdGFP; 310±34, F-AdS100A1; 247±16)

(Figure 3.4C). Application of the SERCA2 inhibitor cyclopyazonic acid (10μM) abrogated the gain in function found in AdS100A1-treated failing myocytes (data not shown).

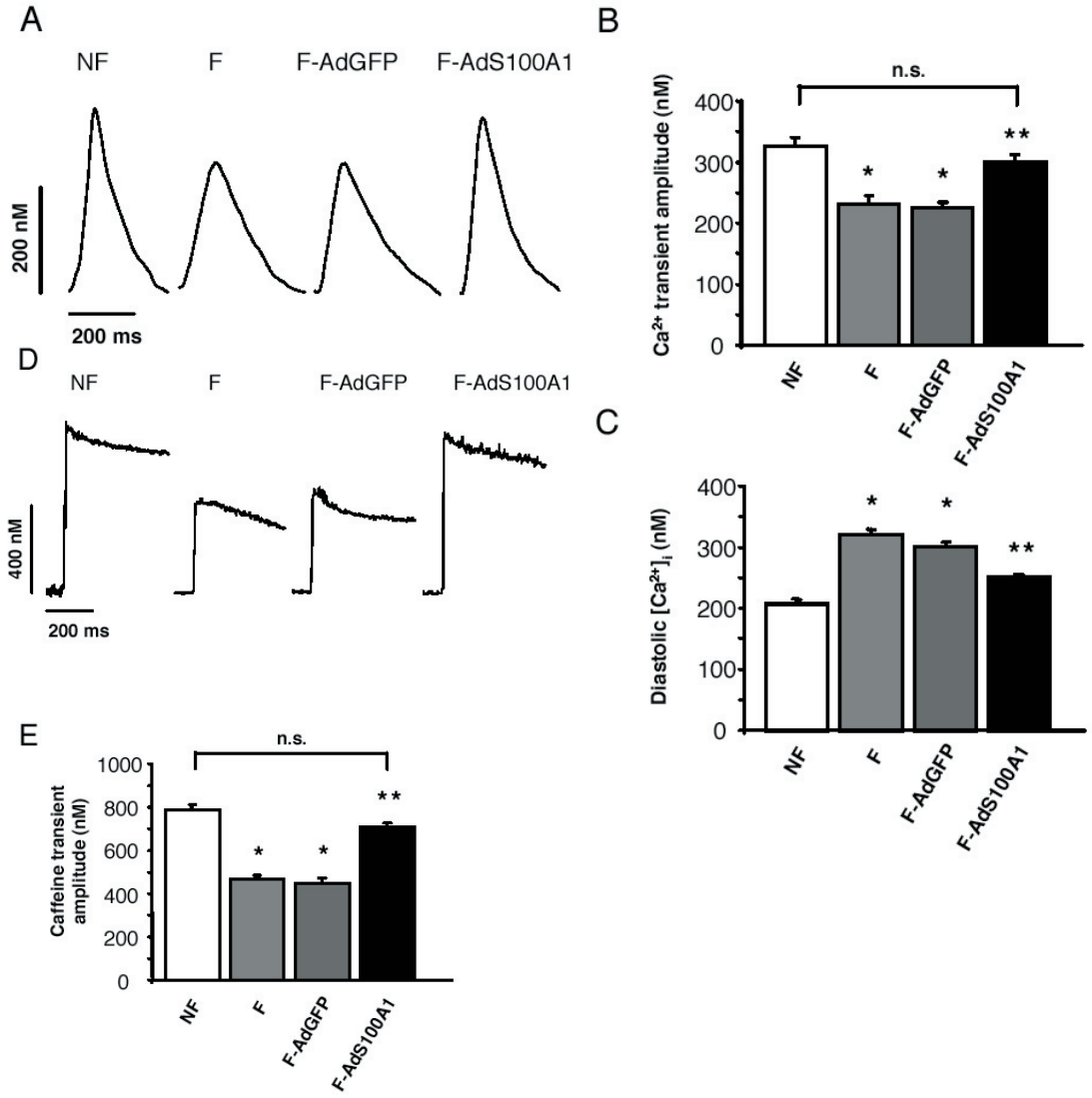

Figure 3.4: Normalization of Ca^{2+}-transients and SR Ca^{2+}-load after S100A1 gene delivery in failing cardiomyocytes (A) Original tracings of Ca^{2+}-transients (shown as upward deflection) from a representative non failing (NF), failing (F), AdGFP-infected (F-AdGFP) and AdS100A1-infected (F-AdS100A1) failing cardiomyocyte. (B) Normalization of Ca^{2+}-transient amplitude (nM) and (C) significant decrease in diastolic [Ca^{2+}] (nM) in failing cells after AdS100A1 treatement. (n=40 cells from four different preparations in each group). (D) Original tracings of cytosolic Ca^{2+}-rise in response to acute caffeine application (10mM) in the presence of Ni2+ (5mM) (shown as upward deflection) from a representative non-failing (NF), failing (NF) and AdGFP-infected (F-AdGFP) and AdS100A1-infected (F-AdS100A1) failing cells. (E) Normalization of SR Ca^{2+}-load estimated from the caffeine-induced cytosolic Ca^{2+}-rise (nM) in failing cells after AdS100A1 gene transfer. (n=40 cells from four different preparations in each group). * P<0.01 NF vs. F and F-AdGFP, ** P<0.01 F-AdS100A1 vs. F and F-AdGFP, P=n.s. NF vs. F-AdS100A1. Data are presented as mean±SEM.

Figure 3.4D provides representative original tracings of cytosolic $[Ca^{2+}]_i$ rise for untreated non-failing (NF), failing cells (F), AdGFP- and AdS100A1-treated failing cardiomyocytes in

response to rapid application of caffeine (10mM) and Ni^{2+} (5mM) serving as a measure for the SR Ca^{2+}-load. S100A1 gene delivery significantly augmented the amplitude of the caffeine-mediated rise in $[Ca^{2+}]_i$ to levels observed in non-failing control (nM: NF; 787±33, F; 469±44, F-AdGFP; 449±29, F-AdS100A1; 709±19) (Figure 3.4E) indicating restoration of SR Ca^{2+}-content in failing cells by S100A1. In contrast, infection of failing cardiomyocytes with AdGFP did not improve diminished SR Ca^{2+}-load (Figure 3.4E).

S100A1 interacts with SERCA2 and enhances SR Ca^{2+}-ATPase activity *in vitro*

Subcellular location of adenovirally expressed S100A1 in failing cardiomyocytes was investigated by confocal laser scanning microscopy. Anti-S100A1 immunolabelling of AdS100A1-treated failing cardiomyocytes revealed a fine granular network-like distribution for S100A1 (blue) throughout the cell that was periodically enhanced nearly every 2μm. (Figure 3.5B, see 3-fold magnified inlet). A similar pattern was obtained for SERCA2 (red) (Figure 3.5C). Superimposing of both images revealed substantial colocalization of S100A1 and SERCA2 (violet) (Figure 3.5D). This finding was further corroborated by Ca^{2+}-dependent co-immunoprecipitation for S100A1 with SERCA2 in the presence of 1 mM Ca^{2+} (Figure 3.5E). Lower free Ca^{2+} (1μM) also supported this interaction (data not shown). Interestingly, co-immunoprecipitations carried out for SERCA2 and PLB revealed no apparent alteration of the PLB/SERCA2 interaction by S100A1 (data not shown).

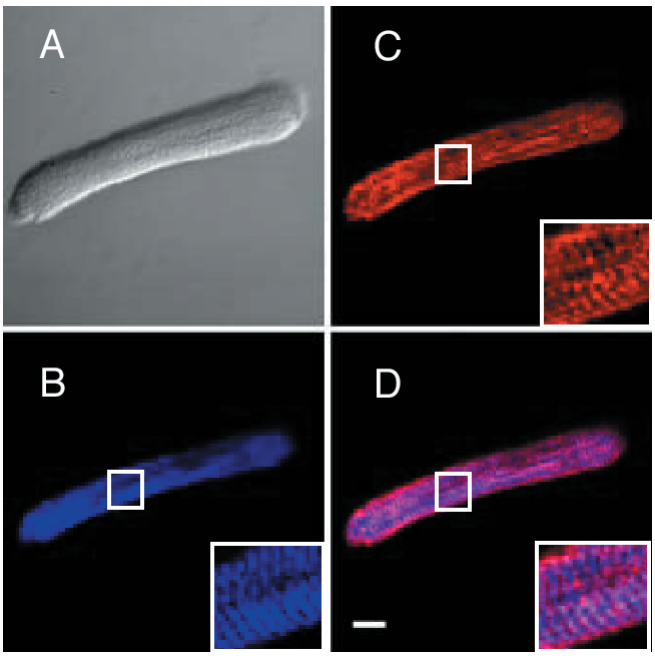

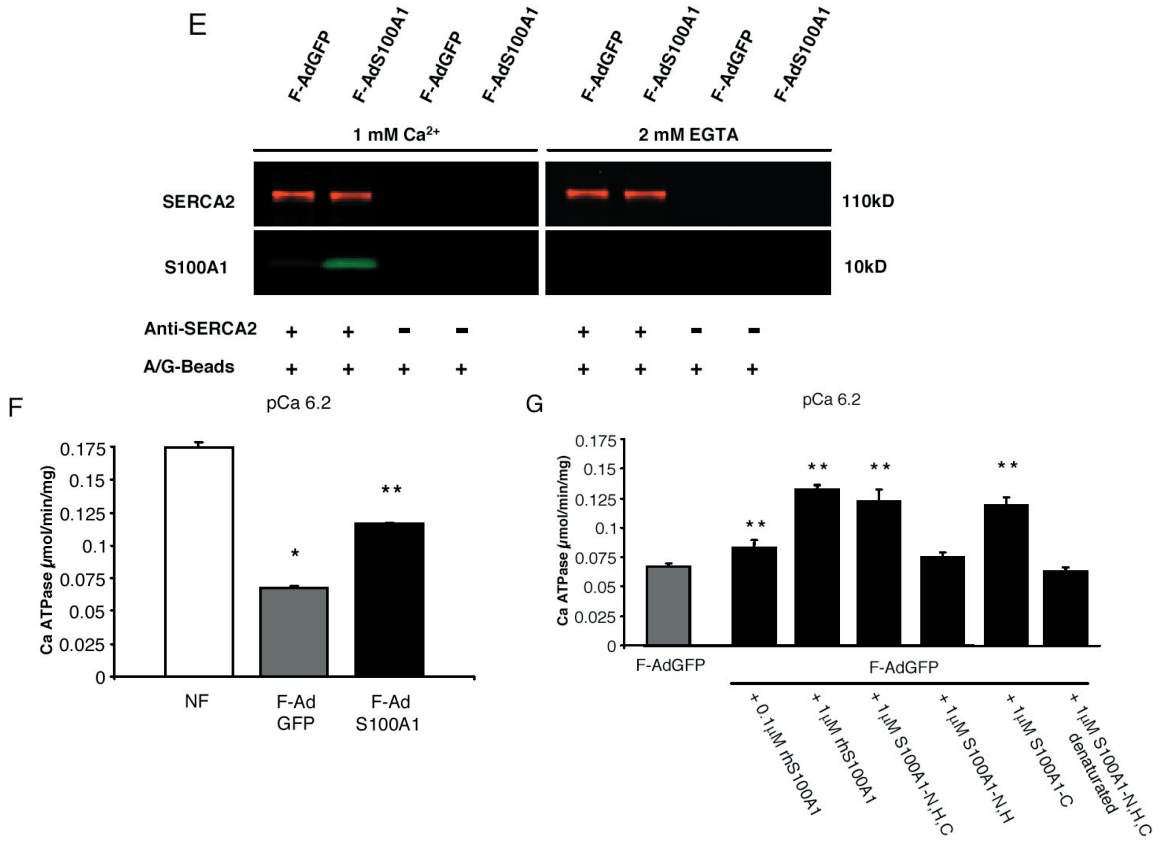

Figure 3.5: S100A1 interacts with SERCA2 and increases activity of the SR Ca^{2+}-pump in failing myocardium. (A) Nomarski image of an AdS100A1 treated failing cardiomyocyte. Immunolabeling of (B) S100A1 (blue) and (C) SERCA2 (red) in the same cell. (D) Overlay of G and H depicts co-localization of SERCA2 and S100A1 (violet). Bar, 20μm. (E) Ca^{2+}-dependent co-immunoprecipitation of SERCA2 (red) and S100A1 (green). Samples were immunoprecipated with anti-SERCA2 antibody and co-stained for S100A1. Controls were carried out with A/G-Sepharose beads (A/G-Beads) only. (F) Enhancement of Ca^{2+}-dependent Ca^{2+}-ATPase activity in homogenates of AdS100A1-treated failing cardiomyocytes. (G) Co-incubation of F-AdGFP homogenates with human recombinant S100A1 protein (rhS100A1) and S100A1 peptides enhances SERCA2 activity. Experiments were carried out at pCa 6.2. (n=6). * P<0.01 NF vs. F, ** P<0.01 F-AdS100A1 and F-AdGFP + S100A1 protein or peptides vs. F-AdGFP. Pooled cardiomyocyte samples were obtained from four different preparations in each group. Data are presented as mean±SEM.

SERCA2 activity was measured in SR preparations derived both from AdS100A1- and AdGFP-treated failing cells as well as non-failing cardiomyocytes by the use of a pyruvate/NADH coupled reaction at pCa 6.2. SERCA2 activity in AdGFP-treated failing cells (F-AdGFP) was significantly decreased compared with non-failing control (NF) (Figure 3.5F). However, SR preparations from AdS100A1 myocytes had significantly improved Ca^{2+}-dependent SERCA2 activity (μmol/min/mg protein: NF; 0.175±0.03, F-AdGFP; 0.07±0.01, F-AdS100A1; 0.121±0.02) (Figure 3.5F). Further in accordance with these data, incubation of SR vesicles isolated from F-AdGFP myocytes with recombinant human S100A1 protein showed a similar increase in SERCA2 activity (Figure 3.5G). Testing of distinct regions of

S100A1 using oligopeptides revealed that the S100A1-mediated increase in SERCA2 activity is through the carboxyl terminal domain (S100A1-C) of the protein (Figure 3.5G).

S100A1 interacts with SERCA2 and increases SR Ca^{2+}-ATPase activity in COS cells

Co-expression of S100A1 and SERCA2 in COS cells was carried out to confirm the impact of S100A1 on SR Ca^{2+}-handling seen in myocardial tissue. COS cells were incubated with 100 viral particles per cell to achieve 100% transfection (data not shown). Figure 3.6A shows representative western blot images for adenovirally overexpressed SERCA2 and S100A1 protein in COS cell lysates. Staining for ß-actin served as a control for equal protein loading. Assessment of Ca^{2+}-ATPase activity in COS microsomal fractions were carried out in the presence of 600 nM free Ca^{2+}-concentration (pCa 6.2). As displayed in Figure 3.6B (left panel) co-expression of S100A1 enhanced Ca^{2+}-ATPase activity of SERCA2 by 44%. Notably, the S100A1 mediated increase in SERCA2 activity could be prevented by addition of an anti-S100A1 antibody (10 μl SA 5632) whereas application of the antibody preincubated with an S100A1 blocking peptide (S100A1 amino acids 42-54) did not abrogate the S100A1-mediated effect. Thapsigargin (10–6 M) completely abolished the ATPase activity both in SERCA2 and S100A1/SERCA2 overexpressing COS cells confirming specificity of the measurements. Likewise co-expressed S100A1 protein, addition of 1 μM of human recombinant S100A1 protein also significantly increased the Ca^{2+}-ATPase activity in SERCA2 overexpressing COS cells (Figure 3.6B, right panel).

Co-immunoprecipitations carried out for adenovirally expressed S100A1 and SERCA2 confirmed the Ca^{2+}-dependent interaction of both molecules observed in myocardium.

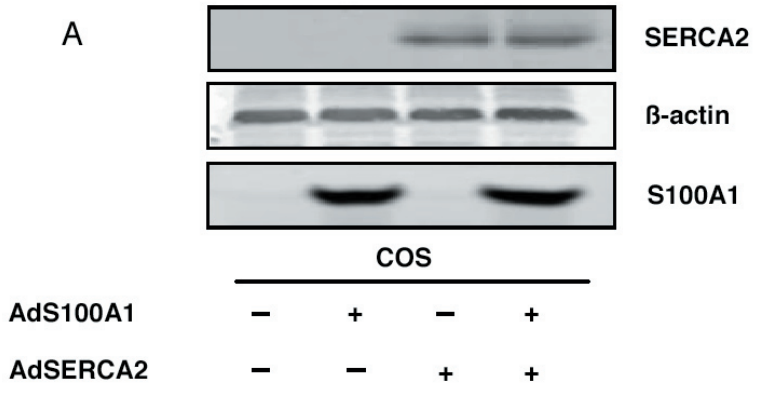

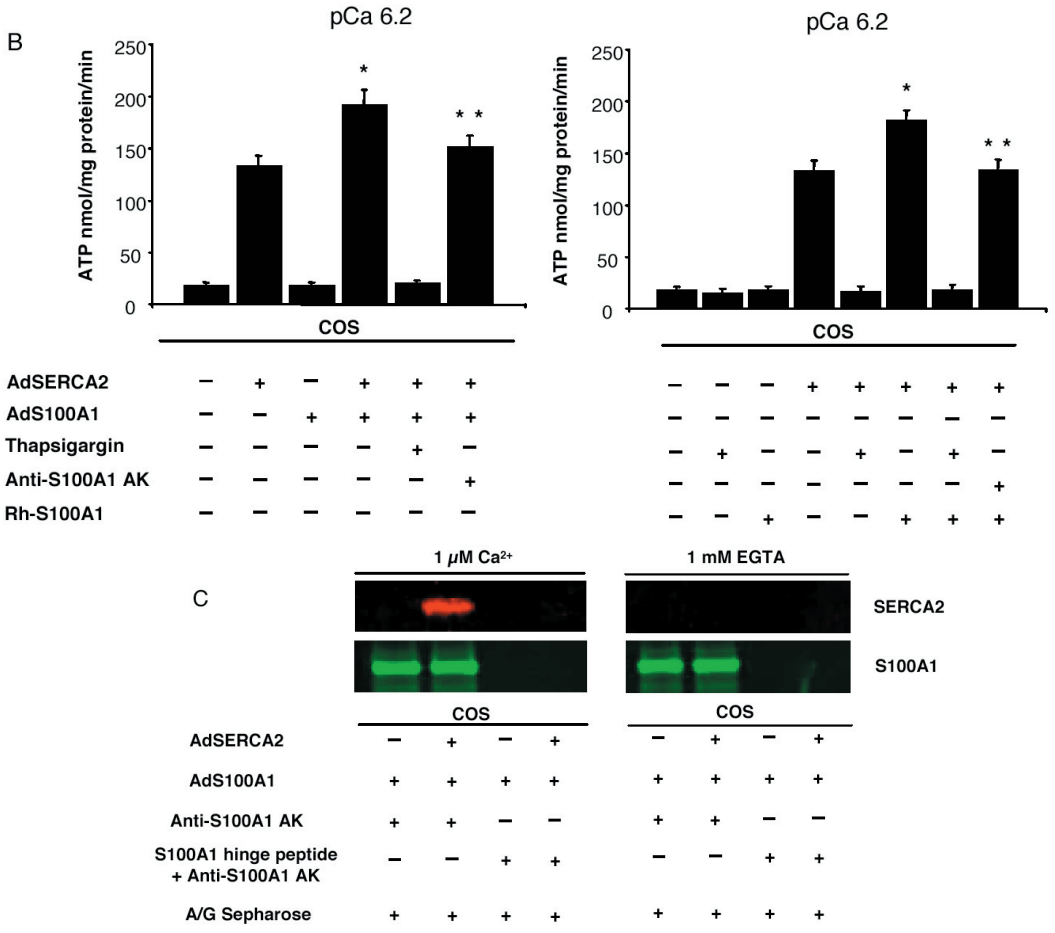

Figure 3.6: S100A1 interacts with SERCA2 and increases activity of the SR Ca^{2+}-pump in COS cells. (A) Representative Western Blots given for adenovirally expressed S100A1 and SERCA2 in COS cells. ß-actin staining served as leading control. (B) (Left panel) Enhanced Ca^{2+}-dependent ATPase activity in SERCA2 expressing COS cells by co-expressed S100A1 protein. Expression of S100A1 alone did not alter Ca^{2+}-dependent ATPase activity in COS cells. Note that addition of anti-S100A1 antibody (SA 5632) abrogated the S100A1 mediated increase in Ca^{2+}-dependent ATPase activity. (Right panel) Increased Ca^{2+}-dependent ATPase activity in SERCA2 expressing COS cells following application of human recombinant S100A1 protein (1μM). Application of anti-S100A1 antibody (SA 5632, 10μl) abrogated the S100A1 mediated enhancement of Ca^{2+}-dependent ATPase activity. Application of the SERCA2 inhibitor thapsigargin (10-6 M) abolished Ca^{2+}-dependent ATPase activity in AdSERCA2 infected COS cells. Experiments were carried out at pCa 6.2. (n=3). * P<0.01 vs. AdSERCA2, ** P<0.01 vs. AdS100A1/AdSERCA2. Data are presented as mean±SEM. (C) Ca^{2+}-dependent co-immunoprecipitation of SERCA2 (red) and S100A1 (green). Samples were immunoprecipated with anti-S100A1 antibody and co-stained for SERCA2. Controls were carried out with an anti-S100A1 antibody preincubated with an blocking peptide.

As shown in Figure 3.6C, S100A1 co-immunoprecipates SERCA2 only in the presence of 1 μM free Ca^{2+}-concentration but not in the presence of EGTA. S100A1 also co-precipitates with SERCA2 in the presence of 1 mM Ca^{2+} (data not shown). Specificity of this finding was confirmed by testing the S100A1 antibody preincubated with an S100A1 blocking peptide that neither precipated S100A1 protein nor co-precipated SERCA2.

S100A1 interacts with the RyR2 and reduces the SR Ca^{2+}-leak

Since S100A1 has been shown to interact with RyR in striated muscle (14), we investigated whether adenoviral expressed S100A1 might associate with the SR Ca^{2+}-release channel in failing cardiomyocytes. Figure 3.7 shows representative confocal images for S100A1 (blue) (Figure 3.7B) and RyR2 (red) (Figure 3.7C) in myocytes after AdS100A1 treatment. Merging the corresponding pictures revealed partial colocalization for S100A1 with the RyR2 (violet) (Figure 3.7D, see 3-fold magnified inlet).

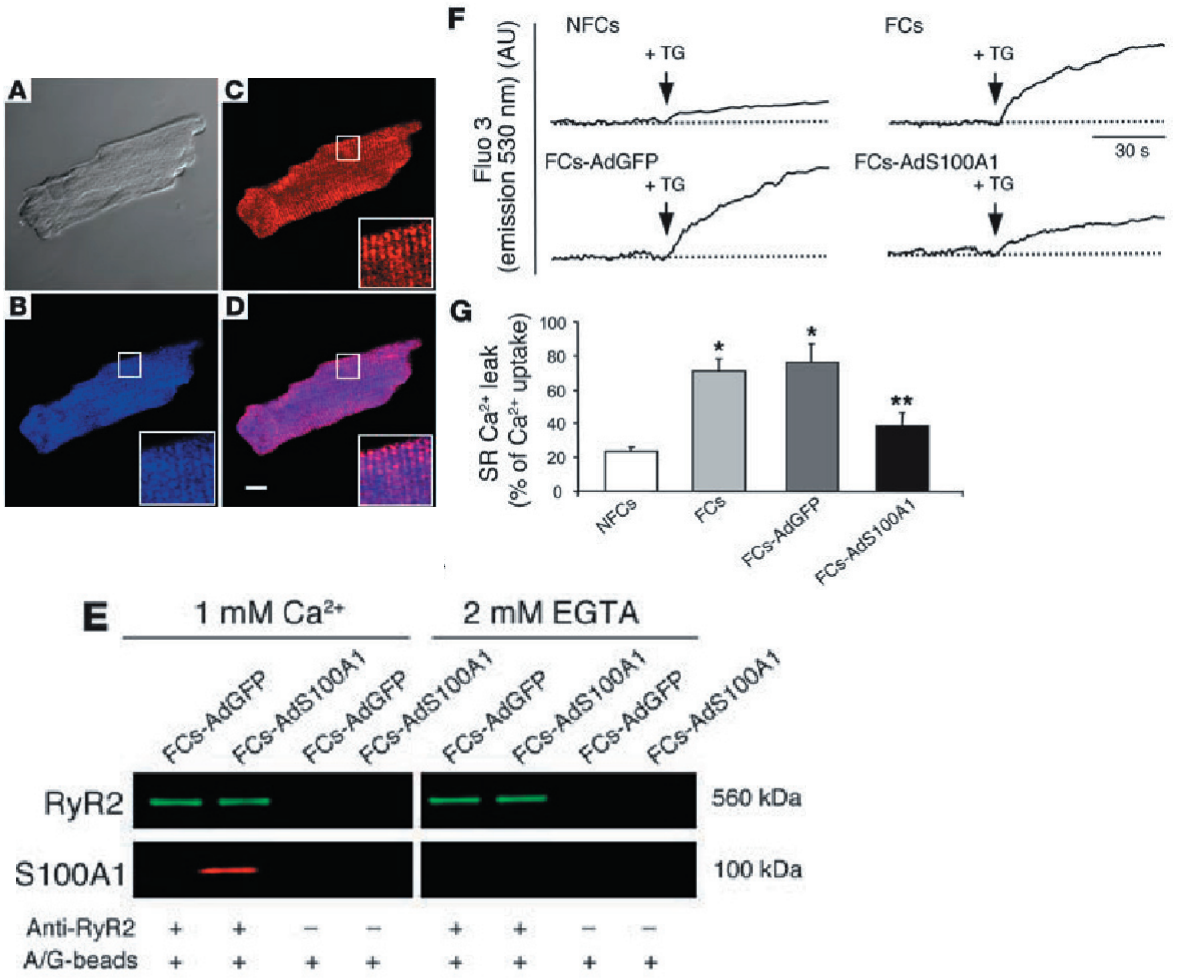

Figure 3.7: S100A1 interacts with RyR2 and reduces the SR Ca^{2+}-leak in failing myocardium. (A) Nomarski image of an AdS100A1-transfected failing cardiomyocyte. Immunolabelling of (B) S100A1 (blue) and (C) RyR2 (red) in the same cell. (D) Overlay of B and C depicts colocalization of S100A1 and RyR2 (violet). Bar, 20μm. (E) Ca^{2+}-dependent co-immunoprecipitation of RyR2 (green) and S100A1 (red). Controls were carried out with A/G-Sepharose beads (A/G-Beads) only. (F) Typical tracings of the time course (upper panel) and averaged values (%) (lower panel) of the SR Ca^{2+} leak in non-failing (NFCs), failing (FCs) and AdGFP- and AdS100A1-transfected failing myocardium. Arrow indicates addition of thapsigargin (+TG; 1μM) (n=4). * P<0.01 NFCs vs. FCs and FCs-AdGFP, ** P<0.01 FCs-AdS100A1 vs. FCs and FCs-AdGFP, P=n.s. NFCs vs. FCs-AdS100A1. Data are presented as mean±SEM.

As shown in Figure 3.7E, Ca^{2+}-dependent (1mM) co-immunoprecipitation of S100A1 with RyR2 in failing cells provides further evidence for the association of both proteins. This was also evident with lower Ca^{2+} (1μM, data not shown). Since S100A1 gene transfer resulted in restored SR Ca^{2+}-content and decreased diastolic $[Ca^{2+}]_i$, we investigated whether S100A1 might affect the SR Ca^{2+}-leak in failing myocardium. Figure 3.7F (upper panel) shows the representative time course of the Ca^{2+}-leak from SR vesicles derived from non-failing as well as AdGFP- and AdS100A1-treated failing myocardium in the presence of thapsigargin (+TG, 1μM) after Ca^{2+}-uptake induced by MgATP. In contrast to non-failing SR vesicles, a prominent Ca^{2+}-leak was observed in non-treated and AdGFP-treated failing myocardium that was significantly reduced after AdS100A1 treatment.

S100A1 modulates activity of the cardiac SR Ca^{2+}-release channel

The influence of S100A1 on RyR2 activity was further investigated in S100A1-depleted cardiac SR vesicle preparations. RyR2 activity was indirectly measured by assessment of Ca^{2+}-dependent RyR2 [^{3}H]-ryanodine binding in the presence and absence of 1 μM human recombinant S100A1. As depicted in Figure 3.8, S100A1 modulates RyR2 [^{3}H]-ryanodine binding in a biphasic manner. Applied S100A1 apparently reduced [^{3}H]-ryanodine binding and RyR2 open probability, respectively, at least in the presence of 150 nM. However, in the presence of increasing Ca^{2+} concentrations, S100A1 enhanced [^{3}H]-ryanodine binding implicating increased activity of the RyR2. Thus, decreased RyR2 activity at diastolic Ca^{2+}-concentrations might account at least in part for the S100A1-caused decrease in the SR Ca^{2+}-leak whereas enhanced RyR2 activity at supra-diastolic Ca^{2+}-concentrations might contribute to the S100A1-mediated increase in Ca^{2+}-transient amplitude in normal (7, 8) and even failing cardiomyocytes.

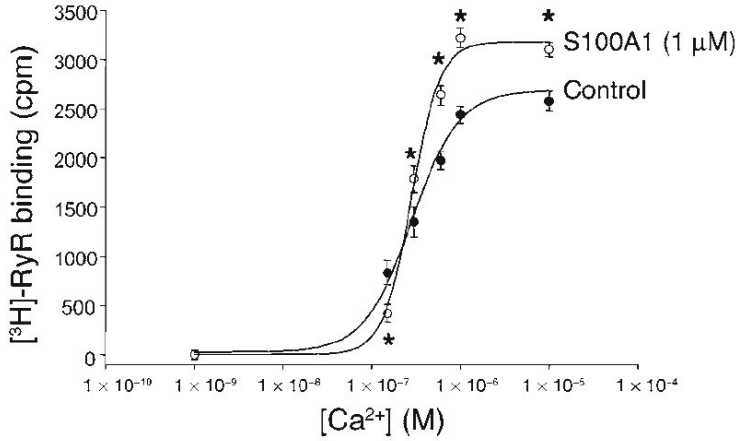

Figure 3.8: S100A1 modulates RyR2 activity in biphasic manner. Control SR vesicles show a Ca^{2+}-dependent increase of [^{3}H]-ryanodine binding in the presence of 0.5 mM Mg^{2+} and 10 mM caffeine. Addition of 1μM S100A1 protein decreased [^{3}H]-ryanodine at 150 nM free Ca^{2+} concentrations while ≥ 300 nM free Ca^{2+} S100A1 increased [^{3}H]-ryanodine binding to the cardiac SR Ca^{2+}-release channel. Data are presented as mean±SEM and expressed as counts per minute (CPM). Experiments (n=3) were carried out in triplicates.

Fetal gene expression in failing ventricular cardiomyocytes *in vitro* is reversed after AdS100A1 treatment

As assessed by quantitative real-time PCR, normalization of S100A1 protein levels in failing cardiomyocytes significantly suppressed increased mRNA expression of ANF (Figure 3.9A) (arbitrary units: NFCs; 1, FCs; 42±06, FCs-AdGFP; 37±07, FCs-AdS100A1; 24±05) and essentially normalized NCX mRNA (Figure 3.9B) (arbitrary units: NFCs; 1, FCs; 2.7±0.5, FCs-AdGFP; 2.9±0.3, FCs-AdS100A1; 1.23±0.2) within 24 hrs, whereas AdGFP infection revealed no alterations of these genes.

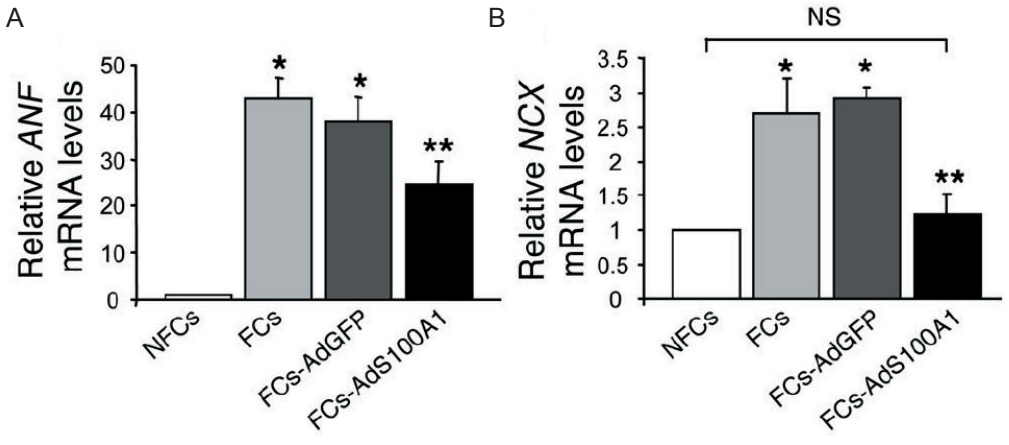

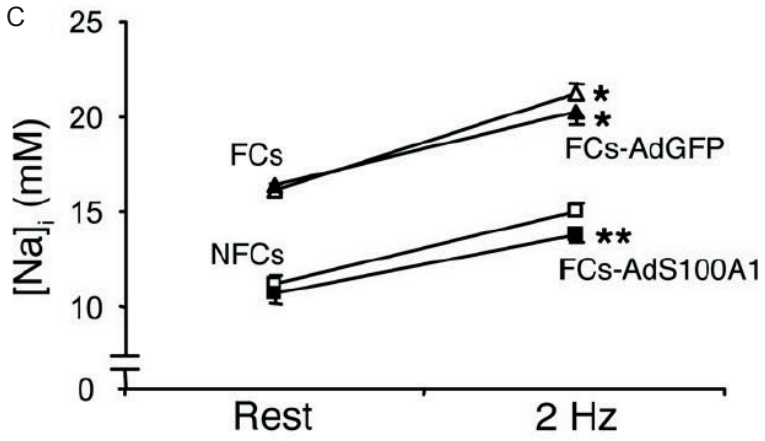

Figure 3.9. Effect of adenovirally expressed S100A1 on fetal gene expression and Na^+-handling in failing cardiomyocytes. (A) Average relative mRNA expression for ANF (upper panel) and (B) NCX (lower panel). 18S rRNA signals were used for normalization. (n=6) (C) Normalization of $[Na^+]_i$ in FCS following S100A1 gene transfer. (n=40 cells from four different preparations; FCs [open triangles], FCs-AdGFP [filled triangles], NFCs [open squares], FCs-AdS100A1 [filled squares]. * P<0.01 compared with NFCs; **P. Data <0.01 compared with FCs and FCs-Ad GFP; P=NS, NFCs vs. FCs-AdS100A1. Data are presented as mean±SEM.

AdS100A1 treatment normalizes intracellular Na^+-concentration in failing ventricular cardiomyocytes *in vitro*

We next addressed the impact of S100A1 gene-transfer on disturbed intracellular Na+-handling in failing cardiomyocytes by the measurement of the Na^+-fluorescent indicator SBFI-AM. Steady state $[Na^+]_i$ was found to be significantly increased both in untreated and AdGFP-treated failing cardiomyocytes compared with non-failing control (NFC) both under rest (mM: FCs 16.12±0.36, FCs-AdGFP 16.12±0.36, NFCs 11.21±0.41) and electrical stimulation (2Hz) (mM: F 20.21±0.49, FCs-AdGFP 20.24±0.68, NFCs 15.04±0.39) (Figure 3.9C). However, S100A1 gene transfer decreased elevated $[Na^+]_i$ in failing cardiomyocytes under both conditions to levels observed in non-failing cells (mM: rest FCs-AdS100A1 10.67±0.49, 2Hz FCs-AdS100A1 13.80±0.47) (Figure 9C).

Improved contractile reserve in failing ventricular cardiomyocytes after AdS100A1 treatment *in vitro*

AdS100A1 infection significantly improved the blunted β-adrenergic contractile response of failing cardiomyocytes compared with AdGFP-treated and untreated failing cells (Figure 3.10A). However, phosphorylation of PLB serine-16, reflecting cAMP-dependent protein kinase (PKA) activity was unchanged in AdS100A1-infected failing cardiomyocytes com-

pared to controls (Figure 3.10B). Note that treatment of non-failing cells with isoproterenol resulted in a visible higher amount of PLB Serine-16 phosphorylation than in failing cardiomyocytes.

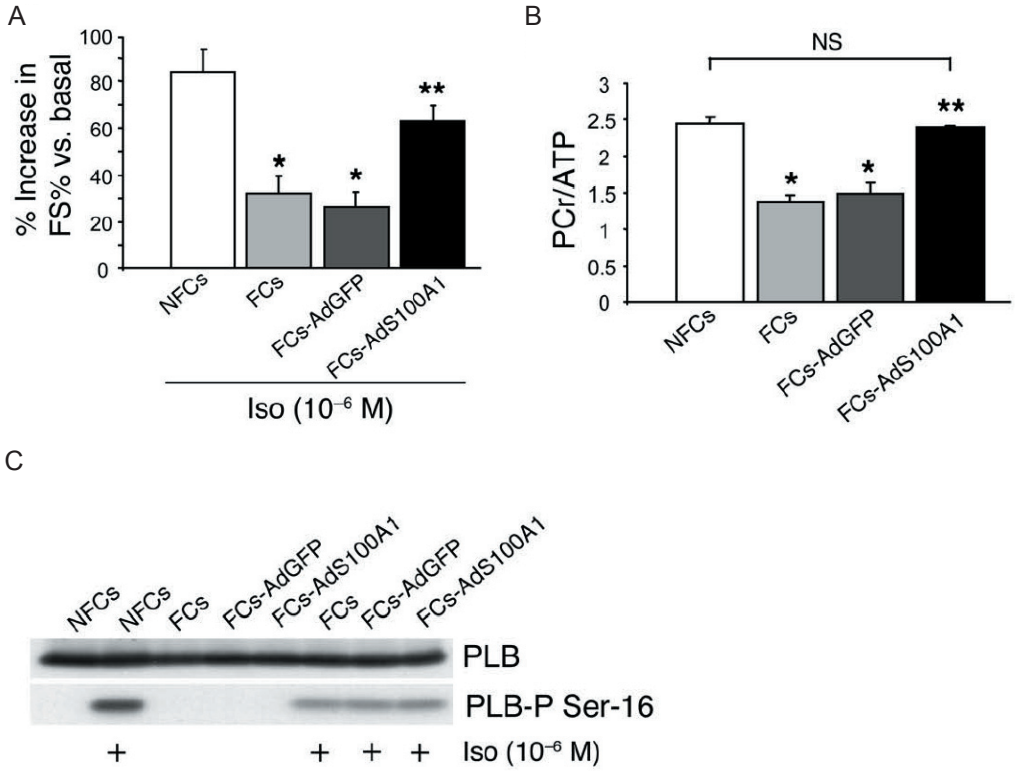

Figure 3.10: Adenoviral S100A1 gene delivery improves contractile reserve and normalizes energy supply in FCs. (A) Improved β-adrenergic stimulated contractility due to S100A1 gene addition in failing cardiomyocytes. (n=30 cells from three different preparations. (B) Representative Western blots for total PLB (upper panel) and phosphorylated PLB (PLB-P Serine-16, lower panel) levels in NFCs, FCs, FCs-AdGFP, and FCs_AdS100A1-infected FCs under basal conditions and in response to isoproterenol (Iso, 10–6 M). (C) Normalization of PCr/ATP ratio in FCs following S100A1 gene addition. Average results for PCr/ATP ratio of each experimental group. (n=4). * P<0.01 compared with NFCs, ** P<0.01 compared with FCs and FCs-AdGFP, P=NCS, NFCs vs. FCs-AdS100A1. Data are presented as mean±SEM.

AdS100A1 gene transfer rescues high energetic phosphate production in failing ventricular cardiomyocytes *in vitro*

High energetic phosphates in non-failing and failing cardiomyocytes were determined by high performance liquid chromatography. Figure 3.10C shows that the ratio of total amounts of phosphocreatine (PCr) to adenosine triphosphate (ATP) was significantly lower in failing than in non-failing cardiomyocytes indicating impaired energy production. Importantly, AdS100A1 treatment recovered the PCr/ATP ratio to values of non-failing cells (arbitrary units: NFCs; 2.43±0.1, FCs; 1.39±0.1, FCs-AdGFP; 1.48±0.2, FCs-AdS100A1; 2.4±0.1).

Cardiac AdS100A1 gene transfer restores S100A1 protein levels in failing hearts *in vivo*

Having shown that S100A1 gene transfer normalized function of failing ventricular cardiomyocytes *in vitro*, we next adressed the question whether *in vivo* intracoronary adenoviral-mediated S100A1 delivery might restore contractile function of failing rat hearts. We applied a catheter-based adenoviral delivery technique that has previously been shown to achieve global and relatively homogenous transgene expression throughout rat myocardium (15). Figure 3.11 shows representative confocal Nomarski and GFP fluorescence images of midventricular cyrosections of sham-OP (A/B) as well as AdS100A1 (C/D) and AdGFP (E/F) treated post-infarct rat hearts, respectively. To assess the amount of gene expression in these hearts 7 days after AdS100A1 (n=7) and AdGFP (n=7) intracoronary gene transfer, we analyzed cardiac S100A1 and GFP protein levels by Western blotting. As shown in Figure 3.11G, infection with AdGFP did not alter downregulated S100A1 protein compared with failing saline-treated hearts (n=7) (arbitrary units: F-AdGFP 0.7±0.2, F-saline; 0.6±0.3, P=n.s. F-AdGFP vs. F-saline, n=4), whereas delivery with AdS100A1 resulted in normalized cardiac S100A1 protein compared with sham-operated non-failing hearts (n=9) (F-AdS100A1; 2.2±0.3, sham-OP; 2.5±0.4, P=n.s. F-AdS100A1 vs. sham-OP, P<0.05 F-AdS100A1 vs. F-AdGFP and F-saline, n=4). The data are given as relative arbitrary units normalized to unchanged CSQ for each group. Note that GFP protein expression was only detected in treated hearts (Figure 3.11G).

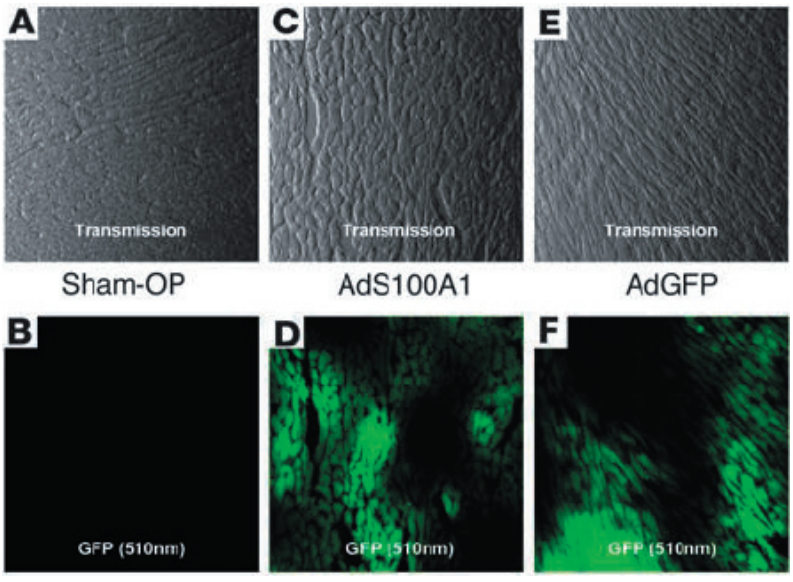

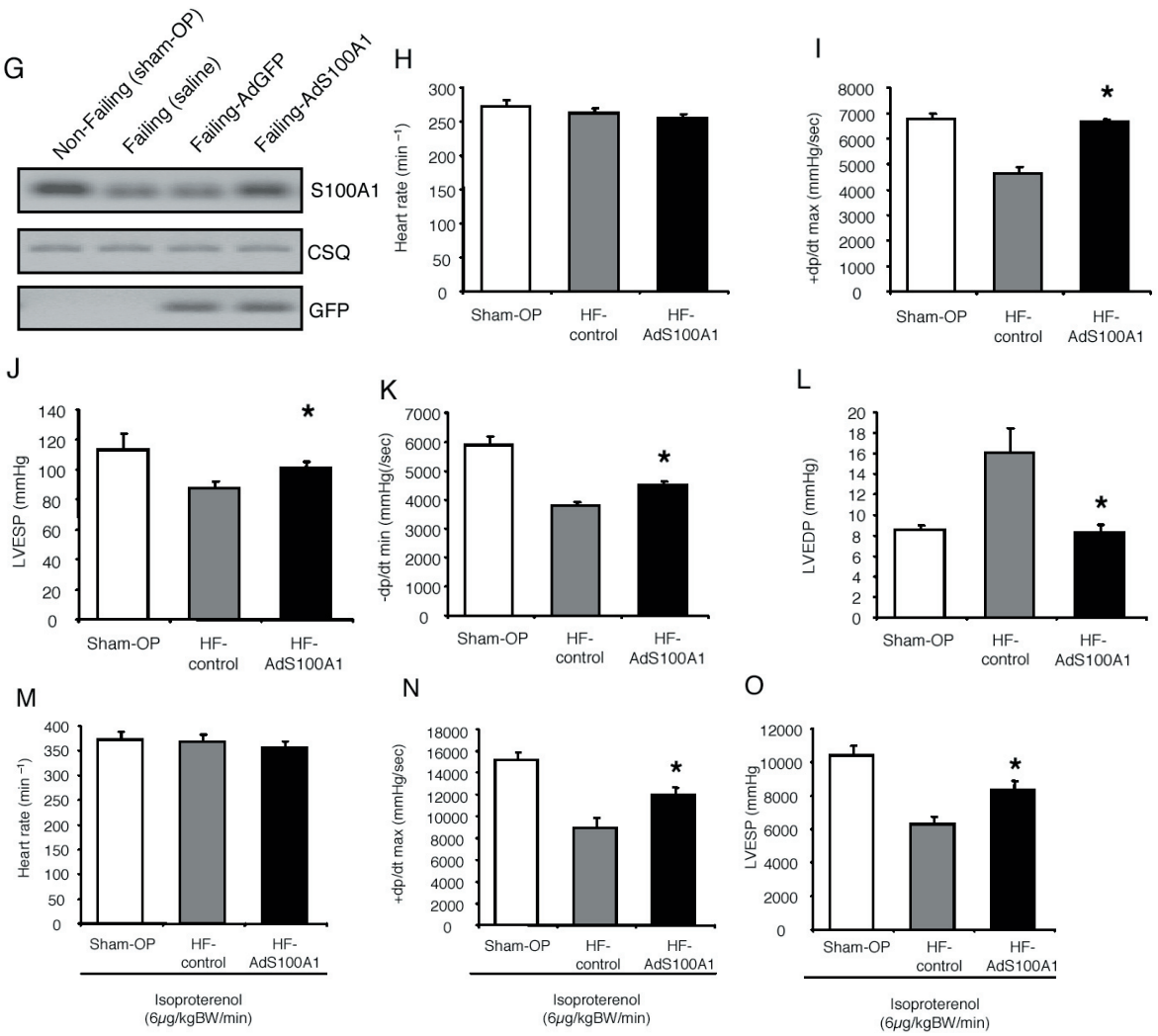

Figure 3.11: Intracoronary adenoviral S100A1 gene delivery rescues contractile dysfunction *in vivo*. (A-F) Representative corresponding Nomarski and GFP-fluorescence images from midventricular cyrosections of non-failing (A/B) and AdS100A1- (C/D) and AdGFP-treated (E/F) failing myocyardium. Magnification 40-fold. (G) Cardiac S100A1 gene transfer reconstitutes S100A1 protein levels in failing myocardium *in vivo*. Representative Western blot of S100A1, CSQ and GFP expression in sham-operated non-failing, saline-treated failing, and adenovirally-treated (AdGFP/AdS100A1) failing myocardium. (H-L) Restoration of basal cardiac contractile performance after AdS100A1 gene transfer in vivo. (M-O) Preserved gain-in-function of AdS100A1-treated failing hearts in vivo after isoproterenol stimulation. Saline- and AdGFP-treated failing hearts displayed no significant difference in functional parameters and were combined to heart failure control group (HF-control; n=14). Data were obtained in isoflurane-anesthetized animals 7 days after intracoronary gene transfer or saline injection. Sham-OP; n=7, HF-AdS100A1; n=7. * P<0.05 HF-AdS100A1 vs. HF control.

AdS100A1 gene transfer recovers contractile function of failing hearts *in vivo*

To gain further insight into the physiological consequences of restored cardiac S100A1 protein levels in failing myocardium in vivo, we re-examined LV contractile properties by cardiac catheterization via the right carotid artery 7 days after gene transfer to 12 week post-infarcted rat hearts. Since saline- and AdGFP-treated failing hearts displayed no significant difference in functional parameters, both groups were pooled and further refered to as HF-control (n=14). As shown in Figure 3.11H, heart rate (HR) was not significantly

different among groups 7 days following gene delivery. However, cardiac S100A1 gene transfer significantly enhanced systolic function of failing hearts in vivo, reflected by a normalized peak rate of LV pressure rise (+dp/dtmax) (+mmHg/sec: HF-AdS100A1; 6640±149, HF-control; 4634±267, sham-OP; 6777±209, P=n.s. HF-AdS100A1 vs. sham-OP, P<0.05 HF-AdS100A1 vs. HF-control) and increased LV end-systolic pressure (LVESP) (mmHg: HF-AdS100A1; 101±4, HF-control; 88±4, sham-OP; 113±11, P=n.s. HF-AdS100A1 vs. sham-OP, P<0.05 HF-AdS100A1 vs. HF-control) (Figure 3.11I/J). In addition, the peak rate of LV pressure decline (-dp/dtmin) (-mmHg/sec: HF-AdS100A1; 4501±129, HF-control; 3808±121, sham-OP; 5887±282, P<0.05 HF-AdS100A1 vs. HF-control), an index of diastolic function, was also significantly improved in response to S100A1 gene delivery (Figure 3.11K). LV end-diastolic pressure (LVEDP) was also normalized after AdS100A1 delivery (mmHg: HF-AdS100A1; 8.5±0.5 mmHg, HF-control; 16.1±2.4 sham-OP; 8.3±0.8, P=n.s. HF-AdS100A1 vs. sham-OP, P<0.05 HF-AdS100A1 vs. HF-control) (Figure 3.11L). Importantly, the S100A1-mediated in vivo gain in cardiac function was preserved after b-adrenergic stimulation. As shown in Figure 3.11M, the isoproterenol-stimulated increase in heart rate was not significantly different between AdS100A1-treated and control failing hearts, however, AdS100A1-treated failing myocardium displayed improved systolic contractile function in response to isoproterenol (Figure 3.11N/O). In line with these findings, LV cardiomyocytes isolated from AdS100A1-infected hearts displayed increased contractility (FS%: HF-AdGFP; 4.2±0.13, HF-AdS100A1; 8.1±0.51, P<0.05 HF-AdS100A1 vs. HF-AdGFP, n=60 cells; isolated from three different animals in each group) and intracellular Ca^{2+}-transients (nM: HF-AdGFP; 188±10, HF-AdS100A1; 309±37, P<0.05 HF-AdS100A1 vs. HF-AdGFP, n=60 cells; isolated from three different animals in each group) compared with failing cardiomyocytes derived from AdGFP-treated hearts.

Cardiac AdS100A1 gene delivery *in vivo* reverses fetal gene expression

RT-PCR analysis of in vivo AdS100A1-treated failing rat hearts revealed a significant attenuation of elevated mRNA levels for ANF , NCX and α-sk-actin mRNA levels 7 days after gene transfer (Figure 3.12A). Moreover, Western blot analysis of failing rat myocardium

after AdS100A1 intracoronary delivery yielded a significant decrease in elevated NCX protein levels (arbitrary units: sham-OP; 1.3±0.4, HF-control; 2.4±0.3, F-AdS100A1; 1.6±0.3, n=4, P<0.05 HF-S100A1 vs. HF-control) and a significant increase in SERCA2 (sham-OP; 3.5±0.8, HF-control; 1.4±0.6, F-AdS100A1; 2.9±0.3, n=4, P<0.05 HF-S100A1 vs. HF-control) and PLB (sham-OP; 4.1±0.5, HF-control; 2.3±0.7, F-AdS100A1; 3.6±0.2, n=4, P<0.05 HF-S100A1 vs. HF-control) protein amount compared with HF-control (Figure 3.12B). Protein data are given as relative arbitrary units normalized to CSQ that did not change among the groups (data not shown).

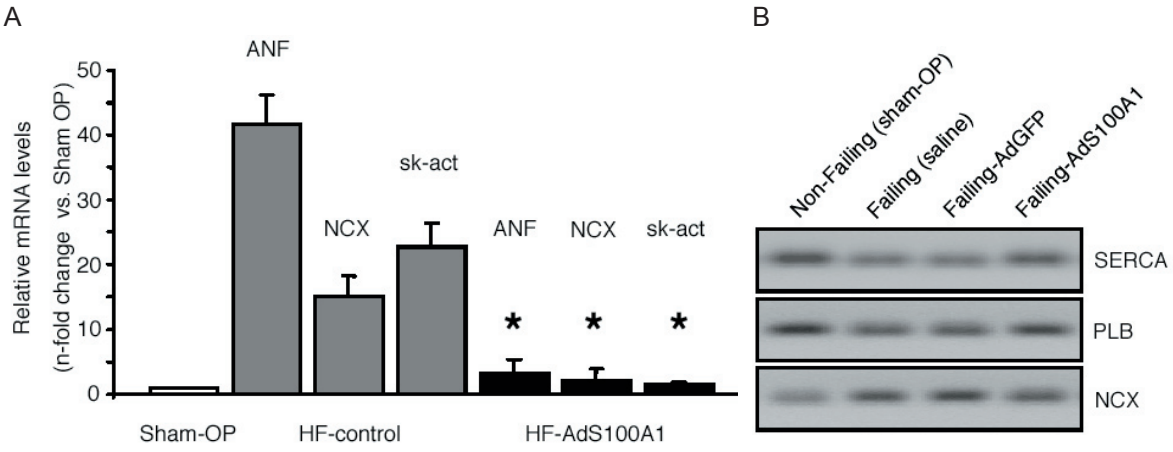

Figure 3.12: Intracoronary adenoviral S100A1 gene delivery reverses fetal gene expression and aberrant protein expression in failing myocardium *in vivo*. (A) Reversed fetal gene expression after S100A1 gene delivery in failing myocardium *in vivo* (* P<0.05 HF-AdS100A1 vs. HF-control, n=4, samples were obtained from 3 different animals in each group). (B) Impact of S100A1 gene addition on SERCA2, PLB and NCX protein amount in failing myocardium *in vivo* compared with saline-treated and AdGFP-treated failing myocardium (n=4, samples were obtained from 3 different animals in each group). Data are presented as mean±SEM.

3.5 Discussion

S100A1 has recently been identified by our group as a novel positive regulator of cardiac contractility as its cardiac-restricted overexpression improves cardiac contractile performance *in vitro* and *in vivo* in a cAMP-independent manner (7, 8). Since S100A1 protein has been shown to be down-regulated in human and animal HF models (5, 6), we undertook this study to address whether S100A1 gene addition may reverse ventricular contractile dysfunction in failing myocardium. Using a post-infarct HF model in the rat, we provide evidence,

for the first time, that adenoviral-mediated myocardial S100A1 gene delivery can restore S100A1 protein expression in failing myocardium and rescue contractile dysfunction both *in vitro* and *in vivo*. Restored S100A1 protein levels normalized dysfunctional intracellular Ca^{2+}- and Na^{+}-handling, reversed fetal gene expression associated with HF and restored energy supply in failing myocardium. These results strongly support the hypothesis that altered expression of S100A1 in HF significantly contributes to Ca^{2+}-signaling abnormalities and cardiac dysfunction and S100A1 is a key factor in the regulation of cardiac excitation-contraction coupling.

Adenoviral-mediated S100A1 gene transfer *in vitro* increased contractile performance of isolated failing cardiomyocytes to levels observed in non-failing ventricular cells. Moreover, S100A1 gene addition almost totally normalized b-adrenergic contractile response in failing ventricular myocytes, which was significantly attenuated under control conditions. This response was independent of any S100A1-mediated change in post-bAR signaling. For example, S100A1 overexpression did not alter serine-16 phosphorylation of PLB after isoproterenol addition. This lack of altered bAR signalling in failing myocardium after S100A1 gene addition is similar to previous findings in transgenic mouse hearts overexpressing S100A1 protein (8). Thus, normalized S100A1 protein levels in failing cardiomyocytes appear to have cAMP-independent and additive positive inotropic effects with b-adrenergic stimulation. This is also supported by previous findings in S100A1 deficient mouse hearts, which had impaired contractility despite normal b-adrenergic signalling (12).

Depressed contractility in HF is inherently linked to abnormal intracellular Ca^{2+}-homeostasis. To gain further insight into the mechanisms by which S100A1 restores contractility in failing myocardium, we explored the impact of S100A1 gene addition on dysfunctional Ca^{2+}-cycling in failing cardiomyocytes. S100A1 gene delivery was found to normalize Ca^{2+}-transients and decreased diastolic Ca^{2+}-overload in failing cardiomyocytes. Overall, it seems that normalized S100A1 expression in failing cardiomyocytes enhances contractility by restoring cytosolic Ca^{2+}-handling, which was suggested by previous studies in normal myocardium (7-9). Since impaired SR Ca^{2+}-load is a major hallmark of HF (16) and contributes to depressed cytosolic Ca^{2+}-cycling (2), we were interested in whether S100A1 restoration

after gene delivery improved this aspect of SR Ca^{2+}-signaling in failing cardiomyocytes. Importantly, S100A1 restores SR Ca^{2+}-load in failing cardiomyocytes, which may account, at least in part, for reconstituted f-transients and improved cardiac contractile performance in AdS100A1-treated failing cardiomyocytes.

Using confocal laser microscopy we found a colocalization in the SR between S100A1 and SERCA2 after AdS100A1 treatment and also found a Ca^{2+}-dependent association between these two proteins in failing cardiomyocytes. Accordingly, we assessed the influence of normalized S100A1 levels on SERCA2 activity in failing myocardium since the above results with increased SR Ca^{2+}-load may be due to increased Ca^{2+}-uptake. Importantly, S100A1 was found to enhance SERCA2 activity indicating that restored SR Ca^{2+}-content seen in AdS100A1-treated failing cardiomyocytes might be the result of this mechanism enhancing SR Ca^{2+}-uptake. This was further supported by the finding that inhibition of SERCA2 abrogated this functional gain in S100A1 overexpressing failing cardiomyocytes. Moreover, testing of distinct S100A1 oligopeptides revealed that the carboxyl terminus of S100A1 is responsible for its enhancement of SERCA2 activity. Interestingly, this result is consistent with previous studies showing that this domain of S100A1 is involved in modulating the activity of target proteins such as RyR1 in skeletal muscle (11). S100A1 was also found both to enhance Ca^{2+}-dependent SERCA2 activity and to interact with the SR Ca^{2+}-pump in the context of a non-cardiac cellular environment. Therefore, normalized S100A1 protein expression in HF appears to enhance SR Ca^{2+}-load in failing myocardium by increasing SERCA2 activity through a Ca^{2+}-dependent interaction with the carboxyl domain of this S100 family member. Further studies are needed to determine the specific mechanism responsible for this domain of S100A1 to enhance SERCA2 activity in myocardial SR.

SR Ca^{2+}-load is balanced both by diastolic Ca^{2+}-uptake and Ca^{2+}-leak and enhanced diastolic Ca^{2+}-leakage in failing myocardium can contribute to impaired SR Ca^{2+}-content (2, 16). Interestingly, normalized S100A1 protein levels after AdS100A1 treatment lead to a decrease in the SR Ca^{2+}-leak in failing cardiomyocytes. This could be due to an effect of S100A1 on RyR2 as we found a colocalization between these two SR proteins as well as a Ca^{2+}-dependent association. This notion is further supported by the finding that S100A1 ap-

parently reduces RyR2 activity at diastolic Ca^{2+}-concentrations as indicated by reduced [^{3}H]-ryanodine binding. Overall, these results suggest that restored SR Ca^{2+}-load in response to S100A1 gene addition is caused both by enhanced Ca^{2+}-uptake and decreased Ca^{2+}-leakage. This is significant as it could mean that this mechanism is responsible for the decreased diastolic $[Ca^{2+}]_i$ in AdS100A1-treated failing cardiomyocytes. However, our results suggest that S100A1 apparently influences RyR2 activity in a biphasic manner. Increasing free Ca^{2+}-concentrations ≥ 300 nM resulted in enhanced [^{3}H]-ryanodine binding suggesting that S100A1 enhances RyR2 activity at supra-diastolic Ca^{2+}-concentrations. Given the fact that S100A1 has previously shown to enhance Ca^{2+}-induced SR Ca^{2+}-release in non-failing myocardium (8), enhanced RyR2 activity might also contribute to normalized excitation-contraction coupling in failing cardiomyocytes after S100A1 gene addition. Further studies are required to detail the biphasic mechanisms of S100A1 on diastolic and systolic SR Ca^{2+}-release channel function in failing and normal myocardium.

Since abnormal intracellular Na^+-handling has also been associated with HF (17), we addressed the impact of S100A1 gene transfer on $[Na^+]_i$ overload in failing cardiomyocytes *in vitro*. Importantly, this defect that can cause pro-arrythmogenic actions and ventricular remodeling (17) was also normalized by S100A1 gene transfer. Since suppressed SR function in HF can favor diastolic Ca^{2+}-efflux via the NCX forward-mode (17), this SR dysfunction might essentially contribute to increased $[Na^+]_i$ in failing myocardium. Considering normalized SR Ca^{2+}-load after S100A1 gene transfer, it is possible that S100A1-mediated enhancement of Ca^{2+}-uptake enables the SR to better compete with NCX for diastolic $[Ca^{2+}]_i$ elimination. In turn, this effect might therefore reduce sarcolemmal $[Na^+]_i$-influx and contribute to reduction in $[Na^+]_i$. However, with regard to the complex network of ion channels and transporters regulating both cardiac Ca^{2+}- and Na^+-homeostasis (17), elucidating the exact mechanisms underlying S100A1 beneficial effects on Ca^{2+}- and Na^+-handling in failing cardiomyocytes warrants further investigation.

Decreased energy reserve via the creatine kinase reaction is also a characteristic finding both in human and experimental HF (18). Normalization of S100A1 protein in failing cardiomyocytes restored the depressed PCr/ATP ratio to normal values. Since SERCA2 activity is

the most vulnerable reaction to a decrease in free energy released from ATP hydrolysis (19), normalized energy transfer might also account for improved SR Ca^{2+}-uptake in our experimental setting despite sustained suppression of the Ca^{2+}-pump. Thus, S100A1 gene addition also appears to normalize impaired energy supply in failing cardiomyocytes. With regard to diastolic $[Ca^{2+}]_i$ overload that essentially contributes to impaired mitochondrial function in failing myocardium, the S100A1-mediated decrease of diastolic $[Ca^{2+}]_i$ might in part contribute to the correction of the decreased PCr/ATP ratio. Since S100A1 has previously been shown to also reside in the outer membrane of mitochondria within cardiomyocytes (20), this finding strongly supports the notion that this Ca^{2+}-binding protein might also support mitochondrial function, which is the subject of current investigations. Moreover, we speculate, that the increase of free energy released from ATP hydrolysis might also restore, at least in part, depressed Na^+/K^+-ATPase activity in failing cardiomyocytes (17) that might also contribute to the S100A1-mediated normalized $[Na^+]_i$ discussed above.

Our *in vitro* results indicate that S100A1 normalization via gene transfer to the heart may represent a novel therapeutic strategy for HF. However, the ultimate question is whether similar results may occur *in vivo* after myocardial gene delivery of S100A1. To test this, we delivered AdS100A1 via the coronary arteries to post-infarcted rat hearts that were in overt HF. Importantly, 7 days after intracoronary S100A1 gene delivery S100A1 protein was normalized in failing myocardium and this resulted in markedly improved contractile function of failing hearts *in vivo*. Although gene delivery to the rat heart was shown to be global in nature it was not entirely homogenous and regional overexpression may account for the overall normalization of S100 in failing rat hearts. Important however, this normalized myocardial S100A1 protein levels essentially restored to almost normal both the peak rate of LV pressure rise and LV end-systolic pressure, reflecting a rescue of *in vivo* cardiac systolic function. This is significant due to the continued presence of a large LV infarct. Similarly, S100A1 gene transfer subsequently decreased elevated LV end-diastolic filling pressure to levels seen in non-failing hearts demonstrating improved diastolic function as well. In contrast, delivery of the control AdGFP (or saline) did not alter the diminished cardiac levels of S100A1 nor was there any improvement in cardiac function *in vivo* of the

failing rat hearts. This *in vivo* rescue of myocardial function due to S100A1 restoration was also preserved after b-adrenergic stimulation and importantly, S100A1 gene treatment did not alter heart rate.

In addition to *in vivo* hemodynamics, we also isolated ventricular myocytes from Ad100A1 or AdGFP treated failing hearts. Importantly, we found that AdS100A1 positive cells had enhanced cellular contractility and intracellular Ca^{2+}-cycling both under basal conditions and in response to β-AR stimulation (data not shown) supporting the hypothesis that that S100A1-mediated HF rescue *in vivo* is due to an increase in myocyte contractile function. Overall, this *in vivo* rescue appears to be due to similar mechanisms of restored SR function as found above in our *in vitro* study.

As in the failing cardiac myocytes *in vitro*, *in vivo* HF rescue via S100A1 gene delivery was associated with a reversal of up-regulated fetal gene expression. Further, there was an apparent normalization of aberrant SERCA2/PLB ratios and NCX protein expression. These results are consistent with previous findings in non-failing cardiomyocytes *in vitro* where S100A1 addition prevented fetal gene expression in response to a1-adrenergic stimulation (6). Thus, the down-regulation of S100A1 protein in HF might be permissive for the induction of genes that underlie myocardial hypertrophy and failure, whereas restoration of S100A1 protein both participates in thwarting expression of fetal genes and may maintain the genetic program that defines normal cardiac function. However, attenuated fetal gene expression may also be simply a secondary result to normalized Ca^{2+}-cycling and end-diastolic pressure by S100A1 gene transfer.

Overall, we have shown for the first time that restoring S100A1 protein expression can rescue defective contractile performance of failing myocardium *in vitro* and *in vivo* due to improved cytosolic and SR Ca^{2+}-cycling. The apparent mechanism involves enhancement of SERCA2 activity and modulation of RyR2 function. Importantly, the therapeutic effects of S100A1 normalization was not limited to improved Ca^{2+}-cycling and contractile function since normalized protein levels also restored impaired Na^{+}-homeostasis, cardiac energetic and attenuation of fetal gene expression occuring in HF. Since S100A1 protein is down-regulated in end-stage human HF, the present study clearly validates this Ca^{2+}-sensor as a key

regulator of cardiac function and its normalization appears to be a novel therapeutic target. Moreover, targeting S100A1 and SR Ca^{2+}-cycling differ in many ways from conventional positive inotropic agents that increase chronotropy and energy consumption of failing myocardium counterbalancing the positive effects on contractile strength. Our study does have its limitations including the use of a first-generation adenoviral vector that limits our study duration as it will be important to examine the chronic effects of HF rescue by S100A1 gene delivery, and studies with improved vectors (i.e. AAV) may translate these findings into future S100A1 HF gene therapy clinical trials.

Acknowledgments

This work was supported in part by grants from the Deutsche Forschungsgemeinschaft (P.M.; Mo 1066/1-1) (A.R.; 1083/1-1), the Forschungsförderungsprogramm Medizinische Fakultät der Universität Heidelberg (P.M.; 93/2002), and the National Institutes of Health (W.J.K.; R01 HL56205 and R01 HL59533).

Abbreviations

Heart failure (HF), sarcoplasmic reticulum (SR), green fluorescent protein (GFP), adenovirus (Ad), plaque forming units (pfu), left ventricular (LV), triphenyltetrazolium chloride (TTC), end-diastolic pressure (EDP), systolic ejection pressure (ESP), medium 199 (M199), SR Ca^{2+}-ATPase (SERCA2), sodium-calcium exchanger (NCX), calsequestrin (CSQ), phospholamban (PLB), α-skeletal actin (α-sk-actin), phosphocreatine (PCr), adenosine triphosphate (ATP), multiplicity of infection (MOI).

3.5 References

1. AHA. Heart Disease and Stroke Statistics--2004 Update. Dallas, Tex: American Heart Association; 2003.
2. Marks, A.R. 2003. Calcium and the heart: a question of life and death. J Clin Invest:597-600.
3. Hasenfuss, G. 1998. Alterations of calcium-regulatory proteins in heart failure. Cardiovasc Res 37:279-289.
4. Donato, R. 2003. Intracellular and extracellular roles of S100 proteins. Microsc Res Tech 60:540-551.
5. Remppis, A., Greten, T., Schafer, B.W., Hunziker, P., Erne, P., Katus, H.A., and Heizmann, C.W. 1996. Altered expression of the Ca(2+)-binding protein S100A1 in human cardiomyopathy. Biochim Biophys Acta 1313:253-257.
6. Tsoporis, J.N., Marks, A., Zimmer, D.B., McMahon, C., and Parker, T.G. 2003. The myocardial protein S100A1 plays a role in the maintenance of normal gene expressi on in the adult heart. Mol Cell Biochem 242:27-33.
7. Most, P., Bernotat, J., Ehlermann, P., Pleger, S.T., Reppel, M., Borries, M., Niroomand, F., Pieske, B., Janssen, P.M., Eschenhagen, T., et al. 2001. S100A1: a regulator of myocardial contractility. Proc Natl Acad Sci U S A 98:13889-13894.
8. Most, P., Remppis, A., Pleger, S.T., Löffler, E., Ehlermann, P., Bernotat, J., Kleuss, C., Heierhorst, J., Ruiz, P., Witt, H., et al. 2003. Transgenic overexpression of the Ca^{2+} binding protein S100A1 in the heart leads to increased in vivo myocardial contractile performance. J Biol Chem. 278:33809-33817.
9. Remppis, A., Most, P., Löffler, E., Ehlermann, P., Bernotat, J., Pleger, S.T., Börries, M., Repper, M., Fischer, J., Koch, W.J., et al. 2002. The small EF-hand Ca^{2+} binding protein S100A1 increases contractility and Ca^{2+} cycling in rat cardiac myocytes. Basic Res Cardiol 97:I/56-I/62.
10. Remppis, A., Pleger, S.T., Most, P., Lindenkamp, J., Ehlermann, P., Löffler, E., Weil, J., Eschenhagen, T., Koch, W.J., and Katus, H.A. 2004. S100A1 gene transfer : A strategy to strenghten engineered cardiac grafts. J Gene Medicine 6:387-

394.

11. Most, P., Remppis, A., Weber, C., Bernotat, J., Ehlermann, P., Pleger, S.T., Kirsch, W., Weber, M., Uttenweiler, D., Smith, G.L., et al. 2003. The C-terminus (aa 75-94) and the linker region (aa 42-54) of the Ca^{2+} binding protein S100A1 differentially enhance sarcoplasmic Ca^{2+} release in murine skinned skeletal muscle fibres. J Biol Chem 278:26356-26364.
12. Du, X.J., Cole, T.J., Tenis, N., Gao, X.M., Kontgen, F., Kemp, B.E., and Heierhorst, J. 2002. Impaired cardiac contractility response to hemodynamic stress in S100A1-deficient mice. Mol Cell Biol 22:2821-2829.
13. Most, P., Boerries, M., Eicher, C., Schweda, C., Ehlermann, P., Pleger, S.T., Löffler, E., Koch, W.J., Katus, H.A., Schoenenberger, C.A., et al. 2003. Extracellular S100A1 protein inhibits apoptosis in ventricular cardiomyocytes via activation of the extracellular-regulated kinase (ERK1/2) pathway. J Biol Chem 278:48404-48412.
14. Treves, S., Scutari, E., Robert, M., Groh, S., Ottolia, M., Prestipino, G., Ronjat, M., and Zorzato, F. 1997. Interaction of S100A1 with the Ca^{2+} release channel (ryanodine receptor) of skeletal muscle. Biochemistry 36:11496-11503.
15. Hajjar, R.J., Schmidt, U., Matsui, T., Guerrero, J.L., Lee, K.H., Gwathmey, J.K., Dec, G.W., Semigran, M.J., and Rosenzweig, A. 1998. Modulation of ventricular function through gene transfer in vivo. Proc Natl Acad Sci U S A 95:5251-5256.
16. Bers, D.M. 2002. Cardiac excitation-contraction coupling. Nature 415:198-205.
17. Pieske, B., and Houser, S.R. 2003. [Na+]i handling in the failing heart. Cardiovasc Res 57:874-886.
18. Balaban, R.S. 2002. Cardiac Energy Metabolism Homeostasis: Role of Cytosolic Calcium. J Mol Cell Cardiol 34:1259-1271.
19. del Monte, F., Harding, S.E., Schmidt, U., Matsui, M., Bin Kang, Z., William, D., Gwathmey, J., Rosenzweig, A., and Hajjar, R.J. 1999. Restoration of Contractile Function in Isolated Cardiomyocytes From Failing Human Hearts by Gene Transfer of SERCA2a. Circulation 1000:2308-2311.

20. Haimoto, H., and Kato, K. 1988. S100a0 (alpha alpha) protein in cardiac muscle. Isolation from human cardiac muscle and ultrastructural localization. Eur J Biochem 171:409-415.

21. He, T.C., Zhou, S., da Costa, L.T., Yu, J., Kinzler, K.W., and Vogelstein, B. 1998. A simplified system for generating recombinant adenoviruses. Proc Natl Acad Sci U S A 95:2509-2514.

22. Parsa, C.J., Matsumoto, A., Kim, J., Riel, R.U., Pascal, L.S., Walton, G.B., Thompson, R.B., Petrofski, J.A., Annex, B.H., Stamler, J.S., et al. 2003. A novel protective effect of erythropoietin in the infarcted heart. J Clin Invest 112:999-1007.

23. Miyamoto, M.I., del Monte, F., Schmidt, U., DiSalvo, T.S., Kang, Z.B., Matsui, T., Guerrero, J.L., Gwathmey, J.K., Rosenzweig, A., and Hajjar, R.J. 2000. Adenoviral gene transfer of SERCA2a improves left-ventricular function in aortic-banded rats in transition to heart failure. Proc Natl Acad Sci U S A 97:793-798.

24. Strock, C., Cavagna, M., Pfeiffer, W., Sumbilla, C., Lewis, D., and Inesi, G. 1998. Direct demonstration of Ca^{2+} binding defects in sarco-endoplasmic reticulum Ca^{2+} ATPase mutants overexpressed in COS-1 cells transfected with adenovirus vectors. Journal of Biological Chemistry 273:15104-15109.

25. Yano, M., Ono, K., Ohkusa, T., Suetsugu, M., Kohno, M., Hisaoka, T., Kobayashi, S., Hisamatsu, Y., Yamamoto, T., Kohno, M., et al. 2000. Altered Stoichiometry of FKBP12.6 Versus Ryanodine Receptor as a Cause of Abnormal Ca^{2+} Leak Through Ryanodibe Receptor in Heart Failure. Circulation 102:2131-2136.

26. Yamaguchi, N., Xu, L., Pasek, D.A., Evans, K.E., and Meissner, G. 2003. Molecular Basis of Calmodulin Binding to Cardiac Muscle Ca^{2+} Release Channel (Ryanodine Receptor). Journal of Biological Chemistry 278:23480-23486.

27. Kiewitz R, Acklin C, Schafer BW, Maco B, Uhri KB, Wuytack F, Erne P, and CW., H. 2003. Ca(2+)-dependent interaction of S100A1 with the sarcoplasmic reticulum Ca(2+)-ATPase2a and phospholamban in the human heart. Biochem Biophys Res Commun. 306(2):550-557.

28. Despa, S., Islam, M.A., Pogwizd, S.M., and Bers, D.M. 2002. Intracellular [Na^+] and Na^+ pump rate in rat and rabbit ventricular myocytes. Journal of Physiology 539:133-143.

29. Arrio-Dupont, M., and de Nay, D. 1988. High-energy phosphates in quiescent, beating and contracted cardiac cells. Biochim Biophys Acta 934:264-268.

Chapter 4

Distinct subcellular location of the Ca^{2+}-binding protein S100A1 differentially modulates Ca^{2+}-cycling in ventricular rat cardiomyocytes

Patrick Most*, Melanie Boerries*, Carmen Eicher, Christopher Schweda, Mirko Völkers, Thilo Wedel, Stefan Söllner, Hugo A. Katus, Andrew Remppis, Ueli Aebi, Walter J. Koch and Cora-Ann Schoenenberger

* Both authors contributed equally to this study

4.1 Abstract

Calcium is a key regulator of cardiac function and is modulated through the Ca^{2+}-sensor protein S100A1. S100 proteins are considered to exert both intracellular and extracellular functions on their target cells. Here we report the impact of an increased intracellular S100A1 protein level on Ca^{2+}-homeostasis in neonatal ventricular cardiomyocytes in vitro. Specifically, we compare the effects of exogenously added recombinant S100A1 to those resulting from the overexpression of a transduced S100A1 gene. Extracellularly added S100A1 enhanced the Ca^{2+}-transient amplitude in NVCMs through a marked decrease in intracellular diastolic Ca^{2+}-concentrations ($[Ca^{2+}]_i$). The decrease in $[Ca^{2+}]_i$ was independent of sarcoplasmic reticulum Ca^{2+}-ATPase (SERCA2a) activity and was likely the result of an increased sarcolemmal Ca^{2+}-extrusion through the sodium-calcium exchanger (NCX). At the same time the Ca^{2+}-content of the sarcoplasmic reticulum (SR) decreased. These effects were dependent on the uptake of extracellularly added S100A1 protein and its subsequent routing to the endosomal compartment. Phospholipase C and protein kinase C that are tightly associated with this subcellular compartment, were found to be activated by endocytosed S100A1.

In contrast, adenoviral-mediated intracellular S100A1 overexpression enhanced the Ca^{2+}-transient amplitude in NVCMs mainly through an increase in systolic $[Ca^{2+}]_{i.}$ The increased Ca^{2+}-load in the SR was based on an enhanced SERCA2a activity while NCX function was unaltered. Overexpressed S100A1 co-localized with SERCA2a and other Ca^{2+}-regulatory proteins at the SR, whereas recombinant S100A1 protein that had been endocytosed did not co-localize with SR proteins. This study provides the first evidence that intracellular S100A1, depending on its subcellular location, modulates cardiac Ca^{2+}-turnover via different Ca^{2+}-regulatory proteins.

4.2 Introduction

S100A1 belongs to a multigenic family of small (Mr 9-13 x 10^3), non-ubiquitous Ca^{2+}-sensing proteins of the EF-hand type. S100 proteins, which exhibit a cell- and tissue-specific expression pattern, play a major role in intracellular Ca^{2+}-homeostasis. In addition, they have been linked to the Ca^{2+}-dependent regulation of a variety of intracellular activities such as cell proliferation and differentiation or the dynamics of cytoskeletal constituents (for review see (Donato, 2003; Heizmann and Cox, 1998; Zimmer et al., 1995). S100A1 is the most abundant S100 protein in striated muscle and predominantly expressed in the adult heart (Haimoto and Kato, 1988; Kato and Kimura, 1985). Recent gain-of function experiments have shown that increasing intracellular S100A1 protein levels in the adult heart and skeletal muscle resulted in enhanced Ca^{2+}-cycling and contractile function *in vitro* and *in vivo* (Most et al., 2001; Most et al., 2003b; Most et al., 2003c; Remppis et al., 2002; Remppis et al., 2004). The identification of S100A1 as a novel intracellular regulator of cardiac and skeletal muscle contractility may provide new impulses in the field of excitation-contraction coupling.

Although S100 proteins apparently lack the classic signaling sequences required for secretion, some S100 proteins seem to reach the extracellular space through secretory pathways that neither involve the common endoplasmic reticulum/Golgi nor the alternative interleukin-1 route (Rammes et al., 1997). From here, S100 proteins may exert an increasing number of downstream functions. For instance, S100B, S100A4 and S100A12 have been shown to promote differentiation of embryonic neurons (Mikkelsen et al., 2001; Novitskaya et al., 2000; Selinfreund et al., 1991). Moreover, S100B that had been secreted by astrocytes, was found to be internalized by neurons, where it influenced intracellular Ca^{2+}-levels ($[Ca^{2+}]_i$) and cellular excitability (Barger and Van Eldik, 1992; Kubista et al., 1999). Some extracellular activities of S100 proteins such as S100A12 and S100B are apparently mediated through interaction with the multiligand receptor for advanced glycation end products (RAGE) (Hofmann et al., 1999; Huttunen et al., 2000). Indeed, Roth and coworkers have shown that the S100A12/RAGE interaction plays an important role in the pathology of chronic inflammatory diseases such as bowel disease (Foell et al., 2003c), cystic fibrosis (Foell et al., 2003d), rheumatoid arthritis (Foell et al., 2003b), and vascular disorders (Foell et al.,

2003a). Importantly, Donato and colleagues have demonstrated that both RAGE-dependent and -independent extracellular effects of S100B are involved in the regulation of cell survival (Huttunen et al., 2000) and muscle development (Sorci et al., 2003; Sorci et al., 2004a; Sorci et al., 2004b). Although there is no evidence for S100A1 secretion from cardiac cells so far, a release into the extracellular space during myocardial damage has been reported (Kiewitz et al., 2000). We have recently shown that extracellularly added S100A1 is endocytosed by neonatal ventricular cardiomyocytes (NVCMs) in a RAGE-independent manner via a Ca^{2+}-dependent clathrin-mediated pathway (Most et al., 2003a). Subsequently, internalized S100A1 protected NVCMs from apoptosis via the specific activation of the extracellular signal-regulated kinase (ERK1/2) prosurvival pathway. Thus, similar to other S100 family members, S100A1 may act 'outside-in' and its extracellular presence may indicate a function as a paracrine factor in protecting the heart.

Since intracellular S100A1 plays an essential role in cardiac Ca^{2+}-handling we examined, whether extracellularly added S100A1 has a similar effect on myocardial Ca^{2+}-homeostasis. The present study compares the consequences of extracellularly added S100A1 to those of virally transduced S100A1 overexpression on Ca^{2+}-cycling in NVCMs *in vitro*.

4.3 Materials and Methods

Reagents

Thapsigargin (T-9033), tetracaine (T-7645), monodansylcadaverine (MDC) (M-4008) and caffeine (C-0750) were purchased from Sigma. Inhibitors for protein kinase A (PKA) (myr-PKI, 476485), protein kinase C (PKC) (calphostin-c, 208725) and phospholipase C (PLC) (U-73122, 662035) were obtained from Calbiochem. NCX inhibitor myr-FRCRCF was custom-made by Eurogentec (Belgium).

Expression and purification of human recombinant S100A1 protein

Human recombinant S100A1 was produced by an isopropylthiogalactosid (IPTG)-driven expression system in Escherichia coli and purified as described previously (Most et al.,

2003c). The coupling of S100A1 to tetramethyl-rhodamine (Rh-S100A1) was carried out by Eurogentec.

Generation of S100A1 adenovirus

The S100A1 adenovirus (AdS100A1) was generated by the use of the pAdTrack-CMV/pAdEasy-1 system as recently reported (Most et al., 2001). To facilitate identification of infected cells, AdS100A1 carried the green fluorescent protein reporter gene (GFP) in addition to the human S100A1 cDNA (accession number X58079). Each transgene was independently expressed under the control of a cytomegalovirus promotor sequence. To rule out that the infection procedure in itself had an effect on the amount of S100A1 in the cell, NVCM were infected with a corresponding adenovirus carrying GFP cDNA alone as a control (Adcontrol). Both replication-deficient adenoviruses were amplified in human embryonic kidney 293 cells (HEK 239), purified and enriched by cesium chloride centrifugation. Activity was tested by plaque assay.

Isolation and primary culture of neonatal rat ventricular cardiomyocytes

Ventricular cardiomyocytes from 1-2 day old neonatal hearts (NVCMs) were prepared as published in detail elsewhere (Most et al., 2003a). NVCMs were cultured in Dulbecco's modified Eagle's medium (DMEM; Biochrom) supplemented with penicillin/streptomycin (100 units/ml), L-glutamine (2 mM), and 1% fetal calf serum (FCS Gold; PAA Laboratories GmbH; DFCS) at 37°C in a 95% air/5% CO2 humidified atmosphere for 2-3 days. Adenoviral infection of NVCMs was carried out in serum-free HEPES-modified medium 199 (M199) with a multiplicity of infection (MOI) of 8 plaque forming units (pfu) per cell. After 4 hours incubation at 37°C in a 95% air/5% CO2 humidified atmosphere, medium was changed to DFCS. Efficiency of adenoviral gene transfer was monitored 24 hours later by GFP fluorescence. Approximately 95% of NVCMs were infected.

Incubation of NVCMs with recombinant S100A1 (1 μM) was performed in DFCS for 24 hours and mock-treated cells served as control.

Indirect immunofluorescence

Imaging of NVCMs was carried out as described (Most et al., 2003a). Briefly, 3-day old NVCMs grown on glass coverslips were either treated with Rh-S100A1 (1 μM) or S100A1 and GFP adenovirus (MOI 8 pfu/cell) as described above. After 24 hours cells were fixed, permeabilized and labeled with a polyclonal anti-S100A1 (SA 5632, Eurogentec; 1/300), a monoclonal anti-S100A1 (Sigma, 1/200), a monoclonal anti-SERCA2a (ABR; 1/500) or anti-RyR2 (ABR; 1/500) antibodies, followed by the corresponding Cy3-conjugated (Jackson Immuno Research Lab; 1/3000), Cy5-conjugated (Jackson Immuno Research Lab; 1/400) and ALEXA Fluor 488-conjugated (Alexis; 1/800) secondary antibodies. Polyclonal rabbit anti-SERCA2a antibody (1/1000) was a kind gift from Dr. F. Wuytack (Department of Molecular Cell Biology, Leuwen). Confocal images (CLSM) were obtained using a 100 x oil objective on a Leica TCS SP laser scanning confocal microscope. Digitized confocal images were processed by Leica software and Adobe Photoshop.

Intracellular Ca^{2+}-calibration and Ca^{2+}-imaging in field-stimulated cardiomyocytes

Calibration and measurement of intracellular Ca^{2+}-transients in field-stimulated NVCMs using the Ca^{2+}-fluorescent dye FURA2-AM was carried out as described in detail by (Most et al., 2003b). Analysis of steady state Ca^{2+}-transients at 1 Hz, 37°C and 2 mM $[Ca^{2+}]_e$ was performed with T.I.L.L Vision software (version 4.01). Baseline data from five consecutive steady-state transients were averaged for analysis of transient amplitude (Ca^{2+} amplitude; [nM]), diastolic Ca^{2+}-levels ([nM]) and transient decay (t; [ms]). The sarcoplasmic reticulum (SR) Ca^{2+}-load and sodium-calcium exchanger (NCX) activity were assessed by changes in the transient amplitude ([nM]) and decay (t; [ms]), respectively, of quiescent NVCMs in modified Tyrode solution (mM: 140 NaCl, 6 KCl, 1 $MgCl_2$, 2 $CaCl_2$, 10 glucose, 5 HEPES), subjected to rapid caffeine application (10 mM) after 5 seconds rest. Exchange against sodium- and calcium-free Tyrode solution (choline chloride and EGTA replaced NaCl and $CaCl_2$, respectively) was used to block NCX current during the decay of the caffeine-induced transient. Myr-FRCRFC (30 μM) was used to inhibit NCX current in field-stimulated NVCMs. Free intracellular Ca^{2+} concentration $[Ca^{2+}]_i$ was calculated by the equation of Grynkiewicz

et al; $[Ca^{2+}]_i$ = Kd x ß x ((R - Rmin)/(Rmax – R)). The Ca^{2+}-transient amplitude was calculated as the difference between calibrated systolic and diastolic $[Ca^{2+}]_i$. Data sets represent analysis of 50 cells from three different preparations.

Protein expression analysis

To assess protein expression of S100A1 (Sigma, S-2407, 1/500), sarcoplasmic reticulum Ca^{2+}-ATPase (SERCA2a; Biomol SA209, 1/5000), sodium-calcium exchanger (NCX; ABR MA3-926, 1/5000), and cardiac actin (Progen Ac1-20.4.2, 1/10000), Western blotting from whole cell homogenates of NVCMs was carried out as previously described (Most et al., 2003b). Briefly, cells were washed three times with EGTA/EDTA buffer (PBS, pH 7.4, containing 2 mM EGTA/EDTA), scraped off the dish, and immediately homogenized in EGTA/EDTA buffer. Homogenates were centrifuged for 10 min at 15.000 g and the supernatant was used for biochemical analysis. S100A1 protein was concentrated by sequential size exlusion centrifugation columns (Amicon; Microcon YM-100 and -3).

Statistical analysis

Data are presented as mean ± s.e.m. Unpaired two-tail student´s t-test and a two way repeated ANOVA analysis was performed to test for differences between groups. A value of $P<0.05$ was accepted as statistically significant.

4.4 Results

Adenoviral-mediated S100A1 overexpression and endocytosis of extracellular S100A1 yield a distinct subcellular location of S100A1 in neonatal ventricular cardiomyocytes

To examine the effects of an increased S100A1 protein level on the cycling of cytosolic Ca^{2+} in neonatal rat ventricular cardiomyocytes (NVCMs), we employed two different procedures (Figure 4.1): the NVCMs were either transduced by means of an adenoviral S100A1-expression construct, (AdS100A1 cells, Figure 4.1A) or incubated for 24 hours with DFCS containing 1 μM recombinant human S100A1 protein (Figure 4.1C). As illustrated in Figure 4.1, overexpressed S100A1 mainly displayed a fine granular network-like pattern. In addi-

tion, small amounts were detected in the nucleus. This pattern corresponds to the distribution of endogenous S100A1 observed in control cells (Figure 4.1B). Westernblotting using an antibody that reacts with both human and rat S100A1 showed that adenoviral-mediated S100A1 gene delivery to NVCMs resulted in approximately 3-fold higher amounts of total S100A1 protein compared to the level of endogenous S100A1 in control cells infected with an adenoviral construct lacking the S100A1 gene (panel Figure 4.1A). Equivalent protein loadings were confirmed by comparable cardiac actin levels.

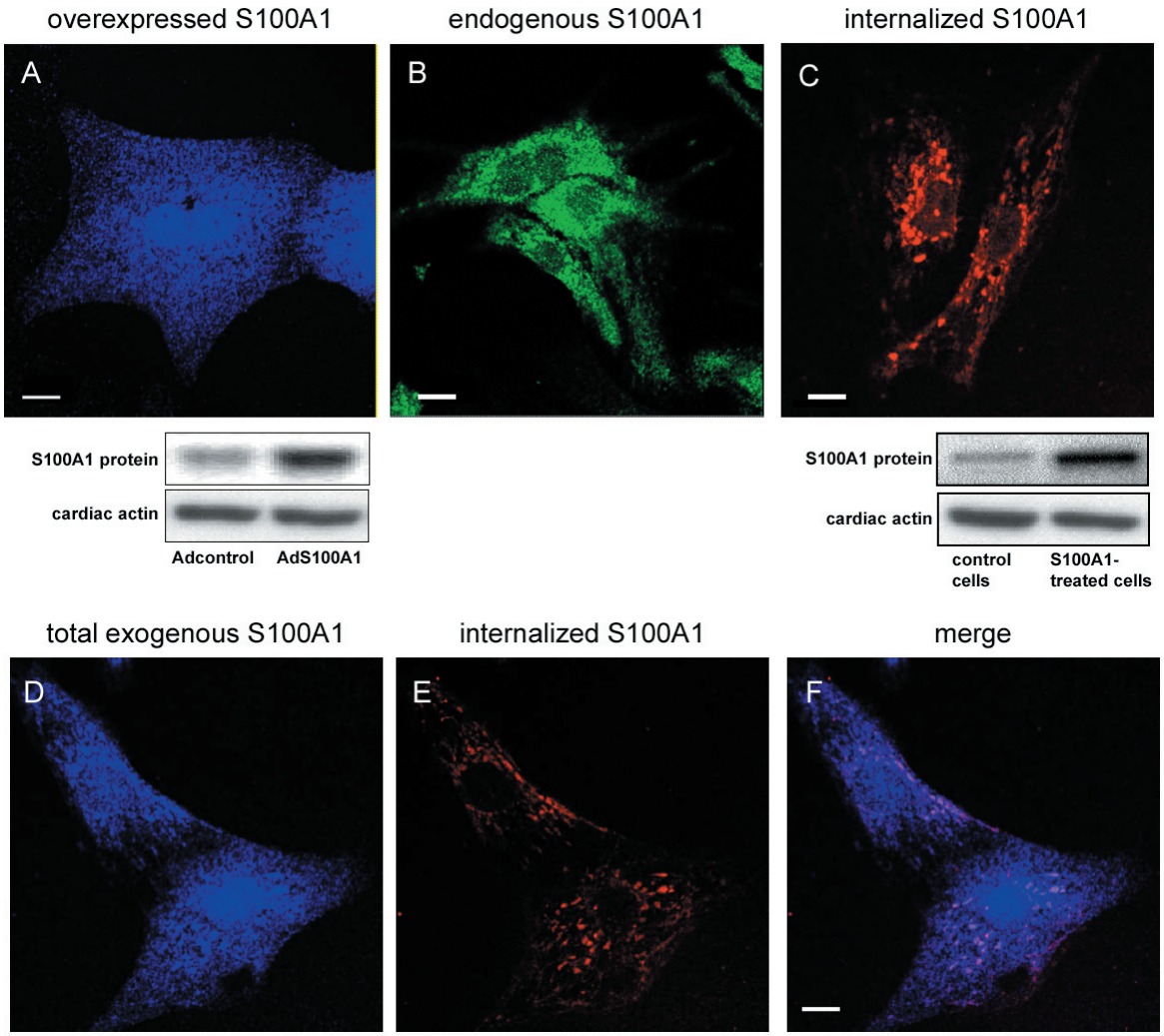

Figure 4.1: Subcellular location of overexpressed, internalized and endogenous S100A1.
A, Overexpressed S100A1 (AdS100A1; blue) is detected by an antibody that specifically reacts with S100A1. Western blot analysis comparing levels of S100A1 (upper panel) and cardiac actin (lower panel) expression in homogenates of Adcontrol and AdS100A1-transduced NVCMs. B, Immunostaining of endogenous S100A1 (green) in untreated NVCMs reveals a fine granular network-like pattern (control). C, Vesicular accumulation of internalized Rh-S100A1 protein (red) in the perinuclear region and in the cytosol of S100A1-treated cells. Western blot analysis comparing levels of S100A1 (upper panel) and cardiac actin (lower panel) in homogenates from S100A1-treated and control NVCMs. D,E,F AdS100A1-transduced cells were incubated for 1 hour with Rh-S100A1 twenty-four hours post infection, and then immunolabeled with an antibody that specifically reacts with human S100A1.

D, The anti-human S100A1/Cy5-anti-rabbit antibody detects internalized Rh-S100A1 as well as overexpressed S100A1 protein (total exogenous S100A1). E, Vesicular accumulation of internalized Rh-S100A1 protein in the perinuclear region and in the cytosol. F, Overlay of both D and F shows that internalized Rh-S100A1 (violet) exhibits a distinct distribution compared to overexpressed S100A1 (blue). Bar, 10 μm.

As an alternative approach to achieve an increase of the intracellular S100A1 level in NVCMs, we incubated cells for 24 hours in medium containing 1 μM rhodamine-coupled recombinant human S100A1 (Rh-S100A1). The CSLM image shown in Figure 4.1C reveals an intracellular perinuclear accumulation of Rh-S100A1. This finding is consistant with our recently published data, which shows that following endocytosis via a Ca^{2+}-dependent calthrin-mediated process, the extracellularly added S100A1 is routed to the endosomal compartment (Most et al., 2003a). The uptake of S100A1 caused an almost 4-fold increase of intracellular S100A1 in NVCMs compared to mock-treated control cells (panel Figure 4.1C). To directly correlate the distribution of exogenous S100A1 resulting from the two different procedures, we incubated AdS100A1 cells for 1 hour with Rh-S100A1 protein (1 μM) 24 hours after adenoviral infection (Figure 4.1D to F). As in the individually treated cells, the internalized recombinant human Rh-S100A1 (red, Figure 4.1E) displayed a vesicular-like endosomal localization in AdS100A1 cells. When immunolabeld with a polyclonal antibody that specifically recognizes the hinge region of human S100A1, both S100A1 populations were recognized in the S100A1-treated AdS100A1 cells (blue, Figure 4.1D). Superimposing the CSLM image of total exogenous S100A1 with the internalized Rh-S100A1 (Figure 4.1F) confirmed that the localization of internalized Rh-S100A1 (violet) was clearly distinct from the fine granular network-like pattern of overexpressed human S100A1 (blue).

Elevated S100A1 enhances cytosolic Ca^{2+}-turnover in neonatal ventricular cardiomyocytes

As illustrated by the Ca^{2+}-transients in Figure 4.2, the overexpression of S100A1 in AdS100A1-transduced NVCMs gave rise to an enhanced cytosolic Ca^{2+}-cycling compared to control cells. The overall enhanced Ca^{2+}-cycling was reflected by an increased amplitude of Ca^{2+}-transients in AdS100A1 cells (Figure 4.2B). The larger amplitude was predominantly due to an S100A1-induced rise of systolic $[Ca^{2+}]_i$ as indicated by the higher peak in

AdS100A1-transduced NVCMs (Figure 4.2A, bar). Concomitantly, S100A1 overexpression also decreased diastolic $[Ca^{2+}]_i$ (Figure 4.2C), which was associated with a reduction in the Ca^{2+}-transient decay-constant t (Figure 4.2D).

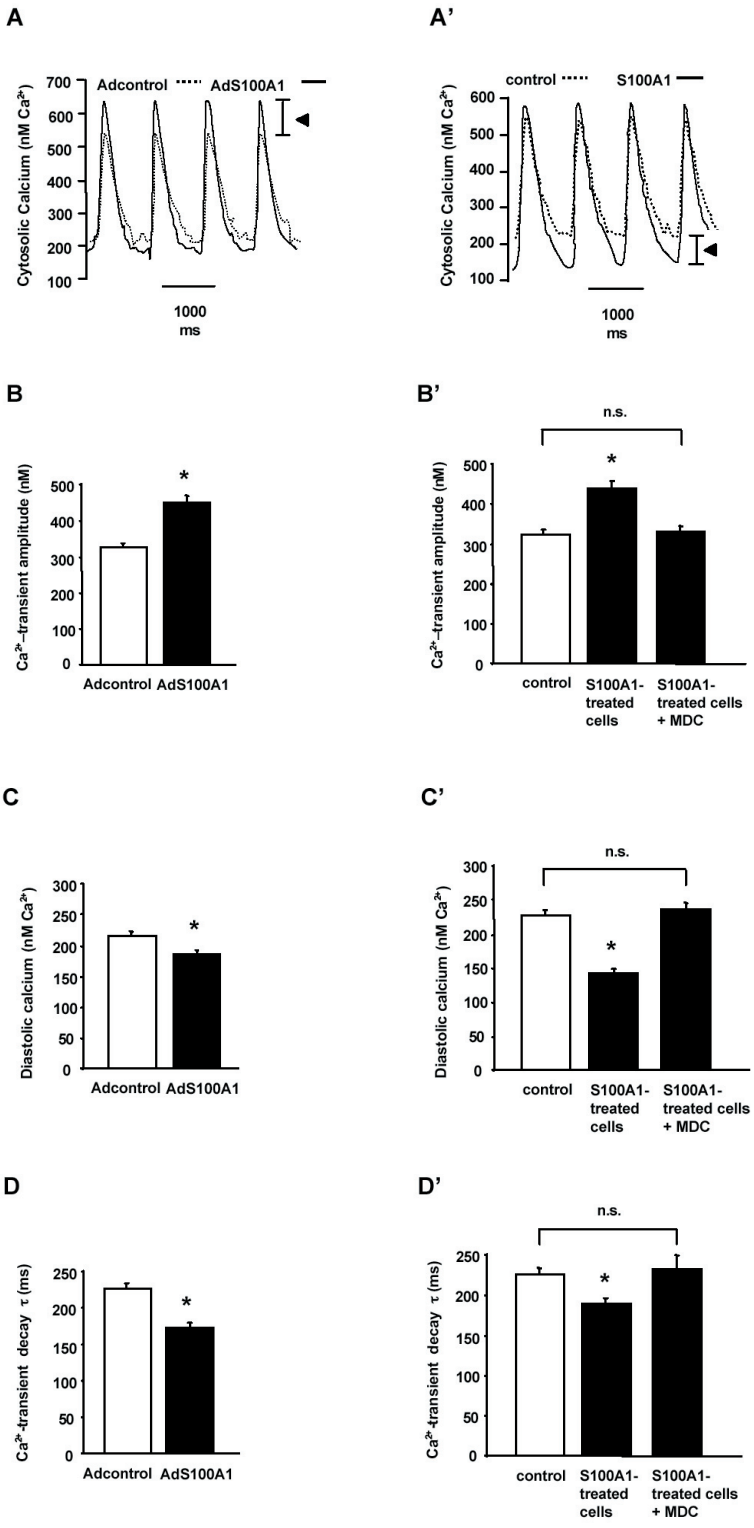

Figure 4.2: Overexpressed and internalized S100A1 enhance cytosolic Ca^{2+}-turnover in neonatal ventricular cardiomyocytes.
A to D, Adenoviral-transduced NVCMs overexpressing S100A1. A, Superimposed tracings of calibrated Ca^{2+}-transients in S100A1-overexpressing (AdS100A1, solid line) and control (Adcontrol, dashed line) NVCMs. Note the gain in systolic $[Ca^{2+}]_i$ in S100A1-overexpressing NVCMs (bar). B, C and D, Effects of increased S100A1 protein level on Ca^{2+}-transients. Compared to control cells expressing endogenous levels of S100A1, S100A1 overexpression significantly increases the Ca^{2+}-transient amplitude (AdS100A1 454±22 nM vs. Adcontrol 311±11 nM; 1B), lowers diastolic $[Ca^{2+}]_i$ (AdS100A1 181±14 nM vs. Adcontrol 219±12 nM; 1C), and accelerates the decay of the Ca^{2+}-transient (t, AdS100A1 172±14 ms vs. Adcontrol 223±11 ms; 1D). n=150 cells from three different cell preparations. Data are given as mean±S.E.M.
A'to D', NVCMs treated with 1 μM human recombinant S100A1. A', Superimposed tracings of calibrated Ca^{2+}-transients in S100A1-treated (S100A1, solid line) and mock-treated (control, dashed line) NVCMs. The decrease in diastolic $[Ca^{2+}]_i$ in S100A1-treated NVCMs is indicated by the bar. B', S100A1-uptake increases the Ca^{2+}-transient amplitude (S100A1-treated 442±23 nM vs. control 324±15 nM). C', The effects of an increased S100A1 level are a reduction of diastolic $[Ca^{2+}]_i$ (S100A1-treated 143±13 nM vs. control 236±14 nM) and D', an accelerated decay of the Ca^{2+}-transient (t, S100A1-treated 182±16 ms vs. control 232±10 ms). Preincubation with monodansylcadaverine (MDC, an inhibitor of clathrin-mediated endocytosis) abolished the effects of extracellularly added S100A1 on the Ca^{2+}-turnover (* P<0.01 vs. no inhibitor).

Similar to S100A1 overexpression in AdS100A1 cells, uptake of S100A1 also had an effect on the Ca^{2+}-transients recorded in S100A1-treated cells (Figure 4.2A'). Accordingly, they exhibited an increased amplitude (Figure 4.2B'), indicating that the rise in intracellular S100A1 caused an increased cytosolic Ca^{2+}-turnover in S100A1-treated NVCMs. However, in contrast to Ca^{2+}-transients of cells with adenoviral-mediated S100A1 overexpression, the amplitude of S100A1-treated cells was primarly increased by a marked reduction of diastolic $[Ca^{2+}]_i$, and to a lesser extent by elevated systolic $[Ca^{2+}]_i$ (Figure 4.2A', bar and 4.2C'). For both, overexpression and uptake from the extracellular environment, increased S100A1 levels accelerated diastolic Ca^{2+}-elimination as indicated by a decrease in the Ca^{2+}-transient decay-constant t (Figure 4.2D and 4.D').

To test whether binding of extracellular S100A1 to NVCMs was sufficient to induce an improved cytosolic Ca^{2+}-cycling or whether endocytosis was required, NVCMs were treated with recombinant S100A1 in the presence of monodansylcadaverine (MDC, 50 μM), which was shown to effectively prevent S100A1 uptake (Most et al., 2003a). As illustrated by the Ca^{2+}-transients, the presence of MDC precluded changes in the amplitude (Figure 4.2B') and diastolic $[Ca^{2+}]_i$ (Figure 4.2C') as well as in the decay of the Ca^{2+}-transient (Figure 4.2D').

Together these results show that an augmented intracellular S100A1 protein level in NVCMs increase cytosolic Ca^{2+}-turnover. More specifically, we observe a differential effect of adenoviral-mediated S100A1 overexpression versus increased S100A1 following endocytosis: higher systolic Ca^{2+}-peaks are responsible for the increased amplitude of Ca^{2+}-transients in NVCMs overexpressing S100A1 while a marked decrease in diastolic $[Ca^{2+}]_i$ largely accounts for the increased amplitude of Ca^{2+}-transients in cells after endoyctosis of extracellular S100A1.

Overexpressed but not endocytosed S100A1 colocalizes with sarcoplasmic Ca^{2+}-regulatory proteins

We next examined whether the differential effect of overexpressed and internalized S100A1 on Ca^{2+}-turnover was associated with the distinct subcellular location of S100A1. Since S100A1 protein has previously been shown to co-immunoprecipitate with cardiac

SR Ca^{2+}-regulatory proteins in human myocardium (Kiewitz et al., 2003), we examined the distribution of the SR Ca^{2+}-ATPase (SERCA2a) and its potential association with S100A1 in NVCMs with an increased level of S100A1 compared to control cells by immunolabeling with anti-SERCA2a antibodies (Figure 4.3).

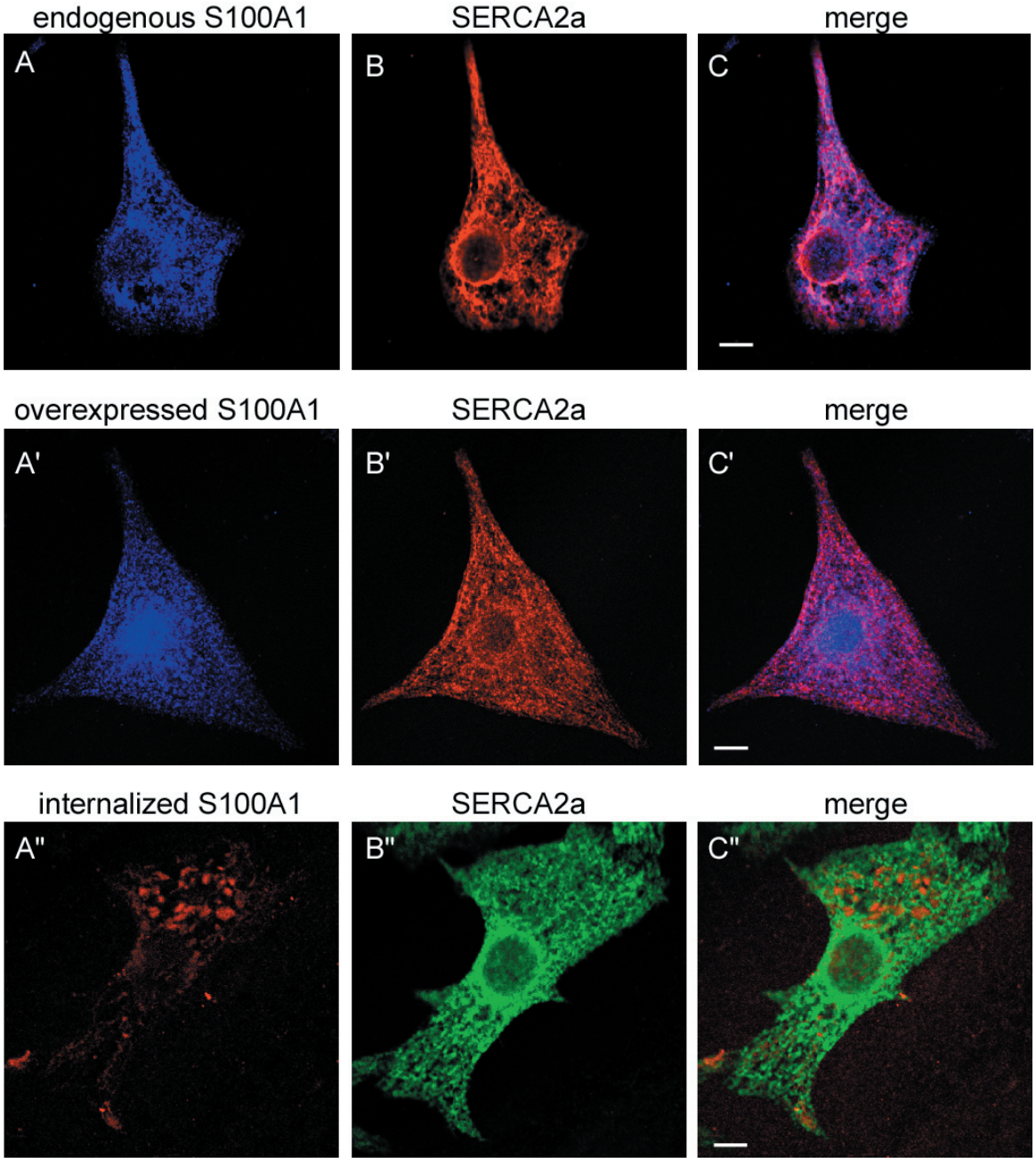

Figure 4.3: Overexpressed but not internalized S100A1 colocalizes with SERCA2a at the SR. Immunolocalization of S100A1 and SERCA2a. A, Endogenous S100A1 labeled with a monoclonal anti-S100A1/Cy5-anti-mouse antibody in control cells. A', Overexpressed S100A1 detected with a polyclonal anti-human S100A1/Cy5–anti-rabbit antibody in AdS100A1-transduced NVCMs. A'', Internalized Rh-S100A1. B, Immunolabeling of SERCA2a in control, B', AdS100A1-infected, B'', and Rh-S100A1-treated NVCMs. C, Overlay of panels A and B, and C', A' and B' depicts colocalization of endogenous and overexpressed S100A1 with SERCA2a (violet). C'', Internalized Rh-S100A1 does not co-localize. Bar, 10 μm (C ') and 5 μm (C,C'').

To rule out that the adenoviral transduction procedure by itself caused a translocation of SERCA2a, we first established that its distribution in cells infected with a control virus was similar to that in uninfected NVCMs expressing only endogenous S100A1 (data not shown). Subsequently, the distribution of S100A1 in control cells (blue, Figure 4.3A,C), in AdS100A1 NVCMs (blue, Figure 4.3A',C') and in S100A1-treated cells (red, Figure 3A'',C'') was compared to the location of immunolabeled SERCA2a (Figure 4.3B,B',B''). Merging the corresponding confocal images clearly showed that overexpressed S100A1 and endogenous S100A1 partially colocalized with the SR Ca^{2+}-pump (violet, Figure 4.3C,C'). Conversely, as illustrated in Figure 4.3A'' to C'', internalized Rh-S100A1 protein (red) did not colocalize with the reticular distribution of SERCA2a (green).

In conclusion, the immuno-localization studies revealed that depending on the experimental procedure employed to increase S100A1 levels, S100A1 was routed to a different cellular compartment. Consequently, an association of S100A1 with the SR was only observed in AdS100A1-transduced NVCMs.

Enhanced Ca^{2+}-turnover in AdS100A1-transduced NVCMs is based on SR Ca^{2+}-cycling

Because overexpressed S100A1 was associated with SERCA2a at the SR, we tested the influence of SERCA2a antagonists on the efficiency of Ca^{2+}-cycling in AdS100A1- as well as in S100A1-treated NVCMs. Because Ca^{2+}-cycling in infected control cells and mock-treated NVCMs was indistinguishable, the two groups were pooled and are hereafter referred to as control NVCMs. As documented in Figure 4.4A, a reduced amplitude in Ca^{2+}-transients of control NVCMs indicated that the SERCA2a-mediated Ca^{2+}-uptake into the SR was inhibited by thapsigargin (1 μM). Incubation of AdS100A1-cells with this SERCA2a inhibitor completely abolished the S1000A1-induced gain in the Ca^{2+}-transient amplitude (Figure 4.4A). The Ca^{2+}-transients in thapsigargin-treated NVCMs did not significantly differ with respect to the diastolic Ca^{2+}-load or the decay rate between AdS100A1-transduced and control NVCMs: thapsigargin inhibition of SERCA2a equally raised diastolic $[Ca^{2+}]_i$ (Figure 4.4B) and prolonged SR resequestration (Figure 4.4C). In contrast, the enhancement

of the Ca^{2+}-transient amplitude in S100A1-treated NVCMs was not affected by thapsigargin (Figure 4.4A).

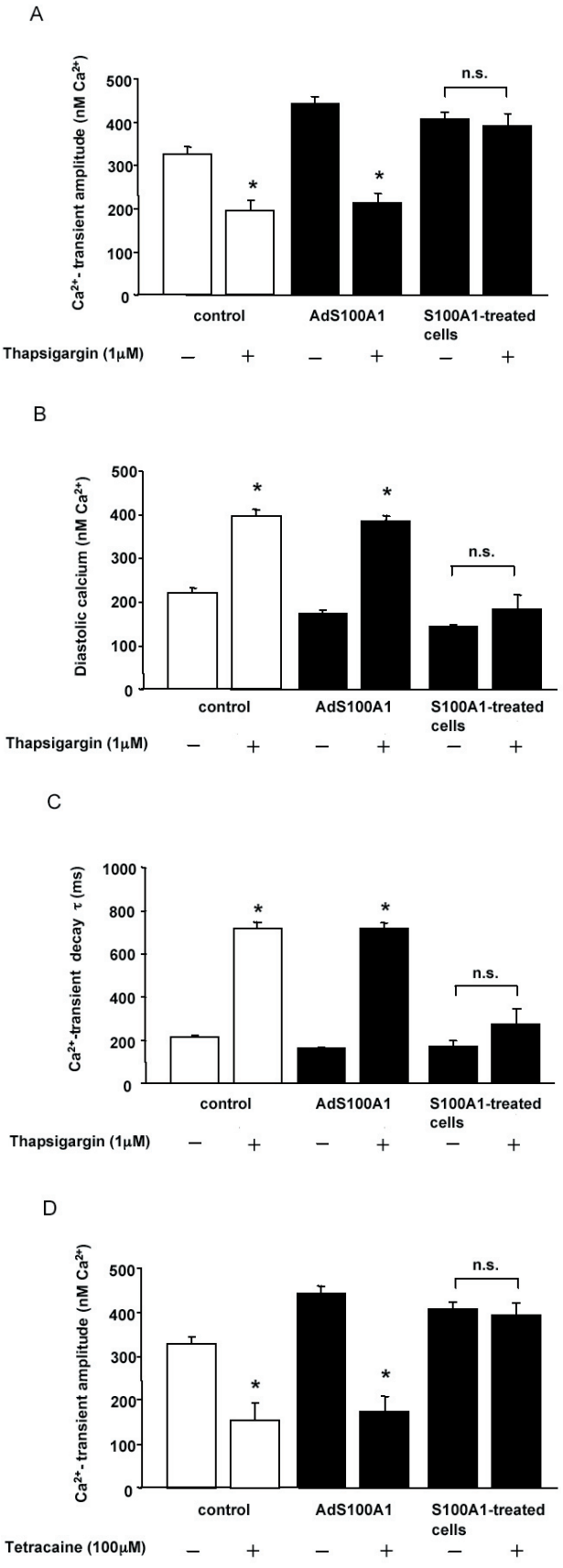

Figure 4.4: Inhibition of SR Ca^{2+}-fluxes abolishes enhanced Ca^{2+}-cycling in S100A1 overexpressing but not in S100A1-treated NVCMs.
A, Addition of the SERCA2a inhibitor thapsigargin (1 μM) abolishes the S100A1-induced increase in the Ca^{2+}-transient amplitude in overexpressing (AdS100A1) but not S100A1-treated NVCMs. B, Thapsigargin reduces diastolic $[Ca^{2+}]_i$ in control and S100A1 overexpressing cells whereas S100A1-treated cells are not significantly affected. C, SERCA2a inhibition raises the decay-constant t in control and AdS100A1-infected NVCMs but does not significantly alter t in S100A1-treated NVCMs. D, Tetracaine (100 μM), an inhibitor of the SR Ca^{2+}-release channel (RyR), abrogates the increased Ca^{2+}-transient amplitude in S100A1 overexpressing NVCMs but does not significantly reduce the augmented amplitude of the Ca^{2+}-transient in S100A1-treated NVCMs relative to tetracaine-treated control cells. * P<0.01 vs. control. Measurements represent n=150 cells from three independent cell preparations. Data are given as mean±S.E.M.

Moreover, inhibition of SERCA2a had virtually no effect on the decreased diastolic $[Ca^{2+}]_i$ (Figure 4.4B) and accelerated cytosolic Ca^{2+}-elimination (Figure 4.4C) in S100A1-treated NVCMs. Like thapsigargin, inhibition of SR Ca^{2+}-release by tetracaine (100 μM), a blocker of the SR Ca^{2+}-release channel/ryanodine receptor (RyR2), decreased the amplitude of the Ca^{2+}-transient in control NVCMs and completely abolished the gain in the Ca^{2+}-transient amplitude in S1000A1 overexpressing NVCMs (Figure 4.4D). However, tetracaine had no effect on the augmented Ca^{2+}-transient amplitude in S100A1-treated NVCMs (Figure 4D). Consistent with these findings, immunofluorescence studies indicated that internalized S100A1 did not colocalize with SERCA2a (Figure 4.3) or RyR2 (data not shown).

Since the data suggested that the increased efficiency of Ca^{2+}-turnover in S100A1 overexpressing but not in S100A1-treated NVCMs depended on SR Ca^{2+}-fluxes, we next investigated the SR Ca^{2+}-load in both groups. To address this issue, AdS100A1-infected and S100A1-treated NVCMs were exposed to caffeine (10 mM) and the amplitude of caffeine-releasable SR Ca^{2+} served as an indirect measure of the SR Ca^{2+}-content. As depicted in Figure 4.5A, S100A1 overexpression caused an increase in the caffeine-induced Ca^{2+}-transient amplitude while internalized S100A1 apparently reduced the SR Ca^{2+}-load compared to the control.

Changes in NCX activity might be involved in modulating sarcolemmal Ca^{2+}-fluxes in response to S100A1

Cytosolic Ca^{2+}-turnover in NVCMs not only invokes the SR, but is simultaneously regulated by sarcolemmal Ca^{2+}-fluxes. The sodium-calcium exchanger (NCX) is a major regulator of sarcolemmal Ca^{2+}-fluxes. Analysis of the decay-constant t of the caffeine-induced Ca^{2+}-transients, which served as a measure for NCX-mediated sarcolemmal Ca^{2+}-extrusion, revealed unchanged kinetics in AdS100A1-transduced NVCMs compared to cells infected with a control construct (Figure 4.5B). Thus, it appears that overexpressed S100A1 does not affect NCX activity. Conversely, in S100A1-treated NVCMs t of the caffeine-induced Ca^{2+}-transients was decreased compared to mock-treated NVCMs (control, Figure 4.5). This finding indicated that the increased S100A1 level in the endosomal compartment could be responsible for the accelerated decay of the caffeine-mediated rise in cytosolic $[Ca^{2+}]_i$.

Since the NCX forward-mode mainly accounts for trans-sarcolemmal Ca^{2+}-efflux, the influence of NCX inhibition in S100A1-treated cells was studied. Selective NCX inhibition was achieved by rapidly replenishing the medium with sodium/calcium-free medium (Bassani et al., 1994; Despa et al., 2002). As documented by the caffeine-induced Ca^{2+}-transients in Figure 4.5C, this regimen effectively abrogated the S100A1-mediated acceleration of the Ca^{2+}-transient decay.

This finding suggests that endocytosed S100A1 decreases diastolic $[Ca^{2+}]_i$ through enhanced sarcolemmal Ca^{2+}-extrusion, possibly involving an increased NCX forward-mode activity.

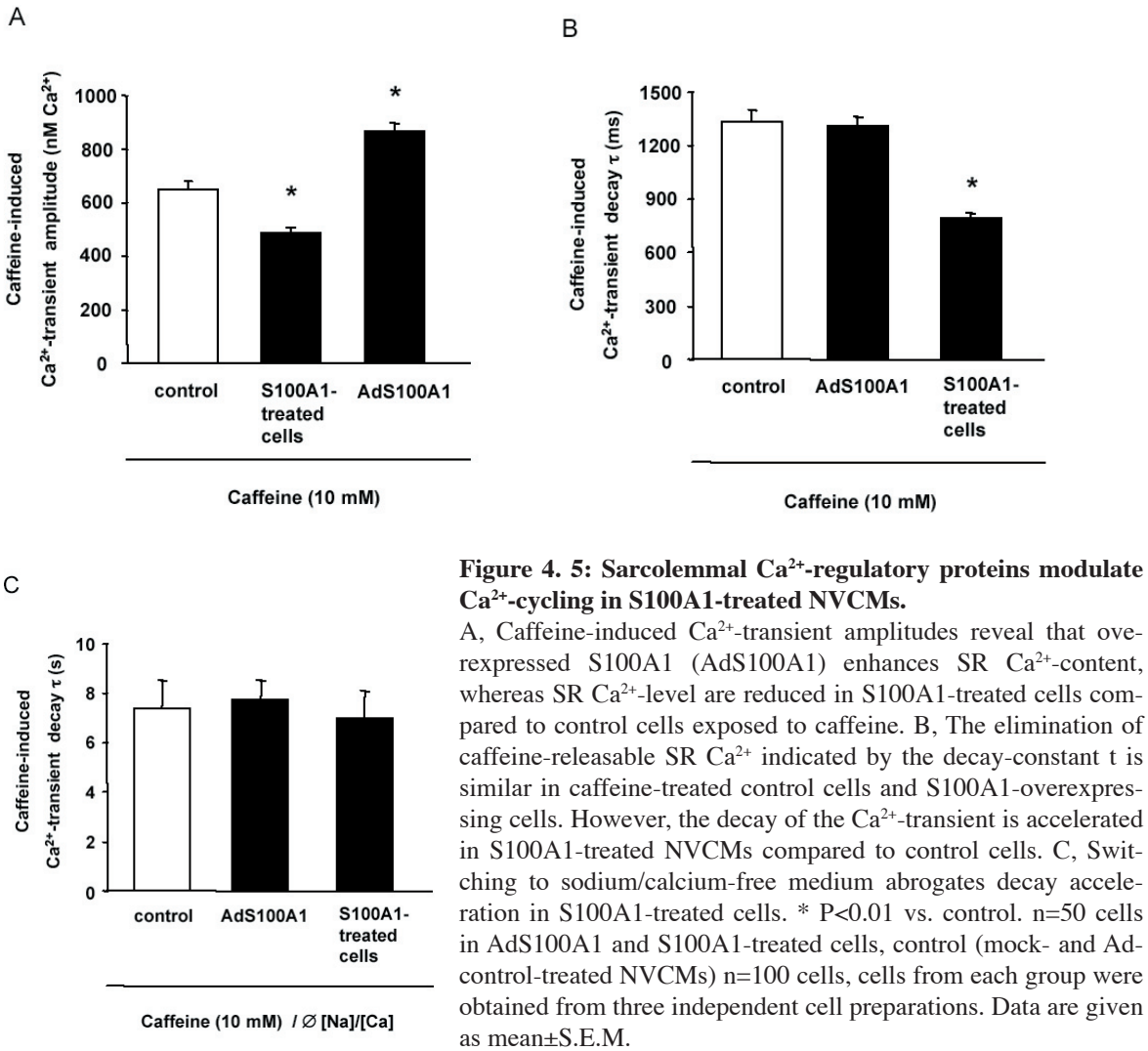

Figure 4. 5: Sarcolemmal Ca^{2+}-regulatory proteins modulate Ca^{2+}-cycling in S100A1-treated NVCMs.
A, Caffeine-induced Ca^{2+}-transient amplitudes reveal that overexpressed S100A1 (AdS100A1) enhances SR Ca^{2+}-content, whereas SR Ca^{2+}-level are reduced in S100A1-treated cells compared to control cells exposed to caffeine. B, The elimination of caffeine-releasable SR Ca^{2+} indicated by the decay-constant t is similar in caffeine-treated control cells and S100A1-overexpressing cells. However, the decay of the Ca^{2+}-transient is accelerated in S100A1-treated NVCMs compared to control cells. C, Switching to sodium/calcium-free medium abrogates decay acceleration in S100A1-treated cells. * $P<0.01$ vs. control. n=50 cells in AdS100A1 and S100A1-treated cells, control (mock- and Ad-control-treated NVCMs) n=100 cells, cells from each group were obtained from three independent cell preparations. Data are given as mean±S.E.M.

To further explore the influence of endocytosed S100A1 protein on NCX activity, we studied the impact of myristylated (myr)-FRCRCFa, a specific NCX blocker on diastolic $[Ca^{2+}]_i$ in S100A1-treated field-stimulated NVCMs. Myr-FRCRCFa is a novel, cell-permeable peptide inhibitor of NCX that alters neither L-type Ca^{2+}-channel/dihydropyridine receptor (LCC) nor Na^+- or K^+-channel activity, and appears to exhibit a higher degree of selectivity compared to other widely used NCX-inhibitors such as KB-R7943 or SEA0400 (Convery et al., 1998; Hobai et al., 1997; Khananshvili et al., 1995; Reuter et al., 2002). Administration of 30 μM myr-FRCRCFa caused a large rise in diastolic $[Ca^{2+}]_i$ in control cells and abrogated the S100A1-mediated decrease in diastolic $[Ca^{2+}]_i$ treated cells (Figure 4.6A).

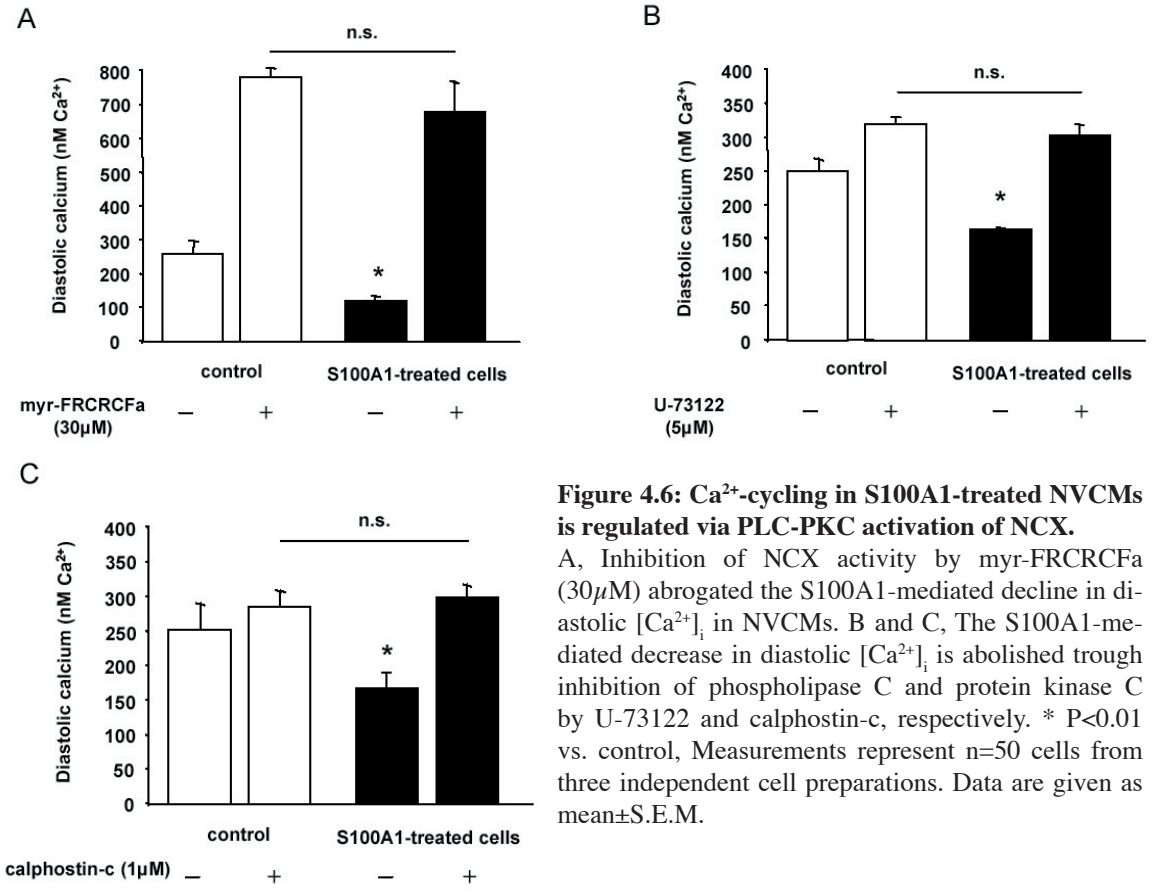

Figure 4.6: Ca^{2+}-cycling in S100A1-treated NVCMs is regulated via PLC-PKC activation of NCX.
A, Inhibition of NCX activity by myr-FRCRCFa (30μM) abrogated the S100A1-mediated decline in diastolic $[Ca^{2+}]_i$ in NVCMs. B and C, The S100A1-mediated decrease in diastolic $[Ca^{2+}]_i$ is abolished trough inhibition of phospholipase C and protein kinase C by U-73122 and calphostin-c, respectively. * P<0.01 vs. control, Measurements represent n=50 cells from three independent cell preparations. Data are given as mean±S.E.M.

Given that endocytosed S100A1 activates the PLC-PKC-p44/42 pathway (Most et al., 2003a) and PKC is known to stimulate NCX function (Iwamoto et al., 1996), we investigated whether triggering a corresponding pathway may be involved in increasing NCX activity in S100A1-treated NVCMs. Incubation with U73122 (5 μM), an inhibitor of PLC, resulted in a significant increase in diastolic $[Ca^{2+}]_i$ in S100A1-treated NVCMs (Figure 4.6B). Similar

results were obtained after addition of calphostin-c (1 μM), a PKC-inhibitor (Figure 4.6C) indicating that enhanced cyotosolic $[Ca^{2+}]_i$ removal by endocytosed S100A1 might involve PLC and PKC. Notably, PD98095 (10 μM) as well as myr-PKI (5 μM), specific inhibitors of MEK1 and PKA, respectively, failed to inhibit the S100A1-mediated decrease in diastolic $[Ca^{2+}]_i$ (data not shown).

Increased S100A1 protein levels do not affect abundance of Ca^{2+}-regulatory proteins

Because increased S100A1 levels in NVCMs impinged on Ca^{2+}-regulatory proteins we assessed the abundance of NCX and SERCA protein in S100A1-treated and AdS100A1-transduced NVCMs. As shown by representative immunoblots in Figure 4.7, neither endocytosis nor overexpression of S100A1 altered the levels of NCX and SERCA2a compared to control cells.

These findings suggest that the changes in Ca^{2+}-cycling seen in response to an increase of intracellular S100A1 are based on the altered activity of Ca^{2+}-regulatory proteins rather than their amounts.

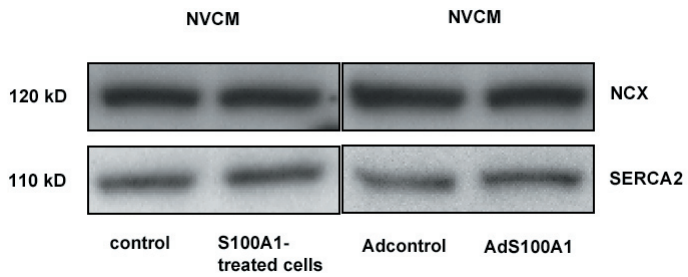

Figure 4. 7: Increased level of S100A1 does not alter expression of Ca^{2+}-regulatory proteins.
A, Western blots of extracts from control, S100A1-treated, AdS100A1- and Adcontrol-transduced cells probed with specific antibodies. Levels of NCX and SERCA2a remain constant despite the increased levels of S100A1.

Discussion

S100 Ca^{2+}-binding proteins have been associated with a variety of intracellular Ca^{2+}-mediated processes (Heizmann and Cox, 1998). Binding of Ca^{2+} induces a conformational change in the three-dimensional structure and enables these proteins to interact with target proteins thereby transducing the intracellular Ca^{2+}-signal (Wang et al., 2001). Recent fin-

dings involving S100A1 gene transfer into ventricular cardiomyocytes have demonstrated that S100A1 overexpression enhances cytosolic Ca^{2+}-cycling and contractile properties both *in vitro* and *in vivo* (Most et al., 2001; Most et al., 2003b; Most et al., 2003c; Remppis et al., 2002; Remppis et al., 2004). Consistently, S100A1-deficient mice display an impaired cardiac contractility in response to hemodynamic stress (Du et al., 2002). These studies promote S100A1 as a novel key regulator of cardiac function. In addition, recent studies from our laboratory provide evidence that S100A1 may also act on ventricular cardiomyocytes through an unrelated mechanism: uptake of S100A1 from the extracellular environment protects cells from apoptosis induced by reactive oxygen species or 2-deoxyglucose (Most et al., 2003a). This downstream effect apparently relies on RAGE-indepedent endocytosis of extracellular S100A1 and involves the activation of the PLC-PKC-ERK1/2 prosurvival pathway. A number of studies support the notion that extracellular S100 proteins may have distinct functions in cellular physiology and pathology. For example, S100A4 was reported to stimulate the outgrowth of neurite cells (Novitskaya et al., 2000), whereas S100B has been shown to be involved in the regulation of cell differentiation and survival (Huttunen et al., 2000; Sorci et al., 2003; Sorci et al., 2004a; Sorci et al., 2004b). Another example is S100A12, which has been implicated as an important pro-inflammatory regulator in numerous chronic inflammatory diseases (Foell et al., 2003a; Foell et al., 2003b; Foell et al., 2003c; Foell et al., 2003d). Notably, release of S100A1 into the extracellular space in reponse to ischemic cadiac injury has been reported (Kiewitz et al., 2000) but it is unclear whether extracellular S100A1 might affect Ca^{2+}-homeostasis in ventricular cardiomyocytes. In the present study we addressed this issue by comparing the effects of S100A1 added to the extracellular environment to the effects of adenoviral-mediated S100A1 overexpression on cardiac Ca^{2+}-cycling *in vitro*.

The model illustrated in Figure 4.8 summarizes the data presented in this paper. First, we show that recombinant S100A1 added to the extracellular environment is internalized and subsequently modulates cytosolic Ca^{2+}-cycling in ventricular cardiomyocytes (Figure 4.8B). Second, compared to the effects of adenoviral-mediated S100A1 overexpression on Ca^{2+}-turnover (Figure 4.8C), internalized S100A1 modulates Ca^{2+}-homeostasis in a different manner, that is likely to involve the NCX.

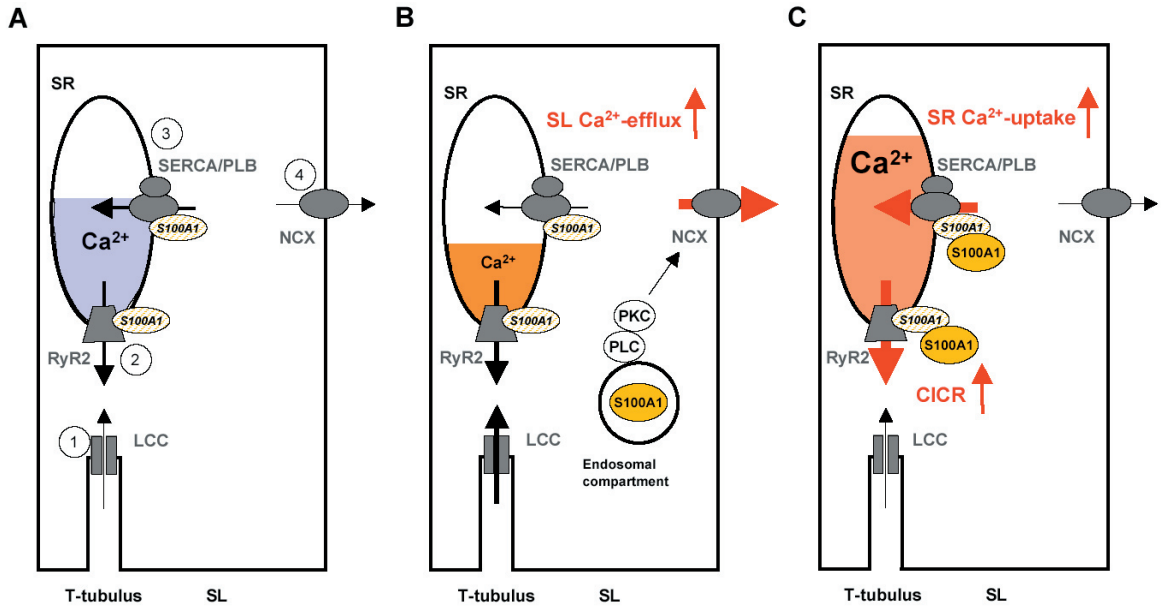

Figure 4. 8: Model of differential effects of endocytosed and overexpressed S100A1 on sarcolemmal and sarcoplasmic Ca^{2+}-cycling.
A, Simplified scheme of intracellular Ca^{2+}-fluxes in a ventricular cardiomyocyte. Endogenous S100A1 (hatched circle) is located at the SR where it interacts with SERCA2a and RyR2. (1) Electrical depolarization of the transverse tubule membrane (T-tubulus) activates inward Ca^{2+}-flux through L-type voltage-gated Ca^{2+}-channels (LCC), which (2) triggers the release of Ca^{2+} from SR stores via ryandine receptors (RyR2). As a result, contractile filaments are activated. (3) For relaxation to occur, the cytosolic $[Ca^{2+}]_i$ must decline. This process is mainly mediated by the SR Ca^{2+}-ATPase (SERCA2a), which resequesters cytosolic Ca^{2+} in the SR. (4) At the sarcolemma, Ca^{2+} is extruded primarily via the sodium-calcium exchanger (NCX). B, Extracellularly added S100A1 is internalized and subsequently routed to the endosomal compartment, where it increases the activity of PLC and PKC (both associated with the endosomal compartment). Through activation of this signaling pathway, internalized S100A1 eventually modulates intracellular Ca^{2+}-flux through an enhanced sarcolemmal Ca^{2+}-extrusion via NCX. The increased Ca^{2+}-extrusion leads to a decreased SR Ca^{2+}-load. C, Effects of overexpressed S100A1 on the intracellular Ca^{2+}-cycling. Overexpressed S100A1 is located at the SR, where it associates with the SR-regulatory proteins SERCA2a and RyR2. As a result, intracellular Ca^{2+}-cycling is enhanced leading to an increased SR Ca^{2+}-uptake and SR Ca^{2+}-load. This, in turn, gives rise to an enhanced Ca^{2+}-induced SR Ca^{2+}-release (CICR).

The immunofluorescence studies suggest that this mechanistic difference is related to a distinct subcellular location of internalized versus overexpressed S100A1. Both experimental regimens, endocytosis of extracellularly added S100A1 and intracellular S100A1 overexpression led to a 3- to 4-fold increase of intracellular levels of the Ca^{2+}-sensor protein. Because the increase in intracellular S100A1 is comparable, we can largely rule out that the total amount of S100A1 is responsible for the differential effects on cytosolic Ca^{2+}-turnover. S100A1 uptake was found to enhance the cytosolic Ca^{2+}-transient amplitude by a marked decrease in diastolic $[Ca^{2+}]_i$ while systolic $[Ca^{2+}]_i$ were mostly unchanged. In contrast, overexpression of S100A1 enhanced the Ca^{2+}-transient amplitude mainly by a marked increase in systolic $[Ca^{2+}]_i$ in combination with a slight decrease in diastolic $[Ca^{2+}]_i$. The downstream

effect of extracellularly added S100A1 on cardiac Ca^{2+}-handling together with the previously demonstrated cardioprotective effects argue that S100A1 could act as paracrine cardiac factor which also acts on other cardiac cells, such as fibroblasts, smooth muscle and endothelial cells.

Along with a differential Ca^{2+}-handling, we also observed a different location of S100A1 that was taken up from the extracellular environment compared to overexpressed S100A1. The latter is associated with the SR since it colocalized with the SR Ca^{2+}-regulatory proteins SERCA2a (Figure 4.8C) and RyR2 (data not shown). These findings are in line with recently published data showing Ca^{2+}-dependent co-immunoprecipitation of endogenous S100A1 protein with RyR2 and SERCA2a in murine and human myocardium (Kiewitz R et al., 2003; Most et al., 2003b). Like Kiewitz et al., who were able to show a colocalization of endogenous S100A1 and SERCA2a in neonatal cardiomyocytes from mouse (Kiewitz et al., 2003), our data reveal a colocalization in rat neonatal cardiomyocytes. Consistently, when RyR2 and SERCA2a activities were inhibited in S100A1 overexpressing cells, the amplitude of Ca^{2+}-transients display a marked decrease, also diastolic $[Ca^{2+}]_i$ are noticeably increased and the decay of Ca^{2+}-transients is decelerated (Figure 4.8C). In contrast, inhibitors of SERCA2a or RyR2 neither affected the S100A1-induced increase in the Ca^{2+}-transient amplitude nor lowered diastolic $[Ca^{2+}]_i$ in cardiomyocytes following uptake of extracellular S100A1. Thus, enhanced Ca^{2+}-cycling in cardiomyocytes overexpressing S100A1 is presumably based on SR Ca^{2+}-cycling. These findings are consistent with previous studies showing that overexpressed S100A1 increased both, SR Ca^{2+}-uptake and Ca^{2+}-load as well as Ca^{2+}-release from the SR (Most et al., 2001; Most et al., 2003b; Remppis et al., 2002). Since the levels of SERCA2a were unaltered, we conclude that overexpressed S100A1 enhances SR Ca^{2+}-load by an increased SERCA2a activity rather than protein abundance.

Internalized S100A1 on the other hand, does not co-localize with SR Ca^{2+}-regulatory proteins (Figure 4.3) and was also not detected at the sarcolemmal membrane of cardiomyocytes (Most et al., 2003a). Instead, it displays a vesicular-like perinuclear distribution that has recently been identified as part of the endosomal compartment (Most et al., 2003a). Consistent with the distinct location of S100A1, Ca^{2+}-handling by S100A1-treated cells appears

to be independent of SR Ca^{2+}-regulatory proteins (Figure 4.8B). However, since S100A1 uptake decreased the SR Ca^{2+}-levels, another mechanism must be affected that accounts for an enhanced cytosolic Ca^{2+}-elimination. Accordingly, we measured an accelerated decay of the caffeine-induced Ca^{2+}-transient amplitude, which indicates that the enhanced cytosolic Ca^{2+}-elimination is likely to involve a trans-sarcolemmal Ca^{2+}-efflux via NCX. In addition, inhibition of NCX by switching to sodium/calcium-free medium abolished this effect which supports the notion that internalized S100A1 stimulates cytosolic Ca^{2+}-extrusion through the NCX forward-mode rather than through the slow Ca^{2+}-removal systems such as the plasma membrane Ca^{2+}-ATPase (PMCA) and the mitochondrial uniporter (Bassani et al., 1994). Similar effects were seen in S100A1-treated field-stimulated cardiomyocytes in the presence of the specific NCX inhibitor myr-FRCRCFa. The inhibitory cell-permeable hexapeptide abolished the S100A1-mediated decrease in diastolic $[Ca^{2+}]_i$. Based on these results, we propose a mechanism where endocytosed S100A1 decreases diastolic $[Ca^{2+}]_i$ by activating sarcolemmal Ca^{2+}-extrusion via NCX.

Since endocytosed S100A1 was not present at the sarcolemmal membrane, the question arose, how an increased S100A1 protein level confined to the endosomal compartment could trigger NCX activity. However, it has been shown that PKC and PLC play a role in the regulation of NCX in neonatal cardiomyocytes (Iwamoto et al., 1996). Moreover, we have demonstrated that internalized S100A1 activates the ERK1/2 signaling pathway through activation of PLC and PKC (Most et al., 2003a). These findings and our Ca^{2+}-transient measurements in the presence of specific inhibitors of PLC and PKC prompted us to suggest that a S100A1-mediated activation of NCX forward mode might occur through the PLC and PKC signalling pathway.

In conclusion, our data indicates that the enhanced Ca^{2+}-cycling observed in S100A1 overexpressing cardiomyocytes predominantly involves SR Ca^{2+}-fluxes (Figure 4.8C), whereas endocytosed S100A1 apparently alters intracellular Ca^{2+}-turnover through sarcolemmal modulation (Figure 4.8B). According to the model, accumulation of internalized S100A1 in the endosomal compartment somehow triggers endosome-associated PLC and PKC, which then activate NCX to increase sarcolemmal Ca^{2+}-efflux.

This study provides the first insight into the mechanisms through which S100A1 differentially modulates sarcolemmal and sarcoplasmic Ca^{2+}-handling in ventricular cardiomyocytes depending on the subcellular location of this protein. Endosomal S100A1 protein appears to modulate Ca^{2+}-cycling through an enhanced NCX forward-mode activity, whereas cytosolic S100A1 increases Ca^{2+}-cycling by enhancing SR Ca^{2+}-fluxes. The latter is likely to underlie the positive inotropic and lusitropic effects seen in S100A1 overexpressing myocardium (Most et al., 2001; Most et al., 2003b; Remppis et al., 2002; Remppis et al., 2004). In addition, we have very recently shown that cardiac adenoviral S100A1 gene delivery rescues failing myocardium *in vitro* and *in vivo* (Most et al., 2004), which warrants further studies on the impact of decreased diastolic $[Ca^{2+}]$ and SR Ca^{2+}-load resulting from S100A1 endocytosis on cardiac function *in vivo*.

4.6 **Acknowledgments**

This work was supported in part by grants from the University of Heidelberg to P.M. (Forschungsförderung 93/2002 and 61/2003), the Deutsche Forschungsgemeinschaft (DFG) to P.M. (Mo 1066/1-1), and T. W. (We 2366/3-1), and from the M.E. Müller Foundation of Switzerland and the Kanton of Basel Stadt (to M. B., U.A., and C.-A. S.).

4.7 References

Barger, S. W. and Van Eldik, L. J. (1992). S100 beta stimulates calcium fluxes in glial and neuronal cells. J Biol Chem 267, 9689-94.

Bassani, J. W. M., Bassani, R. A. and Bers, D. M. (1994). Relaxation in rabbit and rat cardiac cells : Species-dependent differences in cellular mechanisms. J Physiol 476, 279-293.

Convery, M. K., Levi, A. J., Khananshvili, D. and Hancox, J. C. (1998). Actions of myristyl-FRCRCFa, a cell-permeant blocker of the cardiac sarcolemmal Na-Ca

exchanger, tested in rabbit ventricular myocytes. Pflugers Arch 436, 581-90.

Despa, S., Islam, M. A., Pogwizd, S. M. and Bers, D. M. (2002). Intracellular [Na^+] and Na^+ pump rate in rat and rabbit ventricular myocytes. Journal of Physiology 539, 133-143.

Donato, R. (2003). Intracellular and extracellular roles of S100 proteins. Microsc Res Tech 60, 540-51.

Foell, D., Ichida, F., Vogl, T., Yu, X., Chen, R., Miyawaki, T., Sorg, C. and Roth, J. (2003a).S100A12 (EN-RAGE) in monitoring Kawasaki diesease. Lancet 361, 1270-2.

Foell, D., Kane, D., Bresnihan, B., Vogl, T., Nacken, W., Sorg, C., Fitzgerald, O. and Roth, J. (2003b). Expression of the pro-inflammatory protein S100A12 (EN-RAGE) in rheumatoid and psoriatic arthritis. Rheumatology (Oxford) 42, 1383-9.

Foell, D., Kucharzik, T., Kraft, M., Vogl, T., Sorg, C., Domaschke, W. and Roth, J. (2003c). Neutrophil derived S100A12 (EN-RAGE) is strongly expressed during chronic active inflammatory bowel disease. Gut 52, 847-53.

Foell, D., Seeliger, S., Vogl, T., Koch, H. G., Maschek, H., Harms, E., Sorg, C. and Roth, J. (2003d). Expression of S100A12 (EN-RAGE) in cyctic fibrosis. Thorax 58, 613-7.

Haimoto, H. and Kato, K. (1988). S100a0 (alpha alpha) protein in cardiac muscle. Isolation from human cardiac muscle and ultrastructural localization. Eur J Biochem 171, 409-15.

Heizmann, C. W. and Cox, J. A. (1998). New perspectives on S100 proteins: a multi-functional $Ca^{(2+)}$-, $Zn^{(2+)}$- and $Cu^{(2+)}$-binding protein family. Biometals 11, 383-97.

Hobai, I. A., Khananshvili, D. and Levi, A. J. (1997). The peptide „FRCRCFa“, dialysed intracellularly, inhibits the Na/Ca exchange in rabbit ventricular myocytes with high affinity. Pflugers Arch 433, 455-63.

Hofmann, M. A., Drury, S., Fu, C., Qu, W., Taguchi, A., Lu, Y., Avila, C., Kambham, N., Bierhaus, A., Nawroth, P. et al. (1999). RAGE mediates a novel proinflammatory axis: a central cell surface receptor for S100/calgranulin polypeptides. Cell 97, 889-901.

Huttunen, H. J., Kuja-Panula, J., Sorci, G., Agneletti, A. L., Donato, R. and Rauvala, H. (2000). Coregulation of neurite outgrowth and cell survival by amphoterin and S100 proteins through receptor for advanced glycation end products (RAGE) activation. J Biol Chem 275, 40096-105.

Iwamoto, T., Pan, Y., Wakabayashi, S., Imagawa, T., Yamanaka, H. I. and Shigekawa, M. (1996). Phosphorylation-dependent regulation of cardiac Na+/Ca2+ exchanger via protein kinase C. J Biol Chem 271, 13609-15.

Kato, K. and Kimura, S. (1985). S100ao (alpha alpha) protein is mainly located in the heart and striated muscles. Biochim Biophys Acta 842, 146-50.

Khananshvili, D., Shaulov, G., Weil-Maslansky, E. and Baazov, D. (1995). Positively charged cyclic hexapeptides, novel blockers for the cardiac sarcolemma $Na(^{+})$-Ca^{2+} exchanger. J Biol Chem 270, 16182-8.

Kiewitz R, Acklin C, Schafer BW, Maco B, Uhri KB, Wuytack F, Erne P and CW., H. (2003).$Ca(^{2+})$-dependent interaction of S100A1 with the sarcoplasmic reticulum$Ca(^{2+})$ -ATPase2a and phospholamban in the human heart. Biochem Biophys Res Commun. 306(2), 550-557.

Kiewitz, R., Acklin, C., Minder, E., Huber, P. R., Schafer, B. W. and Heizmann, C. W. (2000). S100A1, a new marker for acute myocardial ischemia. Biochem Biophys Res Commun 274, 865-71.

Kubista, H., Donato, R. and Hermann, A. (1999). S100 calcium binding protein affect neuronal electrical discharge activity by modulation of potassium currents. Neuros cience 90, 493-508.

Mikkelsen, S. E., Novitskaya, V., Kriajevska, M., Berezin, V., Bock, E., Norrild, B. and Lukanidin, E. (2001). S100A12 protein is a strong inducer of neurite outgrowth from primary hippocampal neurons. J Neurochem 79, 767-76.

Most, P., Bernotat, J., Ehlermann, P., Pleger, S. T., Reppel, M., Borries, M., Niroomand, F., Pieske, B., Janssen, P. M., Eschenhagen, T. et al. (2001). S100A1: a regulator of myocardial contractility. Proc Natl Acad Sci U S A 98, 13889-94.

Most, P., Boerries, M., Eicher, C., Schweda, C., Ehlermann, P., Pleger, S. T., Löffler, E.,

Koch,W. J., Katus, H. A., Schoenenberger, C. A. et al. (2003a). Extracellular S100A1 protein inhibits apoptosis in ventricular cardiomyocytes via activation of the extracellular-regulated kinase (ERK1/2) pathway. J Biol Chem 278, 48404-48412.

Most, P., Pleger, S., Völkers, M., Heidt, B., Boerries, M., Weichenhan, D., Löffler, E., Janssen, P. M., Eckhart, A. D., Martini, J. et al. (2004). Cardiac adenoviral S100A1 gene transfer rescues failing myocardium. Journal of Clinical Investigation in press.

Most, P., Remppis, A., Pleger, S. T., Löffler, E., Ehlermann, P., Bernotat, J., Kleuss, C., Heierhorst, J., Ruiz, P., Witt, H. et al. (2003b). Transgenic overexpression of the Ca^{2+}-binding protein S100A1 in the heart leads to increased in vivo myocardial contractile performance. J Biol Chem. 278, 33809-33817.

Most, P., Remppis, A., Weber, C., Bernotat, J., Ehlermann, P., Pleger, S. T., Kirsch, W., Weber, M., Uttenweiler, D., Smith, G. L. et al. (2003c). The C-terminus (aa 75-94) and the linker region (aa 42-54) of the Ca^{2+} binding protein S100A1 differentially enhance sarcoplasmic Ca^{2+} release in murine skinned skeletal muscle fibres. J Biol Chem 278, 26356-64.

Novitskaya, V., Grigorian, M., Kriajevska, M., Tarabykina, S., Bronstein, I., Berezin, V., Bock, E. and Lukanidin, E. (2000). Oligomeric forms of the metastasis-related Mts1 (S100A4) protein stimulate neuronal differentiation in cultures of rat hippo campal neurons. J Biol Chem 275, 41278-86.

Rammes, A., Roth, J., Goebeler, M., Klempt, M., Hartmann, M. and Sorg, C. (1997). Myeloid-related Protein (MRP) 8 and MRP14, Calcium-binding Proteins of the S100 Family, Are Secreted by Activated Monocytes via a Novel, Tubulin-dependent Pathway. J Biol Chem 272, 9496-9502.

Remppis, A., Most, P., Löffler, E., Ehlermann, P., Bernotat, J., Pleger, S. T., Börries, M., Repper, M., Fischer, J., Koch, W. J. et al. (2002). The small EF-hand Ca^{2+}-binding protein S100A1 increases contractility and Ca^{2+} cycling in rat cardiac myocytes. Basic Res Cardiol 97, I/56-I/62.

Remppis, A., Pleger, S. T., Most, P., Lindenkamp, J., Ehlermann, P., Löffler, E., Weil,

J., Eschenhagen, T., Koch, W. J. and Katus, H. A. (2004). S100A1 gene transfer : A strategy to strenghten engineered cardiac grafts. J Gene Medicine 6, 387-394.

Reuter, H., Henderson, S. A., Han, T., Matsuda, T., Baba, A., Ross, R. S., Goldhaber, J. I. and Philipson, K. D. (2002). Knockout Mice for Pharmacological Screening. Testing the Specificity of Na-Ca Exchange Inhibitors. Circ Res 91, 90-92.

Selinfreund, R. H., Barger, S. W., Pledger, W. J. and Van Eldik, L. J. (1991). Neurotrophic protein S100 beta stimulates glial cell proliferation. Proc Natl Acad Sci U S A 88, 3554-8.

Sorci, G., Riuzzi, F., Agneletti, A. L., Marchetti, C. and Donato, R. (2003). S100B inhibits myogenic differentiation and myotube formation in a RAGE-independent manner. Mol Cell Biol 23, 4870-81.

Sorci, G., Riuzzi, F., Agneletti, A. L., Marchetti, C. and Donato, R. (2004a). S100B causes apoptosis in a myoblast cell line in a RAGE-independent manner. Journal of Cellular Physiology 199, 274-83.

Sorci, G., Riuzzi, F., Arcuri, C., Giambanco, I. and Donato, R. (2004b). Amphotericin stimulates myogenesis and counteracts the antimyogenic factors basic fibroblast growth factor and S100B via RAGE binding. Mol Cell Biol 24, 4880-94.

Wang, Z., Zhang, H., Ding, Y., Wang, G., Wang, X., Ye, S., Bartlam, M., Tang, H., Liu, Y., Jiang, F. et al. (2001). Preliminary X-ray crystallographic analysis of a Ca^{2+}-binding protein human S100A1. Acta Crystallogr D Biol Crystallogr 57, 882-3.

Zimmer, D. B., Cornwall, E. H., Landar, A. and Song, W. (1995). The S100 protein family: history, function, and expression. Brain Res Bull 37, 417-29.

Chapter 5

Ca^{2+}-dependent interaction of S100A1 with the F_1-ATPase leads to an increased ATP content in cardiomyocytes

Melanie Boerries*, Patrick Most*, Jonathan R. Gledhill, John E. Walker, Hugo A. Katus, Walter J. Koch, Ueli Aebi, and Cora-Ann Schoenenberger

*Both authors contributed equally to this study

5.1 Abstract

S100A1, a Ca^{2+}-sensing protein of the EF-hand family that is predominantly expressed in cardiac muscle plays a pivotal role in cardiac contractility in vitro and in vivo. It has recently been demonstrated that by restoring Ca^{2+}-homoestasis, S100A1 was able to rescue contractile dysfunction in failing rat hearts. Myocardial contractility is not only regulated by Ca^{2+}-homoestasis, but also by the energy metabolism, in particular the production of ATP. Here we report a novel interaction of S100A1 with the mitochondrial F_1-ATPase, which affects F_1-ATPase activity and cellular ATP production. In particular, cardiomyocytes that overexpress S100A1 exhibited a higher ATP content than control cells, whereas knockdown of S100A1 expression decreased ATP levels. In pulldown experiments, we identified the α- and β-chain of F_1-ATPase to interact with S100A1 in a Ca^{2+}-dependent manner. The interaction was confirmed by colocalization studies of S100A1 and F_1-ATPase and the analysis of the S100A1-F_1-ATPase complex by gel filtration chromatography. The functional impact of this association is highlighted by an S100A1-mediated increase of F_1-ATPase activity. Consistently, ATP-synthase activity is reduced in cardiomyocytes from S100A1 knockout mice. Our data indicate that S100A1 might play a key role in cardiac energy metabolism.

5.2 Introduction

S100 proteins are a family of soluble, EF-hand Ca^{2+}-binding proteins, which exhibit a remarkable cell- and tissue-specific expression pattern. They are involved in numerous intracellular activities such as cell proliferation and differentiation or the dynamics of cytoskeletal constituents (reviewed in references 4, 9 and 30). The most abundant S100 protein in the heart is S100A1 (12; reviewed in reference 4). It has been recognized recently as a positive inotropic intracellular regulator of cardiac as well as skeletal muscle Ca^{2+}-homeostasis and contractility (15, 16, 18, 19, 20). Accordingly, S100A1-deficient mice exhibited an impaired cardiac contractility response to hemodynamic stress (5). Notably, the absence of S100A1 significantly accelerates the development of contractile dysfunction after myocardial infarction with a rapid onset of cardiac remodeling and transition to heart failure combined with excessive mortality (21). Normal contractile function and Ca^{2+}-homeostasis, on the other hand, could be restored in failing myocardium in postinfarcted rat hearts by S100A1 gene delivery (19).

In addition to Ca^{2+}-homeostasis, myocardial workload depends on cardiac metabolism. As the energy demand changes, the flux through the mitochondrial ATP-synthase (F_1F_o-ATPase), which is responsible for the bulk of ATP synthesis in the myocardium must change so that ATP-synthesis matches ATP consumption (reviewed in references 6 and 10). To sustain cardiac function in all possible situations there has to be a strict correlation between energy production, energy transfer and energy utilization (reviewed in reference 29). In this regard, Ca^{2+} has emerged as a major factor for adapting mitochondrial ATP production to the constantly varying energy demand of the cell. Consistently, several studies provided evidence that F_1F_o-ATPase dependent ATP synthesis correlates with Ca^{2+} levels in heart cells (reviewed in reference 1). Furthermore, metabolic pathway abnormalities that result in an imbalance of several metabolic reactions, for example, a decreased PCr (phosphocreatine)/ATP ratio indicative of an increase in ADP, an alteration of oxidative phosphorylation or a decreased ATP/ADP ratio, lead to abnormal contraction and relaxation and eventually result in the failing of the heart. Thus, it is conceivable that energy starvation may contribute to heart failure (reviewed in reference 11).

Because S100A1 is able to restore a reduced PCr/ATP ratio and Ca^{2+}-homeostasis in failing cardiomyocytes (19), we examined whether S100A1 has an influence on cardiac energy homeostasis in neonatal rat ventricular cardiomyocytes (NVCMs). Here, we demonstrate a Ca^{2+}-dependent interaction of S100A1 with the α- and β-chain of the F_1-ATPase in NVCMs and isolated mitochondria. Moreover, this interaction is consolidated by colocalization in immunofluorescence and immunoelectron microscopy studies, and the isolation of an S100A1-F_1-ATPase complex by gel filtration chromatography. Furthermore, the physiological significance of S100A1 in energy metabolism is validated through the effects of S100A1 overexpression and knockdown on ATP production in NVCMs and its influence on F_1-ATPase activity.

Based on the data presented, a new role for S100A1 in cardiac energy metabolism emerges.

5.3 Materials and Methods

Reagents

ATP (disodium salt), phosphoenolpyruvate, NADH, pyruvate kinase, lactate dehydrogenase and isoproterenol were purchased from Sigma.

Generation of S100A1 adenovirus

The generation of an S100A1 adenovirus (AdS100A1) by the pAdTrack-CMV/pAdEasy-1 system has been described elsewhere (15). To facilitate identification of infected cells, AdS100A1 carried the green fluorescent protein reporter gene (GFP) in addition to the human S100A1 cDNA (accession number X58079). Each transgene was independently expressed under the control of a cytomegalovirus promotor sequence. To rule out the possibility that the infection procedure itself had an effect on the amount of S100A1 in the cell, cells were infected with a corresponding adenovirus carrying GFP cDNA alone as a control (Adcontrol). tested by plaque assay.

Isolation and primary culture of ventricular cardiomyocytes from neonatal rats (NVCMs) and adult mice

Ventricular cardiomyocytes from 1-2 day old neonatal hearts (NVCMs) were isolated as published in detail elsewhere (17). NVCMs were cultured in Dulbecco's modified Eagle's medium (DMEM) supplemented with penicillin/streptomycin (100 units/ml), L-glutamine (2 mM), and 1% fetal calf serum (FCS Gold; PAA Laboratories GmbH; DFCS) at 37°C in a 95% air/5% CO_2 humidified atmosphere for 2-3 days. Adenoviral infection of NVCMs was carried out in serum-free M199 medium with a multiplicity of infection (MOI) of 8 plaque forming units (pfu) per cell. After 4 hours of incubation at 37°C, M199 medium was changed to DFCS. Efficiency of adenoviral gene transfer was monitored 24 hours later by GFP fluorescence. Accordingly, approximately 95% of NVCMs were infected.

S100A1-deficient (SKO) mice have been previously described (5). Adult ventricular cardiomyocytes from C57/Bl6 wild type (WT) and SKO mice (2-3 months of age) were enzymatically isolated using a pressure and temperature controlled retrograde coronary perfusion protocol as reported elsewhere (24). Subsequently, WT and SKO cardiomyocytes were pelleted and sonicated in ice-cold EGTA-buffered sonication solution (20 mM HEPES, 1.0 $MgCl_2$, 2.0 mM EGTA, pH 7.2) with a free [Ca^{2+}] of 0.2 mM. Samples were kept on ice until measurements. Free [Ca^{2+}] was calculated applying the program REACT.

S100A1 RNA interference

Custom-designed synthetic S100A1 siRNA and negative control (scrambled) siRNA were purchased from Eurogentec (Seraing, Belgium). S100A1 siRNA is target-specific 20-25 nt siRNA to knockdown gene expression of S100A1 in NVCM's (sense: 5'-UGG-AGA-CCC-UCA-UCA-AUG-UdTdT-3', antisense: 5'-ACA-UUG-AUG-AGG-GUC-UCC-AdTdT-3'). NVCM were transfected with S100A1 and control siRNA (100nM) oligonucleotides using Effectene Transfection Reagent according to the manufature's instructions (Qiagen Inc, Valencia, CA, USA). After incubation at 37°C for 24h, cells were lysed and subjected to Western blotting.

Indirect immunofluorescence

Immunofluoresence labeling of NVCMs was carried out as previously described (17). Freshly isolated NVCMs were cultured for 2 days on glass coverslips and incubated with the fluorescent dye MitoTracker Red (1 μM; Molecular Probes) for 30 min. Cells were fixed, permeabilized and labeled with a monoclonal anti-S100A1 (diluted 1:200; Sigma) and a polyclonal F_1-ATPase antibody (diluted 1:400). The latter was a kind gift from Dr. Pfanner (Institute for Biochemistry and Molecular Biology, Freiburg, Germany). The secondary antibodies used were ALEXA Fluor 488-conjugated anti mouse Ig (diluted 1:800; Alexis) and Cy5-conjugated anti rabbit Ig (diluted 1:400; Jackson Immuno Research Lab). Confocal images (CLSM) were obtained using a 100x oil objective lens on a Leica TCS SP laser scanning confocal microscope. Digitized confocal images were processed by Leica software and Adobe Photoshop.

Immunoelectron microscopy

Isolated mitochondria and pieces of heart tissue from 3-day old neonatal rats were fixed as previously described (25). Ultrathin sections were cut and mounted on carbon/parlodion-coated copper grids. Specimens were blocked with 2% BSA in PBS two times 5 min prior to incubation with S100A1 antibody (diluted 1:100, Sigma) for 2 hours at room temperature. Grids were washed in PBS, blocked in 2% BSA in PBS for two times 5 min, and then incubated with 10 nm gold conjugated goat anti-mouse secondary antibody (BBInternational) for 1 hour at RT.

For double immuno-labeling, sections were sequentially incubated with the primary antibodies and the corresponding gold conjugated secondary antibody (10 nm and 5 nm, respectively) for 2 hours at room temperature (RT). After washing in PBS and water, grids were stained with a mixture of 6% uranyl acetate for 1 hour, rinsed with water and then post-stained for two min with lead-citrate. Electron micrographs were recorded on a Hitachi 7000 at 80 kV.

Isolation of mitochondria:

Mitochondria were isolated from the hearts of adult male rats by differential centrifugation steps as described previously (3). Briefly, minced heart tissue was homogenized with approximately 10 ml/g tissue homogenization buffer (0.1 M KCl, 0.05 M MOPS, 5 mM $MgSO_4$, 1 mM EDTA, 1 mM ATP, 0.2% BSA, pH 7.4) using a Teflon-glass homogenizer with a loose fitting piston. The homogenate was centrifuged at 300 g at 4°C for 10 min. The supernatant was poured through a double layered cheese cloth and centrifuged again at 5,000 g at 4°C for 10 min. Pelleted mitochondria were resuspended in 1 ml homogenization buffer and centrifuged again at 5,000 g at 4°C for 10 min. The pellet was resuspended in 0.15 ml KME buffer (0.1 M KCl, 0.05 M MOPS, 0.5 mM EGTA, pH7.4). The protein concentration in the mitochondrial suspension was determined by the Bradford method (Sigma) using bovine albumin Fraction V as a standard.

Purification of F_1-ATPase/S100A1-F_1-ATPase complex and F_1-ATPase activity

Purification of the bovine F_1-ATPase was carried out as previously described (22). The S100A1-F_1-ATPase complex was prepared as follows: purified F_1-ATPase (15 mg), stored as an ammonium sulfate precipitate, was collected by centrifugation (16,000 g), re-dissolved in complex buffer (CB: 20 mM TRIS, pH 7.4; 100 mM NaCl, 1 mM $MgCl_2$, 2 mM $CaCl_2$) and desalted on a Micro Bio-Spin column (Amersham Pharmacia Biotech). The enzyme was then mixed with a 12.5-fold molar excess of S100A1 over F_1-ATPase and incubated for 30 min at 37°C. 1 mM MgATP was added at 1 and 15 min to yield a final concentration of 2 mM. ATPase activity was measured at 37°C with an ATP-regenerating system as reported by following the oxidation of NADH to NAD^+ at 340 nm in a Hewlett Packard spectrophotometer (2). The assay was carried out in 1 ml assay buffer (50 mM Tris, pH 7.4, 50 mM KCl, 2 mM $MgCl_2$) containing 2 mM ATP, 2 mM phosphoenolpyruvate, 0.4 mM NADH, 12.5U pyruvate kinase, 12.5U lactate dehydrogenase. The reaction was started by adding 10 ml of F_1-ATPase or the S100A1-F_1-ATPase complex in the presence of 2 mM or 0.2 mM $CaCl_2$. The decline of NADH absorbance at 340 nm allows monitoring the rate of ATP hydrolysis (OD/min).

Determination of mitochondrial ATP-synthase activity

The enzymatic activity of the mitochondrial ATP-synthase complex was measured using a spectrophotometric assay as described elsewhere with minor modifactions (7). Briefly, aliquots of cardiomyocyte homogenates from adult WT and SKO mice were added to EGTA-buffered activity solution (mM: 60 sucrose, 50 triethanolamine-HCl, 50 KCl, 4 $MgCl_2$, 2 ATP, 1.5 phosphoenolpyruvate, 2 EGTA, 1 KCN, 0.001 thapsigargin, pH 7.4 with KOH) supplemented with 200 mM NADH, 5 U pyruvate kinase and 5 U lactate dehydrogenase. Thapsigargin was used to block activity of the Ca^{2+}-sensitive sarcoplasmic reticulum Ca^{2+}-ATPase. Free [Ca^{2+}] were adjusted either to 0.2 mM or 0.2 mM determined by the program REACT. The conversion of NADH to NAD^+ was followed spectrophotometrically at 340 nm at 37°C for 3 min. Recombinant human S100A1 protein was added 10 min prior to measurement as indicated. Oligomycin (10 mg/ml) was used to block the mitochondrial ATP-synthase. Mitochondrial ATP-synthase activity was calculated as the difference between total and oligomycin-insensitive conversion of NADH to NAD^+.

Gel filtration chromatography

Upon preparation of the S100A1-F_1-ATPase complex as described above, it was chromatographed at RT at a flow rate of 0.3 ml/min on a HiLoad Superdex 200 column that was pre-equilibrated in CB. The absorbance of the eluant was monitored at 280 nm. Individual fractions (0.3 ml) were analyzed by SDS-PAGE.

Measurement of ATP production

The ATP content of NVCMs was determined by the luciferin-luciferase system according to the manufacturer's protocol (ATP Bioluminescence Assa KIT HS II, Roche).

Recombinant proteins

A human S100A1 cDNA (accession number X58079) was subcloned into the expression vector pGEX-6P1 containing glutathione S-transferase (GST) cDNA. S100A1 was produced as a fusion protein with a 26 kDa glutathione S-transferase (GST) at the NH2-terminus

(GST-S100A1) by an isopropylthiogalactosid (IPTG)-driven expression system in E. coli. The fusion protein was purified using glutathione-Sepharose 4B (Amersham Pharmacia Biotech) and dialyzed against PBS.

The GST fusion constructs of palpha3 and pbeta1 were generated by PCR overlap extension using cDNAs of the α- and β-chain of mitochondrial bovine heart F_1-ATPase (palpha3 and pbeta1). The two external primers for the palpha3 construct used were the following: 5'-EcoRI primer 5'-GAATTCCAGAAACCGGCACT, and 3'-XhoI primer 5'-CTCGAGAG-CTTC AAATCCAGC. The PCR product was digested with EcoR and XhoI and inserted into the pGEX-6P1 vector at the corresponing restriction sites. For the GST-pbeta1 expression construct the two external primers were the following: 5'-Sal1 primer 5'-CGGTCGACT-CATGGCCGCTCAAGCATCTCC and 3'-Not1 primer 3'-CCCGCCGGCCGCTCAT-GAGTGCTCTTCAGCCAAC. The PCR product was digested with Sal1 and Not1 and inserted into the pGEX-6P1 vector at the respective sites. GST-fusion proteins of the a-chain and b-chain of the F_1-ATPase were expressed and purified as described for GST-S100A1.

A recombinant human S100A1 cDNA (accession number X58079) was also subcloned into the expression vector pHis-TRX-1 containing a thrombin cleavage side. S100A1 was produced as a fusion protein with a histidine tag at the NH2-terminus by an isopropylthiogalactosid (IPTG)-driven expression system in E. coli. The fusion protein was purified using a HiTrap Chelating HP column (Amersham Pharmacia Biotech) according to the manufacturer's protocol. Subsequently, the histidine-tag was removed by thrombin cleavage and purified S100A1 was dialysed against 25 mM Tris, pH 7.45.

GST pull-down assays

0.02 mg/ml GST-fusion proteins (GST-S100A1, GST-α-F_1-ATPase, GST-β-F_1-ATPase) or GST alone were bound to glutathione S-Sepharose slurries in an incubation buffer (IB2: 100 mM NaCl, 20 mM Tris, pH 7.4, 0.05% Triton X-100, containing 2 mM $CaCl_2$, 0.2 mM $CaCl_2$ or 2 mM EDTA) for 1.5 hours at 4°C. Isolated neonatal rat cardiomyocytes ($5x10^6$ cells) and 1 mg/ml isolated heart mitochondria were homogenized in a homogenization buffer (100 mM NaCl, 20 mM Tris, pH7.4, 1 mM $MgCl_2$, 1 mM PMSF, 1 μl DNAse, 0.2% Triton

X-100, supplemeted with a Mini complete EDTA free protease inhibitor tablet, Roche) containing either 2 mM $CaCl_2$, 0.2 mM $CaCl_2$ or 2 mM EGTA. Homogenates of neonatal cardiomyocytes, isolated mitochondria, and recombinant S100A1 (1 mM) were incubated with GST-S100A1, GST-α-F_1-ATPase, GST-β-F_1-ATPase or GST slurries for 2.5 hours at 4°C. Incubation of purified F_1-ATPase with GST-S100A1 or GST slurries was carried out at RT for 1 hour. Mixtures were washed 6 times with IB2, applied to spin columns, and centrifuged at 400 g for 1 min. The columns were spin-washed twice with IB2. Unbound protein was removed by spin-wash steps for 3 min at 2,300 g. Bound proteins were eluted with SDS-PAGE sample buffer (5% SDS) and analyzed by SDS-PAGE and mass spectrometry.

Mass spectrometry analysis

For mass spectrometry, gel slices were excised from silver stained SDS-PAGE gels and digested with 0.25 mg trypsin (Promega) in 50 mM ammonium bicarbonate (pH 8.0) at 37°C for 16 h. The resulting peptides were analysed by capillary liquid chromatography (LC/MS/MS) using a Magic C18 100 mm x 10 cm HPLC column (Spectronex) connected to a Finnigan TSQ7000 tandem mass spectrometer (ThermoFinnigan). A linear gradient from 2 to 75% B (0.1% acetic acid and 80% (v/v) acetonitril in water) in A (0.1% acetic acid in water) was generated with a Rheos 2000 HPLC system (Flux) at 100 ml/min. A precolumn flow splitter reduced the flow to approximately 500 nl/min. The eluting peptides were ionized by electrospray ionization, detected, and the peptides were automatically selected and fragmented by collision-induced dissociation (MS/MS). Individual MS/MS spectra were searched in the data bank using the Mascot software (www.matrixscience.com).

Western blotting

To reveal the presence of S100A1 in the SDS-PAGE separated protein mixtures of pulldown experiments, standard Western blotting using a specific polyclonal anti-S100A1 antibody (SA 5632, diluted 1:10,000; Eurogentec) was performed. Blots were developed with the Avidix chemiluminescence detection system (Tropix, Applied Biosystems). To detect the presence of S100A1 on the SDS-PAGE separated protein mixtures of siRNA experiments,

standard Western blotting using an epitope affinity purified anti-S100A1 antibody (SP5355P, diluted 1:5000; Acris) were performed (19). Proteins were visualized with a LI-COR infrared imager (Odyssey), and quantitative densitometric analysis was performed by applying the Odyssey version 1.2 infrared imaging software. Signals were normalized to CSQ densitometric levels that were not different between groups.

Statistical analyses

Data are presented as mean ± SEM. Unpaired student´s t-test and a two-way repeated ANOVA analysis was performed to test for differences between groups. A value of $P < 0.01$ was accepted as statistically significant.

5.4 Results

S100A1 enhances ATP production in neonatal rat cardiomyocytes

To examine the effects of an increased S100A1 protein level on the ATP production in neonatal rat ventricular cardiomyocytes (NVCMs), cells were transduced by means of an adenoviral construct that independently drives the expression of human S100A1 and GFP (AdS100A1). As a control, NVCMs were infected with a corresponding adenovirus carrying only GFP cDNA (Adcontrol). Twenty-four hours postinfection, AdS100A1, Adcontrol and non-transfected (NT) cells were processed for ATP quantification using a luciferase based luminometry reaction.

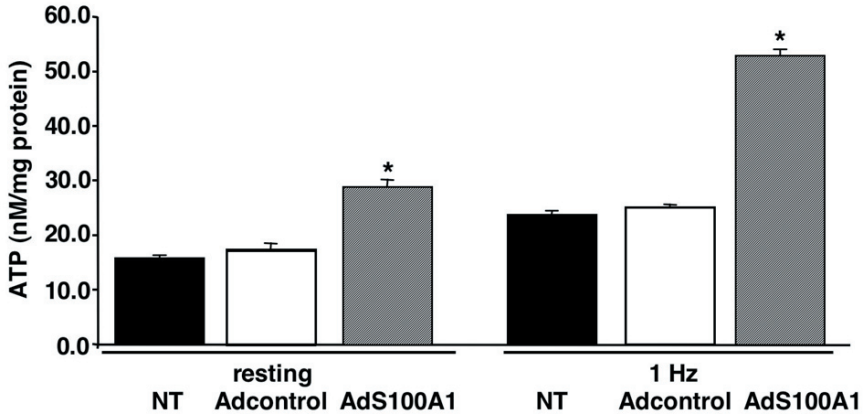

Figure 5.1: S100A1 raises the ATP content in neonatal cardiomyocytes.
(A) In resting cardiomyocytes, adenovirus-mediated S100A1 overexpression (AdS100A1) leads to a significantly higher ATP content (nM/mg protein) than in control transfectants (Adcontrol) and non-transfected (NT) cells. Upon electrical stimulation (1 Hz), AdS100A1 cells are able to increase ATP levels to a greater extent than Adcontrol and NT cells. Data are given as mean ± S.E.M. of five different experiments.

Under resting conditions (without electrical stimulation), the amount of ATP was raised by ~67% in AdS100A1 cells compared to control cells expressing endogenous S100A1 only (Fig. 5.1; Adcontrol and NT cells). In response to electrical stimulation at 1Hz, the ATP production was increased by ~110% in cells overexpressing S100A1. This data suggests that S100A1 is involved in the regulation of the energy metabolism in NVCMs.

Calcium-dependent interaction of S100A1 with mitochondrial proteins

To identify possible target proteins of S100A1 implicated in the ATP increase observed in S100A1 overexpressing cells, we performed GST-S100A1 pulldown assays with different heart homogenates in the presence of 2 mM $CaCl_2$ or 2 mM EGTA (Fig. 5.2). Silver-stained protein bands that were specific to GST-S100A1 pulldown assays in the presence of 2 mM $CaCl_2$ were analyzed by mass spectrometry. In homogenates of isolated NVCMs (Fig. 5.2A), five different mitochondrial proteins, hydroxyl-Coenzyme A dehydrogenase (1), the α-chain of F_1-ATPase (2), isocitrate dehydrogenase 2 (3), annexin V (4) and adenine nucleotide translocase (5), were identified as potential binding partners of S100A1. The corresponding proteins were also pulled down from adult rat heart homogenates (data not shown).

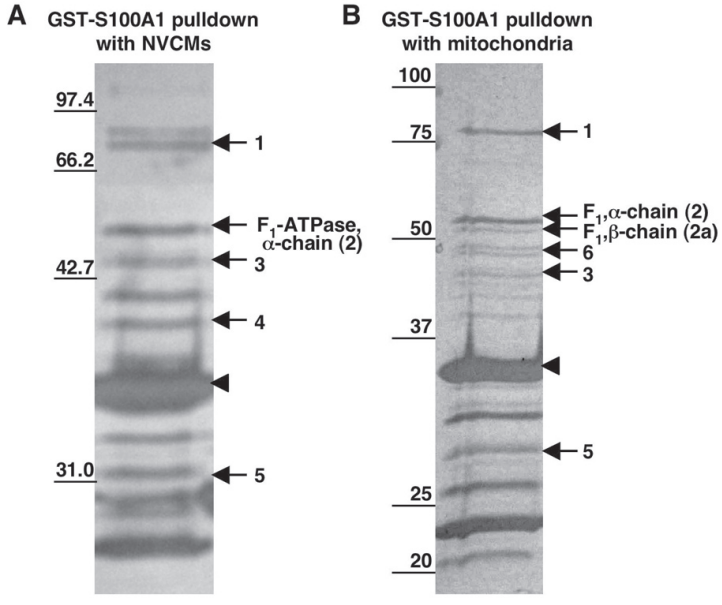

Figure 5.2: GST-S100A1 pulldown assays with different homogenates
Protein eluates from different GST-S100A1 pulldown assays were separated on denaturing SDS-polyacrylamide gels and individual proteins identified by mass spectrometry. (A) Five mitochondrial proteins from a homogenate of NVCMs that interact with GST-S100A1 were identified: hydroxyl-Coenzyme A dehydrogenase (1), α-chain of F_1-ATPase (2), isocitrate dehydrogenase 2 (3), annexin V (4) and adenine nucleotide translocase (5). (B) Similar proteins were pulled down from isolated mitochondria by GST-S100A1 in the presence of 2 mM $CaCl_2$. In addition, the β-chain of the F_1-ATPase (2a) and the hydroxyacyl dehydrogenase (6) were identified. The band representing GST-S100A1 is indicated by an arrowhead.

To substantiate the finding that S100A1 interacts with a number of mitochondrial proteins, we isolated mitochondria from adult rat hearts and prepared corresponding mitochondrial

extracts for pulldown assays with GST-S100A1 (Fig. 5.2B). Analyses by mass spectrometry revealed that the same S100A1-interacting proteins were identified in isolated mitochondria as were detected in isolated NVCMs. In addition, the β-chain of the F_1-ATPase (2a) was identified in mitochondrial extracts.

S100A1 colocalizes with the F_1-ATPase in mitochondria

We used immunofluorescence and immunoelectron microscopy to probe the cellular distribution of S100A1 and its association with the F_1-ATPase in situ. Indirect immunofluorescence labeling of NVCMs with an S100A1 antibody revealed a punctate distribution of S100A1 (green) throughout the cytoplasm (Fig. 5.3A and D) and to a lesser extent in the nucleus. Because NVCMs were incubated in parallel with MitoTracker Red, mitochondria (red) could be identified as 'bullet-shaped' structures (Fig. 5.3B). Merging the two confocal images revealed a partial colocalization of S100A1 with mitochondria (Fig. 5.3C, yellow).

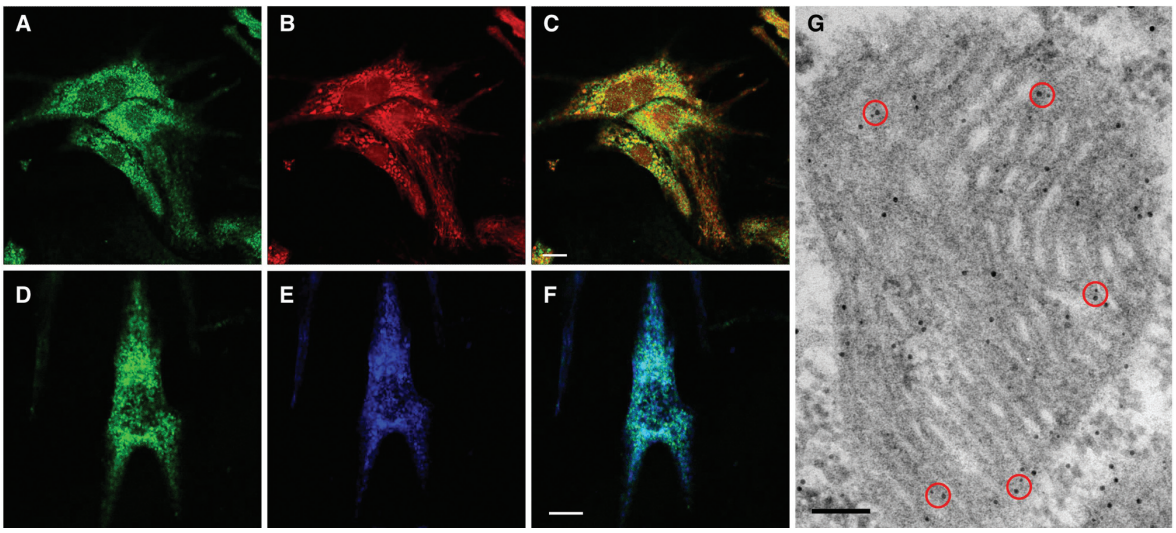

Figure 5.3: S100A1 is present in mitochondria where it colocalizes with the F_1-ATPase
(A and D) S100A1 is labeled with a monoclonal S100A1/Alexa488-mouse antibody in NVCMs (green). (B) Mitochondria are recognized by MitoTracker Red uptake (red). (C) Overlay of panels (A) and (B) reveals a partial colocalization of S100A1 with mitochondria (yellow). (E) F_1-ATPase labeled with a polyclonal F_1-ATPase/Cy5-anti-rabbit antibody (blue). (F) Superposition of panels (D) and (E) reveals a partial colocalization of S100A1 and F_1-ATPase (turquoise). Bar, 10 mm. (G) Ultrastructural colocalization of S100A1 and F_1-ATPase in mitochondria from neonatal rat heart revealed by double immunogold staining. Electron micrograph depicts colocalization of S100A1 and F_1-ATPase as indicated by 10 nm and 5 nm gold particles that are less than 30 nm apart (marked as red circles). Bar, 150 nm

To analyze the interaction of S100A1 and F_1-ATPase at the subcellular level, we performed double-immunolabeling experiments of NVCMs with a monoclonal antibody against S100A1 and a polyclonal antibody that reacts with all 5 subunits of the F_1-ATPase. As

illustrated in Fig. 5.3E, the F_1-ATPase antibody typically revealed 'bullet- shaped' structures (blue), which were similar to mitochondria stained by MitoTracker. Merging the respective confocal images (Fig. 5.3D and E) clearly showed that S100A1 partially localized to the same confocal volume as the F_1-ATPase (Fig. 5.3F, turquoise).

To obtain more detailed information on this colocalization, we used double immunogold labeling of S100A1 and F_1-ATPase on ultrathin sections of a 3-day old neonatal rat heart. As indicated by the red circles in the electron micrograph displayed in Fig. 5.3G, we observed numerous cases where 10 nm gold particles (S100A1) and 5 nm gold particles (F_1-ATPase) appeared in close proximity. Taking the dimensions of the two antibody complexes into account, a spacing of approximately 30 nm between 10 nm and 5 nm gold particles is indicative of a physical interaction between the two binding sites. In conclusion, these immunolocalization studies substantiated the localization of S100A1 in mitochondria and its direct interaction with the F_1-ATPase.

The interaction of S100A1 with the α-and β-chain of the F_1-ATPase depends on calcium and pH

To confirm the direct interaction of S100A1 with the α- and β-chain of the F_1-ATPase, we performed reverse pulldown assays. For this purpose, recombinant GST-α-chain, GST-β-chain fusion proteins or GST alone were coupled to glutathione-Sepharose beads in the presence of 2 mM $CaCl_2$, 0.2 mM $CaCl_2$ or 2 mM EGTA and subsequently incubated with recombinant S100A1 protein. Bound protein was eluted and analyzed by SDS-PAGE and Western-blotting using an S100A1 antibody (Fig. 5.4A).

In the presence of 2 mM $CaCl_2$ and 0.2 mM $CaCl_2$, both the GST-α-chain and the GST-β-chain fusion protein each pulled down two bands with an apparent molecular weight of 10 and 20 kDa, respectively, which were recognized by the S100A1 antibody. The migration behavior of these two bands corresponds to that of the monomeric and dimeric form of recombinant S100A1. Both bands were absent when pulldown assays were carried out in the presence of EGTA or with GST-control beads.

Furthermore, when GST-S100A1 pulldown assays with purified bovine heart F_1-ATPase

were performed under different pH conditions, a pH sensitive interaction was observed (Fig. 5.4B and C). At pH 7.4, the α- and β-chain of F_1-ATPase were pulled down by GST-S100A1 in the presence of 2 mM $CaCl_2$. However, in the presence of 2 mM EGTA the two respective bands were significantly diminished. When the pH was lowered to 6.8, the binding of F_1-ATPase to GST-S100A1 was barely detectable even in the presence of 2 mM $CaCl_2$. In control pulldown assays carried out in the presence of 2 mM EGTA or with immobilized GST alone, no bands were visible (data not shown).

These data confirmed that at pH 7.4 there is a direct interaction between S100A1 and the α-and β-chains of F_1-ATPase in the presence of 2 mM or 0.2 mM $CaCl_2$.

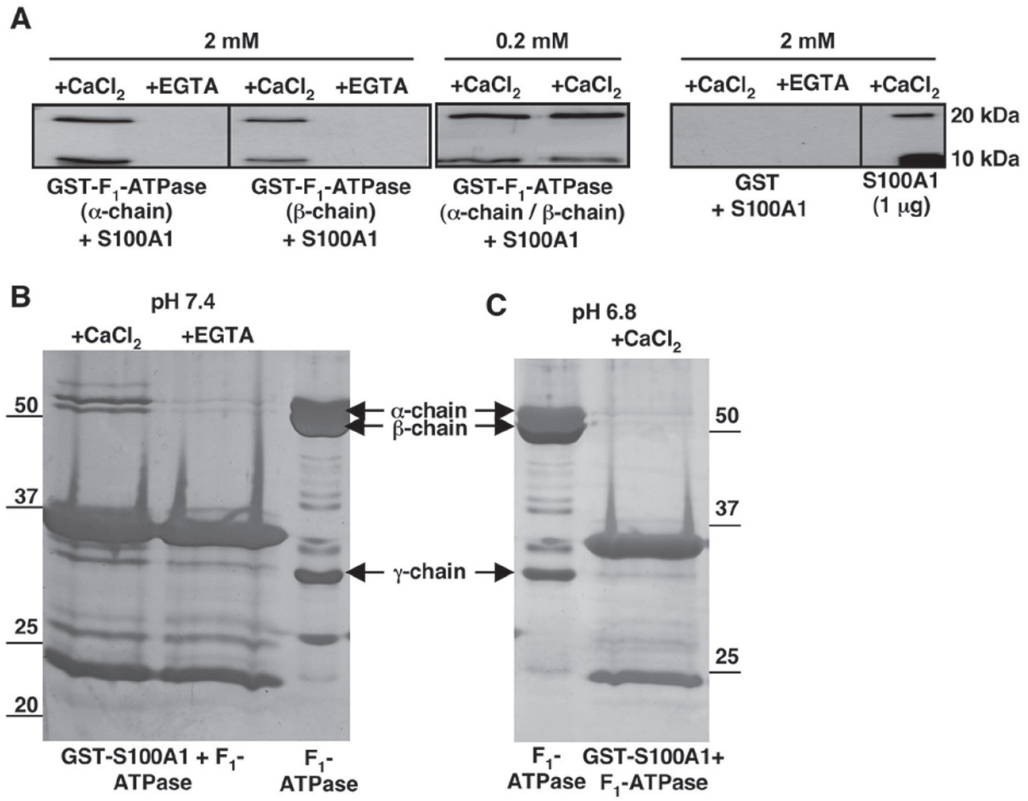

Figure 5.4: Pulldown assays indicate an interaction between S100A1 and the F_1-ATPase
(A) Western blot of eluates of GST-F_1-ATPase α-and β-chain pulldown assays performed with recombinant human S100A1 in the presence of 2 mM $CaCl_2$, 0.2 mM $CaCl_2$ or 2 mM EGTA. Probing with an anti-human S100A1-specific antibody revealed a 10 (monomeric) and 20 kDa (dimeric) S100A1 species which were pulled down by GST-F_1-ATPase α-and β-chain in the presence of 2 mM $CaCl_2$ and 0.2 mM $CaCl_2$. GST alone (control) does not pull down S100A1. (B and C) Pulldown assays with GST-S100A1 and purified F_1-ATPase at different pH. (B) At pH 7.4 in the presence of 2 mM $CaCl_2$, two bands migrating at approximately 55 and 51 kDa are detected. Comparison with purified F_1-ATPase (lane on the right) indicates that these bands represent the α-and β-chain subunits. 2 mM EGTA largely abolishes the interaction between GST-S100A1 and the α-and β-chain of the F_1-ATPase. (C) At pH 6.8, F_1-ATPase subunits are not pulled down by GST-S100A1 even in the presence of 2 mM $CaCl_2$.

S100A1 forms a complex with the F_1-ATPase and increases its activity

To analyze the interaction of S100A1 and the F_1-ATPase in molecular detail, we isolated the S100A1-F_1-ATPase complex by gel filtration chromatography. For complex formation, purified F_1-ATPase was incubated at pH 7.4 with a 12.5-fold molar excess of S100A1 in the presence of 2 mM $CaCl_2$ or 2 mM EGTA for 30 min at 37°C. To maintain F_1-ATPase activity, 1 mM MgATP was added to the mixture at 1 and 15 min. After incubation, the mixture was subjected to gel filtration chromatography on a Superdex 200 HiLoad column and individual fractions were analyzed by SDS-PAGE. In the presence of $CaCl_2$, two prominent peaks were identified in the elution profile (Fig. 5.5A). Based on the apparent molecular masses of the proteins that eluted in the first peak (fractions 36-42), this peak contained the five subunits of the F_1-ATPase (α-, β-, γ-, δ-, and ε-chains) and, as suggested by their electrophoretic mobility, monomeric and dimeric S100A1 (Fig. 5.5A; 10 and 20 kDa bands, respectively, framed in black). The presence of S100A1 was confirmed by Western blotting using an S100A1-specific antibody and by mass spectrometry (data not shown). The elution profile of peak I also displayed a small shoulder (fractions 40-42) that possibly represents aggregation products of S100A1 and F_1-ATPase subunits. SDS-PAGE of the second, smaller peak (fractions 50-54) contained predominantly free S100A1 mono- and dimmers and only traces of the F_1-ATPase subunits.

In the presence of 2 mM EGTA, gel filtration chromatography of the S100A1-F_1-ATPase complex (Fig. 5.5B) produced an elution profile that was clearly distinct from that obtained with 2 mM $CaCl_2$. SDS-PAGE analysis of the first peak (fractions 36-40) revealed the five subunits of the F_1-ATPase but no monomeric or dimeric S100A1 protein (black frames). S100A1 only eluted in fractions corresponding to the second peak (fractions 49-53). This peak, which predominantly contains the free S100A1, was increased by approximately 150% compared to the corresponding peak obtained in the presence of 2 mM $CaCl_2$ (Fig. 5.5A, peak II). Together, the data indicate that S100A1 forms a complex with the F_1-ATPase in the presence of calcium at pH 7.4.

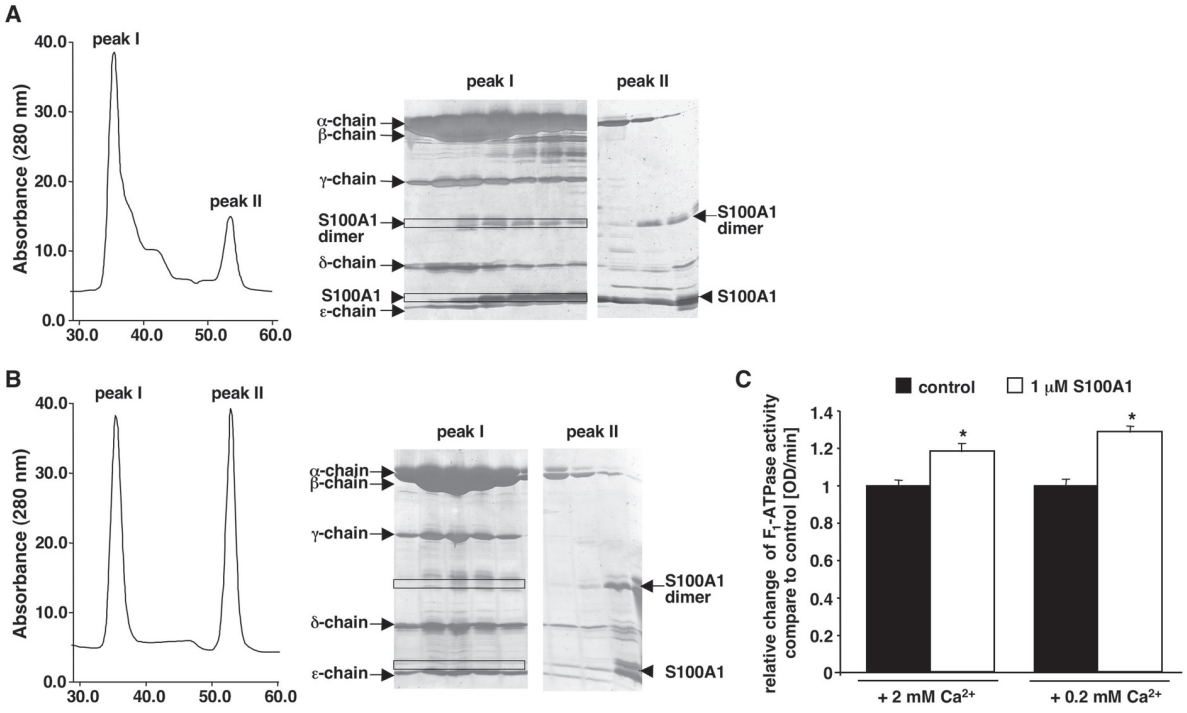

Figure 5.5. Gel filtration chromatography of the S100A1-F_1-ATPase complex and determination of the F_1-ATPase activity

(A) Analysis of the S100A1-F_1-ATPase complex in the presence of 2 mM $CaCl_2$. The absorbance of the eluant was monitored at 280 nm. The elution profile shows two major peaks of different height. Analysis of individual column fractions (X axis) on a 12-22% gradient SDS-PAGE gel reveals that peak I (fractions 36-42) contains the 5 subunits of the F_1-ATPase, as well as S100A1 in form of a dimer and monomer (framed in black). Peak II (fractions 50-54) comprises the excess of recombinant S100A1. Only residual amounts of the F_1-ATPase subunits are detected in this peak. (B) In the presence of 2 mM EGTA, the elution profile of the S100A1-F_1-ATPase complex displays two symmetric peaks of comparable height. The 5 subunits of the F_1-ATPase are eluted in peak I (column fractions 36-40) whereas S100A1 protein appears only in peak II in form of a monomer and dimer (fractions 49-53). S100A1 monomer is indicated by an arrowhead. (C) S100A1 increases F_1-ATPase activity. F_1-ATPase activity was measured with an ATP-regenerating system by following the oxidation of NADH to NAD^+ at 340 nm in the presence of either 2 mM or 0.2 mM calcium. Results are reported as relative change of F_1-ATPase activity in the presence of 1 mM S100A1 compare to control (F_1-ATPase alone). Data are represented as mean ± S.E.M. of 25 experiments. $P<0.01$, indicated by asterisks.10 μm.

To determine the functional effects resulting from the interaction of S100A1 with the F_1-ATPase we measured the activity of isolated F_1-ATPase incubated with S100A1 (Fig. 5.5C). Accordingly, S100A1 caused an ~18% increase of the F_1-ATPase activity in the presence of 2 mM $CaCl_2$ and a ~28% increase in the presence of 0.2 mM $CaCl_2$.

In conclusion, these studies substantiate the direct interaction of S100A1 with the F_1-ATPase and its effects on the F_1-ATPase activity.

S100A1 protein levels affect ATP-synthase activity, ATP content and Ca^{2+}-transient amplitudes in cardiomyocytes

To address the functional significance of an S100A1-F_1-ATPase interaction in cells, we examined the consequences of S100A1 knockdown on both ATP-synthase activity and F_1-ATPase-mediated ATP production in cardiomyocytes.

To examine the relationship between S100A1 levels and ATP-synthase activity we used adult ventricular cardiomyocytes from wild type (WT) and S100A1-deficient (SKO; (5) mice. The significantly higher conversion rate of NADH to NAD^+ observed in WT compared to SKO cardiomyocyte homogenates at 0.2 mM and 0.2 mM free [Ca^{2+}] indicated a higher mitochondrial ATP-synthase activity in WT cardiomyocytes (Fig. 5.6A). Because cardiomyocyte homogenates were prepared in Ca^{2+} buffered solution, which prevented loss of endogenous S100A1 protein in WT as confirmed by immunblotting (data not shown), the higher ATP-synthase activity could be attributed to S100A1. Consistently, addition of recombinant S100A1 protein to SKO cardiomyocyte homogenates significantly increased mitochondrial ATP-synthase activity both at 0.2 mM and 0.2 mM free [Ca^{2+}].

To analyze the ATP content in cardiomoycytes expressing different S100A1 protein levels, NVCMs were transfected with S100A1 small interfering RNA (siRNA) or scrambled control RNA. Efficient suppression of S100A1 protein by the specific siRNA in transfected NVCMs was confirmed by Western blotting (Fig. 5.6B). Parallel NVCM cultures were lysed seventy-two hours post transfection, and subsequently ATP levels were assayed by a luciferase based luminometry reaction. As illustrated in Fig. 5.6B, knockdown of S100A1 expression in unstimulated NVCMs (S100A1 siRNA, basal conditions) caused ATP levels to decrease by an average of 48% compared to control cells transfected with scrambled siRNA or untransfected NVCMs (NT). Consistent with the notion that S100A1 levels influence ATP production, overexpression of S100A1 in NVCMs (Fig. 5.6C; AdS100A1) increased ATP levels by 82% compared to control cells expressing endogenous S100A1 (Adcontrol, NT). Qualitatively similar results were obtained after stimulation of cells with 1 mM isoproterenol, a beta adrenergic receptor agonist, or 10 mM $CaCl_2$: S100A1-deficient NVCMs exhibited a significantly reduced ATP level (approximately 65% for isoproterenol-treated and 53%

for $CaCl_2$-treated knockdown NVCMs compared to control cells) whereas overexpression of S100A1 consistently led to an enhanced ATP level (approximately 118% for isoproterenol-treated, and 127% for $CaCl_2$-treated AdS100A1 NVCMs compared to control cells).

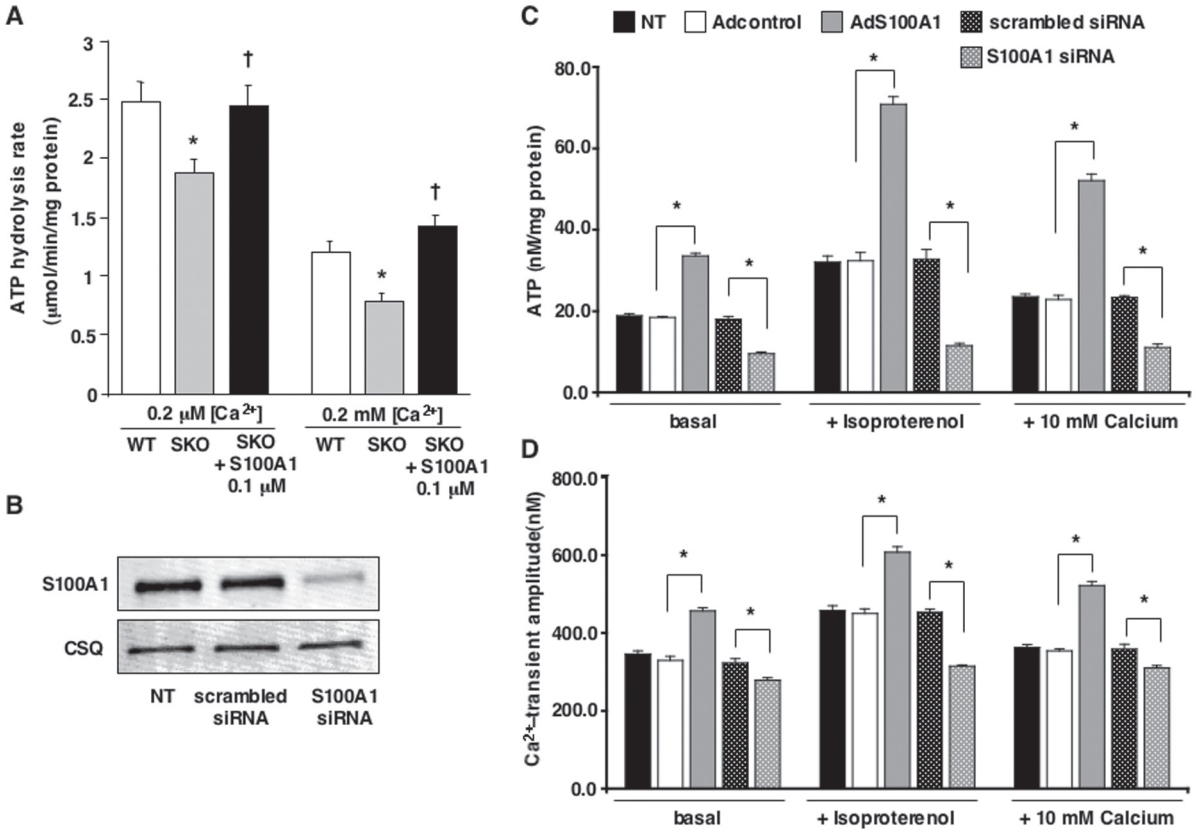

Figure 5.6.S100A1 protein levels affect ATP-Synthase activity, ATP content and Ca^{2+}-transient amplitudes cardiomyocytes

(A) Mitochondrial ATP-synthase activity assessed by monitoring conversion of NADH to NAD^+ in WT and SKO cardiomyocyte homogenates. Compared to WT, mitochondrial ATP-synthase activity is significantly lower in SKO cardiomyocyte homogenates at 0.2 mM and 0.2 mM free [Ca^{2+}]. Preincubation with S100A1 protein (0.1 mM) for 10 min restored mitochondrial ATP-synthase activity in SKO cardiomyocyte homogenates at 0.2 mM and 0.2 mM free [Ca^{2+}]. Values are mean±S.E.M. * $P < 0.05$ vs WT, † $P < 0.05$ vs SKO. n = 4 cell preparations, each experiment was carried out in triplicates. (B) Western Blot of S100A1 or calsequestrin (CSQ, loading control) of extracts from cells transfected with scrambled or S100A1 siRNA and non-transfected (NT) cells. (C) Comparison of the ATP content in NT, adenovirus transduced (AdS100A1 and Adcontrol) and siRNA-treated cells. Under basal conditions, S100A1 overexpression (AdS100A1) results in a significantly higher ATP content compared to control (Adcontrol) and NT cells. In contrast, knockdown of S100A1 protein (S100A1 siRNA) leads to a significant reduction of ATP compared to control cells (scrambled siRNA). Upon isoproterenol stimulation, AdS100A1 cells exhibit a two-fold higher ATP content compared to Adcontrol and NT cells whereas S100A1 suppression caused a two-fold reduction of ATP compared to scrambled siRNA treated cells. Addition of 10 mM calcium also yields to a two-fold increase of ATP content in AdS100A1 cells and likewise to a two-fold reduction in S100A1 siRNA cells. (D) Effects of S100A1 protein levels on Ca^{2+}-transients. Compared to control cells expressing endogenous levels of S100A1, S100A1 overexpression (AdS100A1) significantly increases the Ca^{2+}-transient amplitude under basal conditions as well as when stimulated with isoproterenol or 10 mM calcium. Suppression of S100A1 protein leads to decreased Ca^{2+}-transient amplitude. Data are represented as mean ± S.E.M. of five different experiments in (C), and of 150 cells from the different cell preparations in (D). $P<0.01$, indicated by asterisks.

Furthermore, compared to control or AdS100A1 cells, S100A1-deficient NVCMs were not able to respond with an adequate ATP increase after isoproterenol or $CaCl_2$ stimulation.

To examine the effects of reduced and increased levels of S100A1 on Ca^{2+}-cycling, we recorded Ca^{2+}-transients in NVCMs under basal and stimulated conditions (Fig. 5.6D). In AdS100A1 cells overexpressing S100A1 the increased ATP content was accompanied by an increase in the Ca^{2+}-transient amplitudes compared to control cells (approximately 38% increase for basal, 35% for isoproterenol-treated, and 47% for $CaCl_2$-treated AdS100A1). Consistently, suppression of S100A1 protein by S100A1 siRNA led to decreased Ca^{2+}-transient amplitudes (approximately 14% for basal, 30% for isoproterenol-treated, and 12% for $CaCl_2$-treated AdS100A1 compared to control cells), concomitant with a reduced ATP production.

5.5 Discussion

S100A1 has recently been recognized to act as a regulator of Ca^{2+}-cycling and contractility in the heart (15, 20, 23). However, efficient performance of the myocardium, in particular cardiac contractility, is based not only on Ca^{2+}-homeostasis but to a large extent also on energy metabolism (reviewed in references 6 and 10). Thus, the increase in cardiac contractility brought about by S100A1 overexpression strongly argued for a role of S100A1 in energy metabolism in addition to its role in Ca^{2+}-cycling. Indeed, we found that the ATP content measured in cardiomyocytes overexpressing S100A1 (AdS100A1) was 67% higher in resting AdS100A1 and even 110% higher in electrically stimulated AdS100A1 cells compared to control cells. This ATP increase substantiates the notion that S100A1 is involved in the regulation of the energy metabolism in cardiomyocytes.

Pulldown experiments with GST-S100A1 provided the first clues as to the molecular mechanism underlying the increase in ATP induced by S100A1. Interestingly, several mitochondrial proteins were pulled down by GST-S100A1, and virtually all of these potential S100A1 target proteins are involved in the cell's energy metabolism. In support of our findings, gel overlay experiments revealed glycogen phosphorylase and phosphoglucomutase, which, through their role in glycogenolysis, are also involved in energy production, as potential target proteins of S100A1 (31). In addition, S100A1 was shown to interact in a Ca^{2+}-dependent manner with fructose-1,6-bisphosphate aldolase, thereby increasing its enzymatic activity (32). Fructose-1,6-bisphosphate aldolase is a key regulator of glycolysis and thus essential for energy production. Our data provide the first evidence that S100A1 interacts in a Ca^{2+}-dependent manner with the F_1-ATPase in heart tissue. F_1-ATPase is part of the F_1F_o-ATPase, which is responsible for the ATP synthesis

in the cell. Hence, it is tempting to speculate that the interaction of S100A1 with the F_1-ATPase is responsible for the increased ATP content in cardiomyocytes overexpressing S100A1. At this point, we cannot rule out that any of the other mitochondrial proteins pulled down by GST-S100A1, for example the Ca^{2+}-sensitive dehydrogenase isocitrate or the adenine nucleotide translocase, could also play a role in regulating the ATP content of the cell.

Because we were able to demonstrate a direct interaction of S100A1 with the α- and β-chain

of the F_1-ATPase by reverse pulldown assays using GST-F_1-ATPase α- and β-chain as bait proteins for recombinant S100A1, we have focused our studies on the S100A1-F_1-ATPase interaction. The specificity of this interaction was corroborated by the Ca^{2+}-dependence and pH sensitivity of S100A1 binding to the α- and β-chain of F_1-ATPase. The most convincing piece of evidence that S100A1 biochemically interacts with the F_1-ATPase has been provided by the isolation of a S100A1-F_1-ATPase-complex by gel filtration chromatography.

For a physical interaction of S100A1 and the F_1-ATPase to occur in the cell, the spatial proximity of these proteins is required. While the localization of the F_1-ATPase in mitochondria has been known for quite some years (13), there are only a limited number of studies that report a mitochondrial localization of S100A1. For example, electron microscopy studies have shown that S100A1 is present in the mitochondria of mouse slow-twitch fibers (8) as well as in mitochondria of the human heart (14). Similarly, our data document the presence of S100A1 at the inner and outer mitochondrial membrane, as well as in the matrix of rat heart mitochondria. Furthermore, double immunolabeling experiments, both from confocal light and electron microscopy studies reveal that S100A1 and the F_1-ATPase indeed colocalize in mitochondria, indicating that a physical interaction between S100A1 and the F_1-ATPase is likely to occur in vivo.

A first indication of the functional significance of such an interaction has been reported by Simonian et al., who showed that S100A1 stimulated the ATPase activity in mitochondria isolated from gerbil brain (26). The increased level of ATP we observed in cardiomyocytes that overexpress S100A1 extends the notion of a functional interaction between S100A1 and the F_1-ATPase. Moreover, the effect of S100A1 knockdown on the ATP level consolidates the association of S100A1 with mitochondrial ATP production. Further evidence is provided by the diminished mitochondrial ATPase activity observed in cardiomyocytes from S100A1 knockout mice. A direct indication of the influence of S100A1 on the function of the F_1-ATPase is provided by the determination of the F_1-ATPase activity. Indeed, incubation of S100A1 with isolated F_1-ATPase causes an 18% increase of the F_1-ATPase activity in the presence of 2 mM $CaCl_2$ and a 28% increase at 0.2 mM calcium. The direct impact of S100A1 protein on F_1-ATPase activity is also demonstated by restoring decreased mitochon-

drial ATP-synthase activity in SKO cardiomyocytes through exogenous S100A1.

A potential interaction between the Ca^{2+}-binding protein S100A1 and the F_1-ATPase raises the question of how energy production, as well as cardiac work, and Ca^{2+}-homeostasis are connected. In their recent work, Ventura-Clapier et al. have suggested that Ca^{2+} is one of the main candidates for coupling energy metabolism and cardiac work (reviewed in reference 29). Furthermore, work by Territo and Balaban has shown that cytosolic Ca^{2+} plays an important role in the regulation of cardiac energy metabolism. Of particular interest is their finding that Ca^{2+} activates several steps in oxidative phosphorylation, including F_1F_o-ATPase (27, 28; reviewed in reference 1). It has been proposed that Ca^{2+} as an intermediary may concomitantly control both energy metabolism and cardiac work (28). Because S100A1 not only improves cardiac Ca^{2+}-handling and heart muscle contractility (19) but also increases energy production, we speculate that the Ca^{2+}-sensor might be involved in coupling Ca^{2+}-cycling with Ca^{2+}-dependent regulation of cardiac metabolism. This notion is supported by the finding that Ca^{2+}-transient amplitudes and ATP levels were concomitantly increased when S100A1 levels were raised, whereas knockdown of S100A1 reduced both ATP levels and Ca^{2+}-transient amplitudes. The important question whether improved energy supply is crucial to S100A1 Ca^{2+}-dependent inotropic actions in healthy and diseased myocardium will need to be addressed in future studies.

In conclusion, our data have unveiled a novel role of S100A1 in cardiac metabolism. Undoubtedly, a more detailed knowledge of the molecular interaction between F_1-ATPase and S100A1 and also the other mitochondrial target proteins identified by pulldown assays is needed to more rationally understand the molecular mechanism by which S100A1 participates in the cardiac energy metabolism. Elucidation of this molecular mechanism will ultimately provide insight into the failing heart where the cardiac pump is no longer able to meet the energy requirements of the body.

5.6 **Acknowledgments**

We would like to thank V. Oliveri and U. Sauder (Biozentrum, University of Basel) for their technical support with electron microscopy. This work was supported by the M.E. Müller Foundation of Switzerland and the Kanton of Basel Stadt (MB, UA, and C-AS) and in part by grants from the University of Heidelberg (Forschungsförderung 93/2002 and 61/2003 to PM) and the Deutsche Forschungsgemeinschaft (DFG, Mo 1066/1-1 to PM).

5.7 References

1. **Balaban, R. S**. 2002. Cardiac energy metabolism homeostasis: role of cytosolic calcium. J Mol Cell Cardiol 34:1259-71.

2. **Bosetti, F., G. Yu, R. Zucchi, S. Ronca-Testoni, and G. Solaini**. 2000. Myocardial ischemic preconditioning and mitochondrial F_1F_0-ATPase activity. Mol Cell Biochem 215:31-7.

3. **Cadenas, S., and M. D. Brand**. 2000. Effects of magnesium and nucleotides on the proton conductance of rat skeletal-muscle mitochondria. Biochem J 348 Pt 1:209-13.

4. **Donato, R**. 2003. Intracellular and extracellular roles of S100 proteins. Microsc Res Tech 60:540-51.

5. **Du, X. J., T. J. Cole, N. Tenis, X. M. Gao, F. Kontgen, B. E. Kemp, and J. Heierhorst**. 2002. Impaired cardiac contractility response to hemodynamic stress in S100A1-deficient mice. Mol Cell Biol 22:2821-9.

6. **Duchen, M. R**. 2004. Roles of mitochondria in health and disease. Diabetes 53 Suppl 1: S96-102.

7. **Florholmen, G., V. Aas, A. C. Rustan, P. K. Lunde, N. Straumann, H. Eid, A. Odegaard, H. Dishington, K. B. Andersson, and G. Christensen**. 2004. Leukemia inhibitory factor reduces contractile function and induces alterations in energy metabolism in isolated cardiomyocytes. J Mol Cell Cardiol 37:1183-93.

8. **Haimoto, H., and K. Kato**. 1987. S100a0 (alpha alpha) protein, a calcium-binding protein, is localized in the slow-twitch muscle fiber. J Neurochem 48:917-23.

9. **Heizmann, C. W., and J. A. Cox**. 1998. New perspectives on S100 proteins: a multi-

functional $Ca^{(2+)}$-, $Zn^{(2+)}$- and $Cu^{(2+)}$-binding protein family. Biometals 11:383-97.

10. **Huss, J. M., and D. P. Kelly**. 2005. Mitochondrial energy metabolism in heart failure: a question of balance. J Clin Invest 115:547-55.

11. **Ingwall, J. S., and R. G. Weiss**. 2004. Is the failing heart energy starved? On using chemical energy to support cardiac function. Circ Res 95:135-45.

12. **Kato, K., and S. Kimura**. 1985. S100ao (alpha alpha) protein is mainly located in the heart and striated muscles. Biochim Biophys Acta 842:146-50.

13. **Lehninger, A. L**. 1967. Energy coupling in electron transport. Fed Proc 26:1333-4.

14. **Maco, B., A. Mandinova, M. B. Durrenberger, B. W. Schafer, B. Uhrik, and C. W. Heizmann**. 2001. Ultrastructural distribution of the S100A1 Ca^{2+}-binding protein in the human heart. Physiol Res 50:567-74.

15. **Most, P., J. Bernotat, P. Ehlermann, S. T. Pleger, M. Reppel, M. Borries, F. Niroomand, B. Pieske, P. M. Janssen, T. Eschenhagen, P. Karczewski, G. L. Smith, W. J. Koch, H. A. Katus, and A. Remppis**. 2001. S100A1: a regulator of myocardial contractility. Proc Natl Acad Sci U S A 98:13889-94.

16. **Most, P., M. Boerries, C. Eicher, C. Schweda, P. Ehlermann, S. T. Pleger, E. Loeffler, W. J. Koch, H. A. Katus, C. A. Schoenenberger, and A. Remppis**. 2003. Extracellular S100A1 protein inhibits apoptosis in ventricular cardiomyocytes via activation of the extracellular signal-regulated protein kinase 1/2 (ERK1/2). J Biol Chem 278:48404-12.

17. **Most, P., M. Boerries, C. Eicher, C. Schweda, M. Volkers, T. Wedel, S. Sollner, H. A. Katus, A. Remppis, U. Aebi, W. J. Koch, and C. A. Schoenenberger. 2005**. Distinct subcellular location of the Ca^{2+}-binding protein S100A1 differentially modulates Ca^{2+}-cycling in ventricular rat cardiomyocytes. J Cell Sci 118:421-31.

18. **Most, P., and W. J. Koch**. 2007. S100A1: a calcium-modulating inotropic prototype for future clinical heart failure therapy. Future Cardiol 3:5-11.

19. **Most, P., S. T. Pleger, M. Volkers, B. Heidt, M. Boerries, D. Weichenhan, E. Loffler, P. M. Janssen, A. D. Eckhart, J. Martini, M. L. Williams, H. A. Katus, A. Remppis, and W. J. Koch**. 2004. Cardiac adenoviral S100A1 gene delivery rescues failing myocardium. J Clin Invest 114:1550-63.

20. **Most, P., A. Remppis, S. T. Pleger, E. Loffler, P. Ehlermann, J. Bernotat, C. Kleuss, J. Heierhorst, P. Ruiz, H. Witt, P. Karczewski, L. Mao, H. A. Rockman, S. J. Duncan, H. A. Katus, and W. J. Koch**. 2003. Transgenic overexpression of the Ca^{2+}-binding protein S100A1 in the heart leads to increased in vivo myocardial contractile performance. J Biol Chem 278:33809-17.

21. **Most, P., H. Seifert, E. Gao, H. Funakoshi, M. Volkers, J. Heierhorst, A. Remppis, S. T. Pleger, B. R. DeGeorge, Jr., A. D. Eckhart, A. M. Feldman, and W. J. Koch**. 2006. Cardiac S100A1 protein levels determine contractile performance and propensity toward heart failure after myocardial infarction. Circulation 114:1258-68.

22. **Orriss, G. L., A. G. Leslie, K. Braig, and J. E. Walker. 1998**. Bovine F_1-ATPase covalently inhibited with 4-chloro-7-nitrobenzofurazan: the structure provides further support for a rotary catalytic mechanism. Structure 6:831-7.

23. **Remppis, A., P. Most, E. Loffler, P. Ehlermann, J. Bernotat, S. Pleger, M. Borries, M. Reppel, J. Fischer, W. J. Koch, G. Smith, and H. A. Katus**. 2002. The small EF-hand Ca^{2+} binding protein S100A1 increases contractility and Ca^{2+} cycling in rat cardiac myocytes. Basic Res Cardiol 97 Suppl 1:I56-62.

24. **Sambrano, G. R., I. Fraser, H. Han, Y. Ni, T. O'Connell, Z. Yan, and J. T. Stull**. 2002. Navigating the signalling network in mouse cardiac myocytes. Nature 420:712-4.

25. **Schoenenberger, C. A., S. Buchmeier, M. Boerries, R. Sutterlin, U. Aebi, and B. M. Jockusch**. 2005. Conformation-specific antibodies reveal distinct actin structures in the nucleus and the cytoplasm. J Struct Biol 152:157-68.

26. **Simonian, A., J. Baudier, and K. G. Haglid**. 1989. Modulation of ATPase activities in the central nervous system by the S-100 proteins. Neurochem Res 14:761-4.

27. **Territo, P. R., S. A. French, M. C. Dunleavy, F. J. Evans, and R. S. Balaban**. 2001. Calcium activation of heart mitochondrial oxidative phosphorylation: rapid kinetics of mVO2, NADH, AND light scattering. J Biol Chem 276:2586-99.

28. **Territo, P. R., V. K. Mootha, S. A. French, and R. S. Balaban. 2000**. $Ca(^{2+})$ activation of heart mitochondrial oxidative phosphorylation: role of the $F(_0)/F(_1)$-ATPase. Am J Physiol Cell Physiol 278:C423-35.

29. **Ventura-Clapier, R., A. Garnier, and V. Veksler**. 2004. Energy metabolism in heart failure. J Physiol 555:1-13.

30. **Zimmer, D. B., E. H. Cornwall, A. Landar, and W. Song**. 1995. The S100 protein family: history, function, and expression. Brain Res Bull 37:417-29.

31. **Zimmer, D. B., and J. G. Dubuisson**. 1993. Identification of an S100 target protein: glycogen phosphorylase. Cell Calcium 14:323-32.

32. **Zimmer, D. B., and L. J. Van Eldik**. 1986. Identification of a molecular target for the calcium-modulated protein S100. Fructose-1,6-bisphosphate aldolase. J Biol Chem 261:11424-8.

Chapter 6

Conclusions and Perspectives

6.1 Extracellular S100A1 inhibits apoptosis in ventricular cardiomyocytes via activation of the extracellular signal-regulated protein kinase 1/2 (ERK1/2)

Growing evidence indicates that members of the S100 protein family exert intracellular but also extracellular effects on their target cells (Donato, 2003). Moreover, it has been shown that S100A1 protein is released into the extracellular space in considerable amounts during ischemic myocardial injury (Kiewitz et al., 2000). This observation prompted us to explore the extracellular effect of S100A1 on neonatal ventricular cardiomyocytes (NVCMs).

By directly coupling human recombinant S100A1 protein with rhodamine we were able to trace the uptake of extracellulary added S100A1 into the cytosolic compartment of cultured NVCMs (Chaper 2). Using confocal laser scanning microscopy, we have shown for the first time that S100A1 is internalized by NVCMs via a Ca^{2+}-dependent pathway. The colocalization studies documented that the pathway of S100A1 internalization is clathrin-dependent. By using several inhibitors that are specific for different steps along the intracellular signal transduction pathway, we could identify that S100A1-mediated activation of the ERK1/2 signaling involves activation of PLC and PKC, both of which have been closely linked to the endosomal compartment.

Taken together this part of our study demonstrated extracellular S100A1 to act as a novel anti-apoptotic factor that enhances survival of neonatal cardiomyocytes *in vitro* via activation of the PLC-PKC-MAP kinase kinase1-ERK1/2 pathway.

So far, the receptor for S100A1 internalization is still unknown. Previous studies identified the cell surface receptor for advanced glycosylated end products (RAGE) as possible receptor for S100 proteins (Hofmann et al., 1999; Huttunen et al., 2000). This was shown for the isoforms S100B and S100A12 (Donato, 2003). Because our results suggest that RAGE is not involved in the endocytosis of S100A1 in NVCM, we predict that another cell surface receptor is responsible for S100A1 uptake in NVCMs (Figure 6.1)

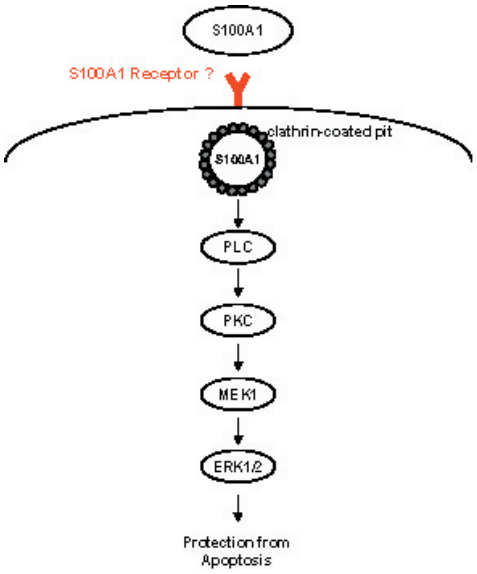

Figure 6.1: Model of S100A1 internalization and involvement in ERK1/2. signaling. The model suggests endocytosis of extracellular S100A1 by NVCM via an unknown receptor (red). *PLC, phospholipase C; PKC, phosphokinase C; MEK1, MAPkinase kinase1; ERK1/2, extracellular signal-regulated kinase 1/2.*

In future studies we will attempt to identify a possible receptor for S100A1 by employing GST-S100A1 fusion protein pull-down assays of plasma membranes. In addition, the cardioprotective effect of internalized S100A1 *in vitro* warrants further research into the release of S100A1 during heart failure. Moreover, our findings should initiate new perspectives on the pathophysiological relevance of the cardioprotective effect of S100A1 protein on cardiac cells *in vivo.*

6.2 Adenoviral-mediated S100A1 gene delivery rescues failing myocard

Since S100A1 protein has been shown to be downregulated in human and animal heart failure (HF) model (Remppis et al., 1996; Tsoporis et al., 2003), we undertook this study to address whether S100A1 gene addition might reserve ventricular contractile dysfunction in failing myocardium (Chapter 3). Using a postinfarct HF model in the rat, we provided evidence that adenoviral-mediated myocardial S100A1 gene delivery can restore S100A1 protein expression in failing myocardium. As a result of restored S100A1 levels, a normalisation of previously dysfunctional intracellular Ca^{2+}- and Na^{+}-handling occured. In additon S100A1 expression abolished aberrant fetal gene expression associated with HF, and most intringuely restored energy supply in failing myocardium.

Overall, we have shown for the first time that restoring S100A1 protein expression can rescue defective contractile performance of failing myocardium *in vitro* and *in vivo* due to improved cytosolic and SR (sarcoplasmic reticulum) Ca^{2+}-cycling. This effect is

caused by both enhanced activity of SERCA (sarco(endo)plasmic reticulum Ca^{2+}-ATPase) and modulation of RyR (ryanodine receptor).

Our studies provide ample vidence that S100A1 is a key-regulator of cardiac function *in vitro* and *in vivo*. The effects of restored S100A1 protein level in failing myocardium argue for a novel clinical approach in the regimen of HF. Athough the study described first results on the application of adenoviral S100A1 expression in failing myocardium, there exist also limitations and open questions. For instance, we have used a first-generation adenoviral vector that limits study duration. Thus, we will analyze chronic effects of HF rescue by S100A1 gene delivery with improved vectors. However, in the future S100A1 HF gene therapy might proof to be a promising clinical treatment.

6.3 Distinct subcellular location of S100A1 differentially modulates Ca^{2+}-cycling in ventricular rat cardiomyocytes

Because S100A1 is a Ca^{2+}-sensor, we investigated the effect of an increasing S100A1 levels on the cycling of cytosolic Ca^{2+} in NVCMs by two different procedures: NVCMs were either transduced by an adenoviral S100A1-expression construct (AdS100A1) or incubated with recombinant human S100A1 protein (S100A1-treated) (Chapter 4). Ca^{2+}-transient measurements revealed an increase on Ca^{2+}-turnover for both procedures. By using different inhibitors of Ca^{2+}-cycling, we have demonstrated that cells overexpressing S100A1 and cells treated with S100A1 use different mechanisms to increase the intracellular Ca^{2+}-cycling. AdS100A1 cells arrived at an enhanced Ca^{2+}-transient amplitude mainly through an increase in systolic $[Ca^{2+}]_i$. In contrast, a marked decrease in diastolic Ca^{2+}-concentrations ($[Ca^{2+}]_i$) was the main cause for the enhanced Ca^{2+}-transient amplitude in S100A1-treated NVCMs. The decreased diastolic $[Ca^{2+}]_i$ in S100A1-treated cells was likely the result of increased sarcolemmal Ca^{2+}-extrusion through the Na^+/Ca^{2+}-exchanger (NCX). Moreover, uptake of S100A1 into the endosomal compartment triggered endosome-associated PLC and PKC, which then activate NCX to increase sarcolemmal Ca^{2+}-efflux.

The enhanced systolic $[Ca^{2+}]_i$ in AdS100A1 cells was brought about by an increased activity of RyR and SERCA. Consistently, immunofluorescence documented a colocalization of intracellular overexpressed S100A1 and these two Ca^{2+}-regulatory proteins.
In conclusion, we demonstrated that intracellular S100A1, depending on its subcellular location, modulates cardiac Ca^{2+}-turnover via different Ca^{2+}-regulatory proteins.

After having shown that internalized S100A1 has a pro-survival effect on cultured cardiomyocytes and that adenoviral S100A1 gene delivery rescues failing myocardium *in vitro* and *in vivo* (Most et al., 2004), we are now facing the challenge of elucidating the effects of internalized S100A1 on cardiac function *in vivo*.

6.4 The Ca^{2+}-dependent dependent interaction of S100A1 with the F_1-ATPase leads to an increased ATP content in cardiomyoctes

Reports on the involvement of S100A1 in energy metabolism (Zimmer et al., 1995; Zimmer and Dubuisson, 1993), have prompted us to examine the effect of S100A1 overexpression on cardiac energy metabolism (Chapter 5). We found that AdS100A1 cells exhibited a significantly higher ATP content compared to control cells (Adcontrol). By using GST-S100A1 fusion protein pull-down assays we were able to identify several mitochondrial proteins, which are all involved in energy metabolism. Based on the relationship between S100A1 and ATP content, we primarily focussed on the interaciton of S100A1 with the F_1-ATPase. Confocal and electron microscopy studies provided further evidence that S100A1 interacts with the mitochondrial F_1-ATPase. Interestingly, several groups have reported the localization of S100A1 in mitochondria, but so far the functional consequence of this localization has not been addressed (Haimoto and Kato, 1988; Maco et al., 2001). In order to fill this gap, we dissected the S100A1-F_1-ATPase complex using different biochemical assays. We found the interaction to be dependent on the presence of Ca^{2+} and on the pH. At physiological pH (7.4) and in the presence of Ca^{2+}, S100A1 and F_1-ATPase form a stable complex.

For further structural analysis of the complex, we initialized a collaboration with the laboratory of Sir John Walkers in Cambridge. In a first step we have isolated an S100A1-F_1-ATPase complex by gel filtration chromatography. To unravel the molecular interactions of S100A1 and F_1-ATPase, we ultimately plan to crystallize the complex.

This part of the projekt unveiled a novel mechanism of S100A1 on cardiac function. The high metabolic demand of the heart requires a close coordination of energy production (ATP) and workload (Cortassa et al., 2003). Approximately 2% of the cellular ATP is consumed with each heartbeat and almost all of this energy is replenished by mitochondrial oxidative phosphorylation under normoxic conditions (Das and Harris, 1991; Harris and Das, 1991). The fact that not only the F_1-ATPase but also other mitochondrial proteins that participate oxidative phosphorylation associate with GST-S100A1 in pull-down experiments, convincingly argues for further investigations of these interactions (Figure 6.2).

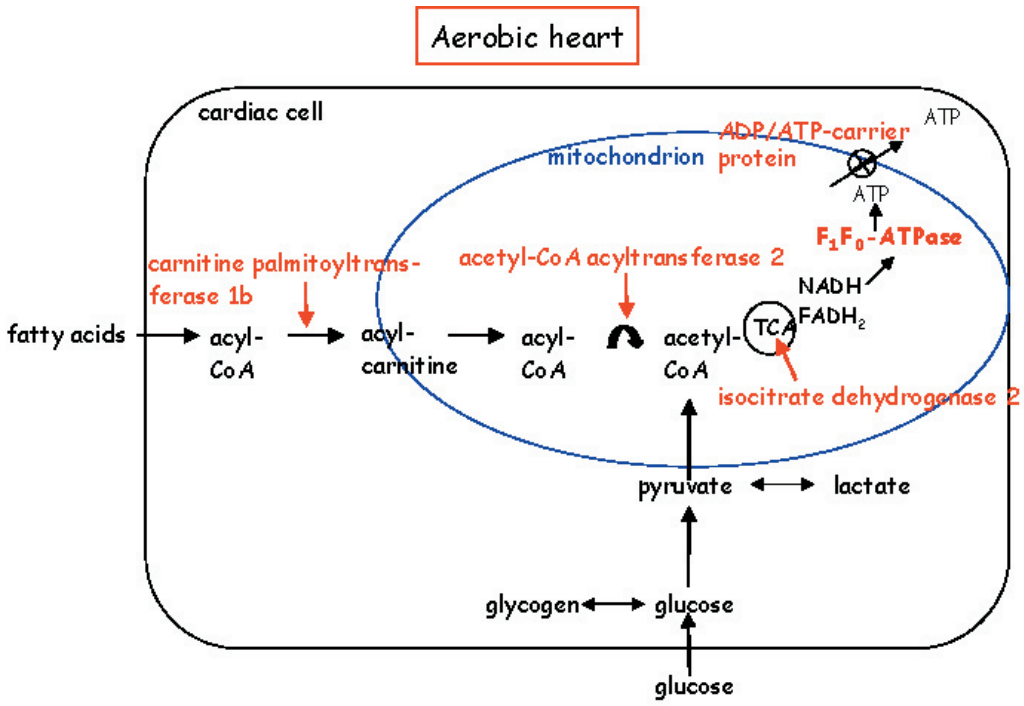

Figure 6.2: Schematic model of S100A1 and its target protein. The model demonstrates a cardiac cell and the energy metabolism of fatty acids and glucose.Identified target proteins of S100A1 are marked in red. *TCA, tricarboxylic cycle.*

6.5 Conclusions

The work presented in this thesis provides essential insights into the molecular mechanisms of S100A1 on cardiac function.

First it reveals novel mechanisms of S100A1. By combining different localization techniques and biochemical assays, the internalization of S100A1 via a Ca^{2+}-dependent, clathrin-mediated process was discovered. Moreover, it is shown that internalized S100A1 exhibits anti-apoptotic effects on cardiomyocytes and increases Ca^{2+}-turnover. Different molecular mechanisms were implicated in Ca^{2+}-handling depending on the localization of the exogenous S100A1. In addition, the rescue of failing myocardium in response to S100A1 gene delivery holds promise for a treatment of heart failure by S100A1 gene therapy. Finally, the identification of new target proteins for S100A1 gives rise to new perspectives on the involvement of S100A1 in the energy metabolism.

6.6 References

Cortassa, S., M.A. Aon, E. Marban, R.L. Winslow, and B. O'Rourke. 2003. An integrated model of cardiac mitochondrial energy metabolism and calcium dynamics. Biophys J. 84:2734-55.

Das, A.M., and D.A. Harris. 1991. Control of mitochondrial ATP synthase in rat cardiomyocytes: effects of thyroid hormone. Biochim Biophys Acta. 1096:284-90.

Donato, R. 2003. Intracellular and extracellular roles of S100 proteins. Microsc Res Tech. 60:540-51.

Haimoto, H., and K. Kato. 1988. S100a0 (alpha alpha) protein in cardiac muscle. Isolaton from human cardiac muscle and ultrastructural localization. Eur J Biochem. 171: 409-15.

Harris, D.A., and A.M. Das. 1991. Control of mitochondrial ATP synthesis in the heart. Biochem J. 280 (Pt 3):561-73.

Hofmann, M.A., S. Drury, C. Fu, W. Qu, A. Taguchi, Y. Lu, C. Avila, N. Kambham, A. Bierhaus, P. Nawroth, M.F. Neurath, T. Slattery, D. Beach, J. McClary, M. Nagashima, J. Morser, D. Stern, and A.M. Schmidt. 1999. RAGE mediates a novel proinflammatory axis: a central cell surface receptor for S100/calgranulin polypeptides. Cell. 97:889-901.

Huttunen, H.J., J. Kuja-Panula, G. Sorci, A.L. Agneletti, R. Donato, and H. Rauvala. 2000. Coregulation of neurite outgrowth and cell survival by amphoterin and S100 proteins through receptor for advanced glycation end products (RAGE) activation. J Biol Chem. 275:40096-105.

Kiewitz, R., C. Acklin, E. Minder, P.R. Huber, B.W. Schafer, and C.W. Heizmann. 2000. S100A1, a new marker for acute myocardial ischemia. Biochem Biophys Res Commun. 274:865-71.

Maco, B., A. Mandinova, M.B. Durrenberger, B.W. Schafer, B. Uhrik, and C.W. Heizmann. 2001. Ultrastructural distribution of the S100A1 Ca2+-binding protein in the human heart. Physiol Res. 50:567-74.

Most, P., S.T. Pleger, M. Volkers, B. Heidt, M. Boerries, D. Weichenhan, E. Loffler, P.M. Janssen, A.D. Eckhart, J. Martini, M.L. Williams, H.A. Katus, A. Remppis, and W.J. Koch. 2004. Cardiac adenoviral S100A1 gene delivery rescues failing myocardium. J Clin Invest. 114:1550-63.

Remppis, A., T. Greten, B.W. Schafer, P. Hunziker, P. Erne, H.A. Katus, and C.W. Heizmann. 1996. Altered expression of the Ca^{2+}-binding protein S100A1 in human cardiomyopathy. Biochim Biophys Acta. 1313:253-7.

Tsoporis, J.N., A. Marks, D.B. Zimmer, C. McMahon, and T.G. Parker. 2003. The myocardial protein S100A1 plays a role in the maintenance of normal gene expression in the adult heart. Mol Cell Biochem. 242:27-33.

Zimmer, D.B., E.H. Cornwall, A. Landar, and W. Song. 1995. The S100 protein family: history, function, and expression. Brain Res Bull. 37:417-29.

Zimmer, D.B., and J.G. Dubuisson. 1993. Identification of an S100 target protein: glycogen phosphorylase. Cell Calcium. 14:323-32.

Acknowledgements

I would like to thank Prof. Ueli Aebi for giving me the opportunity to do my MD-PhD in his laboratory and to continue my medical education in the University Hospital of Bern.
I also thank him for supporting my project and ideas.

I am very grateful to PD Dr. Cora-Ann Schoenenberger for her great supervision. Thank you so much for your continuous support and positive criticism and for teaching me many skills. Thank you for always being there during my MD-PhD (job-related and private).

A huge thank you to Dr. Patrick Most for his close support during my MD and MD-PhD time. Thank you for sharing your knowledge and ideas with me and also for your friendship.

I would also like to thank Sir John Walker for allowing me to conduct the ATPase experiments in his laboratory in Cambridge. I also thank Jonathan Gledhill for his help.

My special thanks go to Dr. Birthe Fahrenkrug and Dr. Joachim Köser for all their scientific and also private support.

Thanks to Ursula Sauder, Vesna Oivieri and Bohumil Maco for their help on the electron microscopy.

Many thanks to the people at the animal facility: Roland Geiser, René Zedi and Urs Berglas.

Thanks also to Teba Al Haboubi and Ulrich Schröder (‘actin-family’); Laurent Kreplak; Sara Paulillo, Kyrill Schwarz-Herion and David Walter (‘the Nups’); Roland Buerki and Margit Jenny (computer support); Marco Marino, Michael Mrosek and Jörg Stetefelder (the ‘Freiburger train group’); Carmen Chan, Kitaro Suda, Röbi Wyss, Röbi Haering, Nicole Taschner, Barbara Merz and Liselotte Walti.

To my family, thanks so much for your support, understanding and encouragement throughout my MD-PhD.

To my husband Oliver, I thank you deeply for always being there, for your understanding and unconditional support and patience. You are the greatest man I have ever met.

Curriculum Vitae

Name:	Dr. med. Melanie Börries
Date of birth:	25. August 1971
Place of Birth:	Oldenburg
Nationality:	German
Family status:	married

Address (business) M.E. Müller Institute for Structural Biology,
Biozentrum, University of Basel
Klingelbergstrasse 70
CH-4056 Basel, Switzerland
Telephon: +41 61 267 2095; Fax: +41 612672109
email: melanie.boerries@unibas.ch

Address (private) Grublach 7
D-79299 Wittnau
Telephon: +49 7621 1307327

Education

2001-2005	MD-PhD program in Cell Biology with Prof. U. Aebi & PD Dr. C-A. Schoenenberger, M.E. Müller Institute for Structural Biology, Biozentrum, University of Basel, Switzerland.
1994-2001	Medical School, University of Luebeck, Germany
1993-1994	Diploma in Nursing, University of Luebeck, Germany
1992-1993	Voluntary, social year
1988-1992	Gymnasium Oedeme, Lüneburg, Abitur

Clinical and Research Experience

2001-Present	Collaboration on the function of S100A1 with the Department of Internal Medicine III (Dr. Most), University of Heidelberg, Germany
2003	Internship in cardiology at the Swiss Cardiovascular Center Bern (3 months)
2002	Internship in cardiology at the Swiss Cardiovascular Center Bern (3 months)
2000-2001	Clinical Experience in anaesthesiology, cardiology and surgery at the Medical University of Luebeck, Germany and University Hospital of Basel, Switzerland.

Teaching Experience

2004	Tutor in the Microscopy Course for biology students, Biozentrum, University of Basel
2003	Tutor in the Microscopy Course for biology students, Biozentrum, University of Basel
2002	Tutor in the Microscopy Course for biology students, Biozentrum, University of Basel
2001	Tutor in the Microscopy Course for biology students, Biozentrum, University of Basel

Publications

Melanie Boerries, Patrick Most, Jonathan R Gledhill, John E Walker, Hugo A Katus, Walter J Koch, Ueli Aebi and Cora-Ann Schoenenberger.

Ca^{2+}-dependent interaction of S100A1 with the F_1-ATPase leads to an increased ATP content in cardiomyoctes.

Mol Cell Biol. 2007 Jun;27(12):4365-73.

Schoenenberger, CA., Buchmeier, S., **Boerries, M.**, Sütterlin, R., Aebi, U. and Jockusch, B.M.

Conformation-specific antibodies reveal distinct actin structures in the nucleus and the cytoplasm.

J Struct Biol. 2005 Dec;152(3):157-68.

Most P, **Boerries M**, Eicher C, Schweda C, Volkers M, Wedel T, Sollner S, Katus HA, Remppis A, Aebi U, Koch WJ, Schoenenberger CA. (Most and Boerries contributed equally to this work).

Distinct subcellular location of the Ca2+-binding protein S100A1 differentially modulates Ca2+-cycling in ventricular rat cardiomyocytes.

J Cell Sci. 2005 Jan 15;118(Pt 2):421-31.

Most P, Pleger ST, Volkers M, Heidt B, **Boerries M**, Weichenhan D, Loffler E, Janssen PM, Eckhart AD, Martini J, Williams ML, Katus HA, Remppis A, Koch WJ.

Cardiac adenoviral S100A1 gene delivery rescues failing myocardium.

J Clin Invest. 2004 Dec;114(11):1550-63.

Most P, **Boerries M**, Eicher C, Schweda C, Ehlermann P, Pleger ST, Loeffler E, Koch WJ, Katus HA, Schoenenberger CA, Remppis A (Most and Boerries contributed equally to this work).

Extracellular S100A1 protein inhibits apoptosis in ventricular cardiomyocytes via activation

of the extracellular signal-regulated protein kinase 1/2 (ERK1/2).

J Biol Chem. 2003 Nov 28;278(48):48404-12.

A. Remppis, P. Most, E. Loeffler, P. Ehlermann, J. Bernotat, ST. Pleger, **M. Börries,** M. Reppel, J. Fischer, WJ. Koch, G. Smith, HA. Katus.

The small EF-hand Ca2+binding protein S100A1 increases contractility and Ca2+cycling in rat cardiac myocytes.

Basic Research in Cardiology Suppl. 1, I/56-I/62. 2002.

P. Most, J. Bernotat, P. Ehlermann, ST. Pleger, **M. Börries**, M. Reppel, F. Niroomand, B. Pieske, PM: Janssen, T. Eschenhagen, P. Karczewski, GL. Smith, WJ. Koch, HA. Katus, A. Remppis. *S100A1: a regulator of myocardial contractility.*

Proceedings of the National Academy of Sciences of the United Staates of America (24): 13889-94. 2001.

Poster

Deutscher Kardiologenkongress 2004:

S100A1 Protein schützt ventrikuläre Kardiomyozyten vor Apoptose.

C. Eicher, M. Börries, Chr. Schweda, M. Völkers, S.T. Pleger, B. Heidt, H.A. Katus, C-A. Schoenenberger, A. Remppis, P. Most

American Society for Cell Biology, 43rd Annual Meeting 2003

Internalized S100A1 inhibits apoptosis via activation of the ERK1/2 signaling pathway in neonatal cardiomyocytes

Melanie Börries, Patrick Most, Carmen Eicher, Ueli Aebi and Cora-Ann Schoenenberger

4th International Ascona Workshop on Cardiomyocyte Cell Biology:

Stem Cells, Differentiation and Cellular Mechanisms, 2003

Cardiac fibroblasts affect the intracellular distribution of S100A1 in neonatal cardiomyocytes and increase their beating rate

Melanie Börries, Patrick Most, Andrew Remppis, Ueli Aebi and Cora-Ann Schoenenberger

Invited talks

March 2005	"Is S100A1 a target protein of F1-ATPase ?" Prof. John Walker, MRC Dunn Human Nutrition Unit, Welcome Trust/MRC Buliding, Cambridge, England.
July 2004	"S100A1: small but powerful" Prof. György Hajnoczky, Department of Pathology, Anatomy and Cell Biology, Thomas-Jefferson-University, Philadelphia, USA.
July 2004	"S100A1: Excitation-Metabolism-coupling" Prof. Walter J. Koch, Center for Translational Medicine, Department of Medicine, Thomas Jefferson University, Philadelphia, USA.